Modular Propulsion System Design for Mid-Speed Vessels

A Sustainable Approach to Reduce Emissions

MSc. Thesis

M.S. Smit

Delft University of Technology

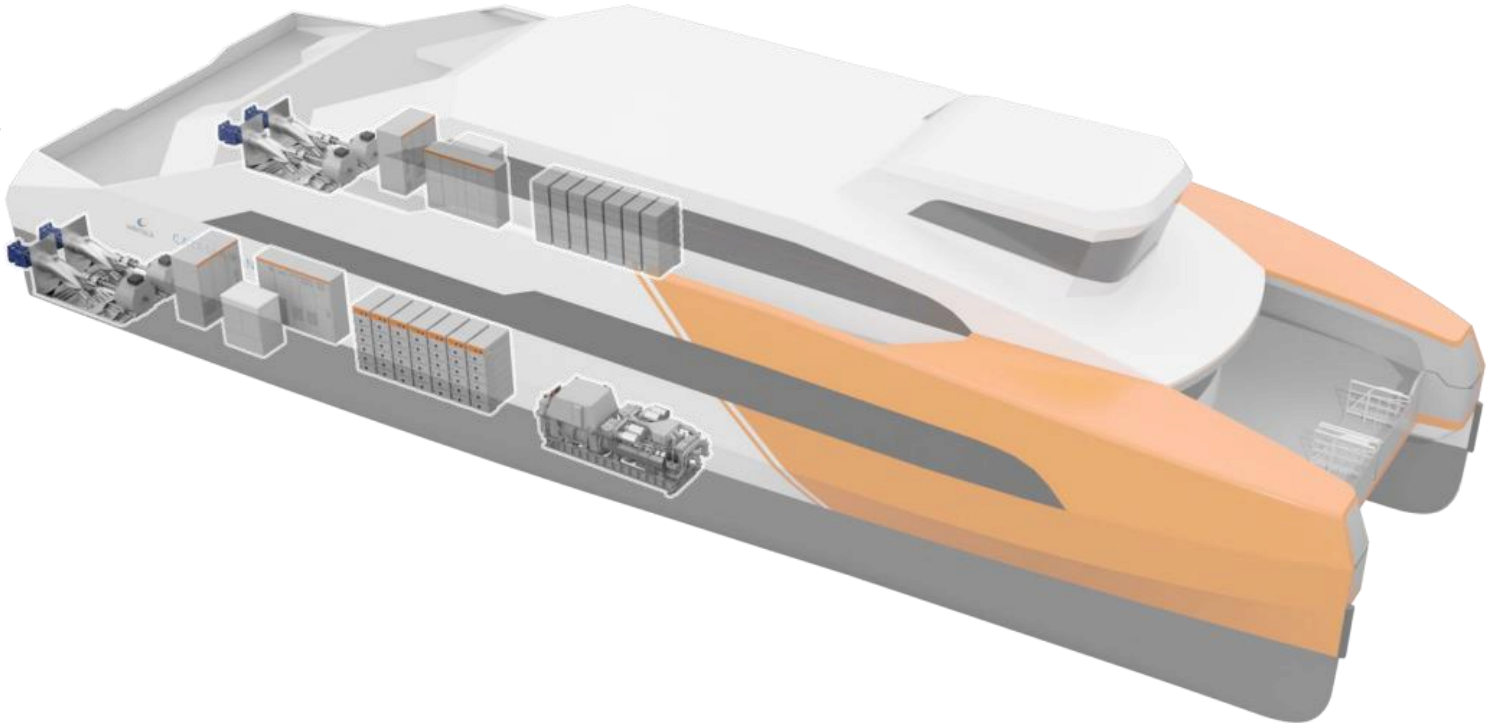

TU Delft

WÄRTSILÄ

Thesis for the degree of MSc. in Marine Technology
in the specialization of Marine Engineering

Modular Propulsion System Design for Mid-Speed Vessels

A Sustainable Approach to Reduce Emissions

by

M.S. Smit

Performed at

Wärtsilä

This thesis (MT.23/24.010.M) is classified as confidential in accordance with the general conditions for projects performed by the TUDelft.

To be publicly defended on November 17th 2023

Student Name	Student Number
Martijn Smit	4927524

Company Supervisor
Supervisor Wärtsilä: Ir. T. van Beek

Thesis Exam Committee

Chair:	Dr.ir. H. Polinder
Staff TU Delft:	MSc. T. Kopka
Staff TU Delft:	Dr.ing. C.H. Thill
Company Member:	Ir. T. van Beek
Project Duration:	February 2023 - November 2023
Faculty:	Maritime and Transport Technology, Delft

Cover: Electric Ferry Concept Wärtsilä

TU Delft

Summary

The climate of the earth is changing, this is due to the emission of greenhouse gasses. The International Maritime Organisation (IMO) will use phased regulation to reduce greenhouse gasses by 80% in 2050 (IMO, 2021). To comply with these regulations solutions need to be investigated for every ship type in the current world fleet. This thesis will focus on mid-speed sailing vessels, specifically a mid-speed sailing ferry. The ferry market is growing due to the growth in population (Transparency Market Research, 2023). The faster sailing vessels will sail slower to reduce energy expenditure and consequently emissions due to the regulations set by the IMO. For the design of the next generation of mid-speed vessels, modularity has to be introduced into the design of the vessel due to uncertainty in alternative fuels. In this research, a framework will be created and evaluated based on a case study to design a modular propulsion system for a mid-speed vessel to reduce or eliminate emissions. To achieve this goal the whole energy chain of the vessel will be investigated on a conceptual design level. This is done to swiftly evaluate and compare different propulsion system designs for specific vessels. The comparison will be done on the basis of five performance indicators: Weight, Volume, Life cycle costing, Modularity and Emissions.

The case study to evaluate the framework is based on a project funded by the EU: Transport – Advanced and Modular (TrAM) fully electric ferry. In combination with the operational profile of a ferry that operates between Harlingen and Terschelling in the Netherlands. Within the framework, the resistance of the reference hull is estimated, and the performance of multiple propulsors are estimated based on first principle models, concluding in an energy requirement to perform the operational profile. The choice of propulsor for this particular vessel in combination with the operational profile is made to create modular concept designs. Furthermore, concept designs have been created and compared based on the aforementioned performance indicators.

To answer the main research question: ”How can a propulsion system for mid-speed vessels be made modular and be made to lower or eliminate emissions?”, the framework is used and results in a hydrogen-fuelled, proton exchange membrane fuel cell in combination with a battery pack to facilitate the dynamic load changes. The conclusion of the framework is that for the mid-speed range of vessels, the best-performing propulsor is a grey area, the differences in performance are close together. For the mid-speed vessels the enemy of a modular propulsion system design to reduce or eliminate emission is weight. The weight increase punishes the design with a steep increase in resistance that will slowly converge to a solution that will be oversized for the task at hand. The framework however can directly compare multiple designs and evaluate them swiftly. The framework can be seen as modular due to the chaining of multiple first principles models that can be adjusted to fit the project’s requirements.

Contents

List of Figures

List of Tables

Nomenclature

Abbreviations

Abbreviation	Definition
AFC	Alkaline Fuel Cell
CAPEX	Capital Expenditure
CCS	Carbon Capture System
CFD	Computational Flow Dynamics
CPP	Controllable Pitch Propeller
CRP	Counter Rotating Propeller
DE	Diesel Engine
DME	Dimethyl Ether
DMFC	Direct Methanol Fuel Cell
DMO	Diesel Marine Oil
DoD	Depth of Discharge
DSM	Design Structure Matrix
EM	Electric Motor
ESS	Energy Storage System
FC	Fuel Cell
FPP	Fixed Pitch Propeller
GHG	Green House Gasses
GT	Gas Turbine
HFO	Heavy Fuel Oil
HT-PEMFC	High-Temperature Proton Exchange Membrane Fuel Cell
ICE	Internal Combustion Engine
IMO	International Maritime Organisation
LNG	Liquified Natural Gas
MCFC	Molten Core Fuel Cell
MDO	Marine Diesel Oil
NG	Natural Gas
NPV	Net Present Value
NPSH	Net Pressure Suction Head
OPEX	Operational Expenditure
PAFC	Phosphoric Acid Fuel Cell
PEMFC	Proton Exchange Membrane Fuel Cell
RNG	Renewable Natural Gas
RPM	Rotations Per Minute
SFC	Specific Fuel Consumption
SI	International System of Units
SLD	Single Line Diagram
SM	Sea Margin
SOFC	Solid Oxide Fuel Cell
TrAM	Transport - Advanced and Modular
WtW	Well to Wake

Symbols

Symbol	Definition	Unit
A_j	Jet Area	m^2
A_p	Propeller Disc Area	
B	Width	m
C_{f0}	Frictional Resistance Coefficient	-
C_T	Thrust Loading Coefficient	-
C_Y	Lateral resistance coefficient	-
D	Propulsor Diameter	m
H	Pump Head	m
h_j	Height Increase Waterjet	m
k	Turning Constant	$^\circ$
LCB	Length Center of Buoyancy	m
L_{wl}	Length Waterline	m
M	Mass	kg
n	Rotational Speed	rps
n_ω	Specific Speed	-
Q	Flow Rate	m^3/s
Q_m	Torque	Nm
r	Radius	m
R	Resistance	N
Re	Reynolds Number	
s	Spacing of Demi Hulls	m
S	Wet Surface Area	m^2
t	Thrust Deduction Factor	-
T	Thrust	N
T	Depth	m
T_q	Shaft Troque	Nm
v	Velocity	m/s
V	Volume	m^3
w	Wake Fraction	-
Y	Thruster Force	N
$(1 + k_2)$	Appendage Form Coefficient	
∇	Water Displacement	m^3
ϵ	Inlet Loss Coefficient	-
ϵ_i	Drag-Lift Coefficient	-
ζ	Transom ventilation depth	m
η	Efficiency	-
μ	Waterjet Velocity Ratio	-
ρ	Density	kg/m^3
σ	Shear Stress Constant	Pa
τ	Pitch angle	$^\circ$
ϕ	Outlet Loss Coefficient	-
ψ	Shaft Angle	$^\circ$
Ω	Rotational Speed	rad/s

Subscripts	
a	Available
ax	Axial
B	Bollard
d	Delivered
dyn	Dynamic
e	Engine
em	Electric Motor
f	Flow
FC	Fuel Cell
gen	Generator
i	Ideal
i	In
j	Jet
l	Lateral
ow	Open Water
p	Propeller
pp	Perpendicular
s	Ship
t	Total
TR	Transom
TRM	Transmission
wl	Waterline
wj	Waterjet

Acknowledgements

This report has been prepared as part of my study for a Master of Science degree in Maritime Engineering at Delft University of Technology. I want to express my gratitude to the individuals assisting me throughout this journey. To begin, I extend my appreciation to my daily supervisor, Teus van Beek, at Wärtsilä. Teus has consistently been a great supervisor for insightful discussions during our meetings and has always been readily available to address my questions. In times when I encountered challenges in the project, his extensive knowledge and skill in posing insightful questions were valuable in redirecting me towards the right path.

I also want to extend my gratitude to my thesis supervisors, Henk Polinder and Timon Kopka, for their guidance, supervision, and constructive feedback they provided, which were critical in navigating me through this academic journey. Additionally, I want to thank Cornel Thill for the guidance and critical questions to better my thesis.

Lastly, I want to extend my appreciation to my friends and family for their support not only during this project but also throughout my educational journey as a whole.

M.S. Smit
Delft, November 2023

1

Introduction

In the pursuit of a low-carbon future by 2050, the global maritime industry stands as a pivotal sector in the battle against climate change. The significance of this effort cannot be overstated, given that carbon and greenhouse gas emissions are primary drivers of global climate change, with acute impacts on ecosystems, economies, and human well-being. The importance extends beyond just large container ships; it entails the entire world fleet, including faster sailing ones. This broad focus is crucial because the shipping industry is a substantial contributor to worldwide emissions. However, this does not tell the entire story. The maritime sector also transports the largest part of the worldwide freight. Which results in low emissions per ton of cargo shipped per nautical mile (Ulreich, 2022).

The involvement of the International Maritime Organization (IMO) adds a layer of international commitment to this cause. As a specialized United Nations agency tasked with regulating global shipping, the IMO plays a central role in setting standards and guidelines. Its plan is to reduce emissions in a phased approach, acknowledging the complexity of this transition and it emphasizes international cooperation. A phased approach provides the industry with the time and flexibility to adapt, invest in new technologies, and minimize economic disruption. The ultimate target of reducing greenhouse gas emissions by 80% by 2050 is a milestone of progress (IMO, 2021). It not only sets a clear objective but also shows a sense of urgency.

1.1. Background and motivation

Ships are intricate machines that demand the expertise of a diverse group of engineers, crafting a vessel involves a blend of theoretical calculations and practical knowledge gathered from past projects. While ship design cannot be classified as a precise science, it requires a balance between various technical aspects, construction methods, and operational needs. As a result, the ultimate ship blueprint often reflects a compromise between competing requirements (A. F. Molland, 2008). This results in an integrated product architecture (Erikstad, 2019). Modularity then can be used to reduce the complexity and standardize the modules within a given system. An important driver for modular design is a reduction of lead time and resource expenditure in responding to tender invitations and future-proofing of designs.

The quest for emission reduction, the need for growth in local ferries and the need for short routes open the quest for lower emissions targeted at ferries with ships' speeds being lowered from 40 kn to 25 kn ((Transparency Market Research, 2023); Wärtsilä Internal). To achieve a significant reduction of emissions various alternatives need to be considered. This calls for a new development for the complete drive train of these vessels.

This thesis will focus on the application of waterjets in combination with hybrid solutions. Given the new lower speed range the waterjet application is being challenged by alternative propulsors such as surface piercing propellers, counter-rotating propellers, linear jets, and fast controllable pitch propellers. Moreover to achieve a significant emission reduction using state-of-the-art technologies today would require alternative fuels, batteries, and electric drive trains (Horton et al., 2022). The thesis is to develop a modular concept that combines the best technologies such that it considers the dependency of the operating profile, and that it fits well with the vessel types requirements. Additionally, this thesis aims to define modules of propulsion systems that can be combined for different applications and power

ranges fitting the type of vessels. The modularity aspect also has to encapsulate the evolving energy transition to future-proof the modular design. To combine all the different aspects that will be covered in this thesis the main research question will be: How can a propulsion system for mid-speed vessels be made modular and be made to lower or eliminate emissions? To support this main research question three extra sub-questions have been phrased.

- What propulsor would be best for mid-speed vessels regarding modularity and emissions?
- What propulsion architecture would facilitate modularity in design and emissions reduction?
- Which future technologies would be feasible and best suited for mid-speed vessels?

1.2. Reference vessel

For this thesis, the TrAM hull shape will be used as a reference vessel. The vessel is designed and established as a fast fully electric ferry and designed with modularity as a driver, this is a good starting point to create a framework for evaluating and designing modular vessels. This hull shape is not the latest hull shape of the TrAM project, but one of the first iterations of the year 2017, due to the availability of the model. The vessel is 31 m long and 9 m wide vessel with a depth of 1.262 m.

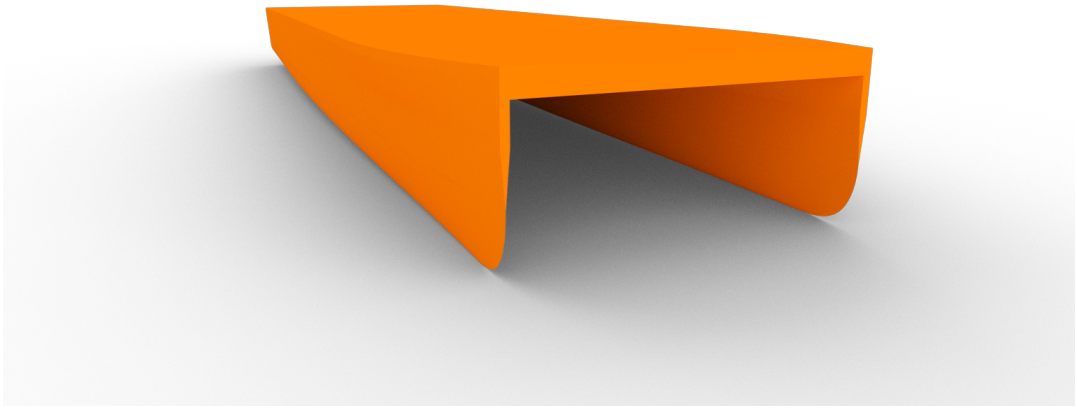

Figure 1.1: Reference vessel TrAM

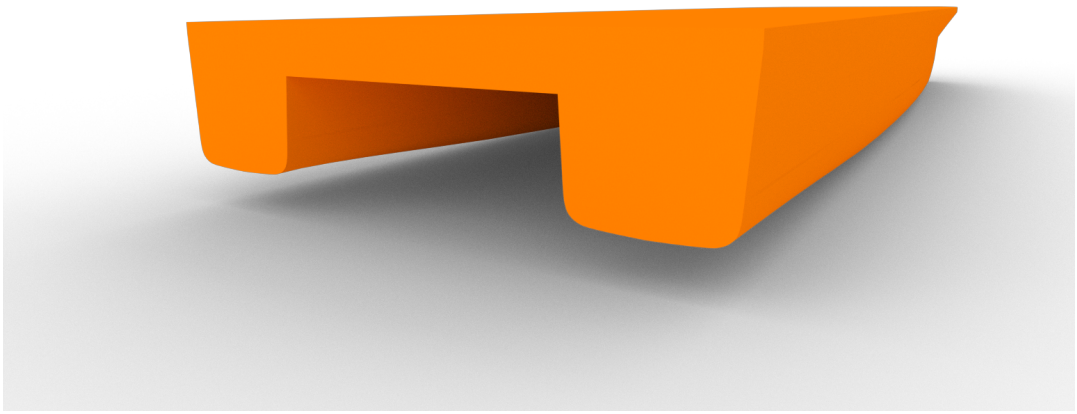

Figure 1.2: Reference vessel TrAM

The operational profile that will be used for this vessel is given in the following timeline (figure 1.3), which is based on the Tiger ferry operating in the Netherlands from Harlingen to Terschelling. The Tiger is a 50 m vessel, the estimated power requirement in figure 1.3 will not be representative due to the size difference. Where the manoeuvring will be described as a crabbing and turning manoeuvre, the transit sailing will be done at 25 knots over a distance of 22 nautical miles. Lastly, the port time will be 30 minutes, where only a hotel load is required for the vessel. This is represented in figure 1.3 which estimates the power required. An additional requirement states that all the power required, either mechanical or electrical, has to come from the vessel's onboard power supply. The standard for these types of vessels are mechanically driven propulsors with a diesel engine and a gearbox. The reference vessel's propulsion system will be taken as a directly driven propulsor via a gearbox, with a diesel generator set for the electrical power generation.

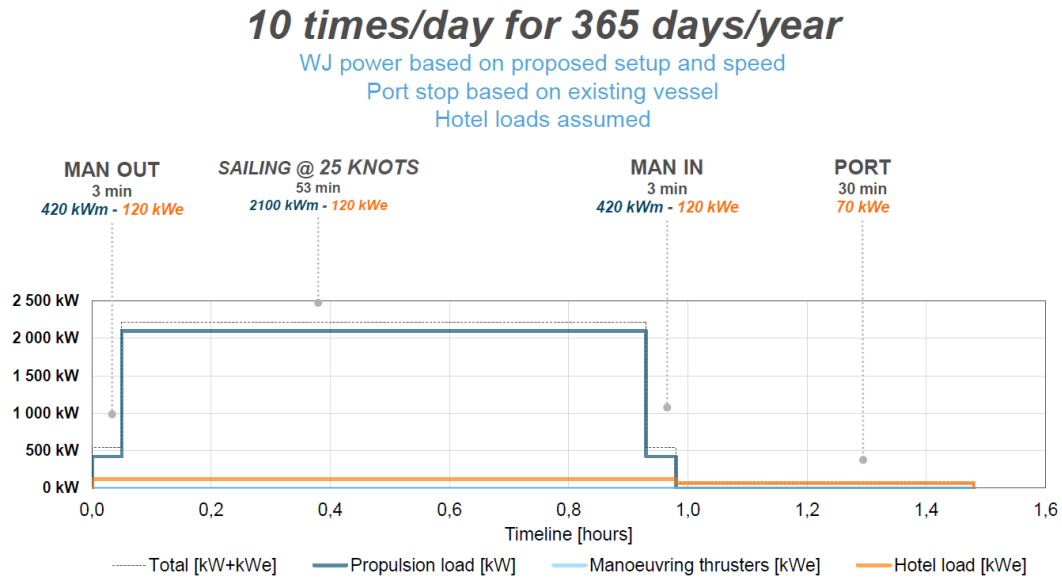

Figure 1.3: Operational Profile (Wärtsilä internal)

1.3. Methodology

To answer the research questions a framework will be created to evaluate and create propulsion systems based on performance indicators. A reference vessel has been introduced in section 1.2. This will be evaluated on the basis of the performance indicators. Based on this vessel, alternative concept propulsion designs will be created to achieve the goal of an increase in modularity and a decrease in emissions. Based on the performance indicators a decision on the feasibility of the propulsion system will be made. The feasibility study will be done on the basis of weight, volume and LCC. When comparing the current and newly generated systems the main drivers will be emissions and modularity. The model created to evaluate efficiency, fuel consumption and emissions will be used here. The emissions will be evaluated on the basis of Well-to-Wake (WtW), which can be directly compared via the CO_2 equivalent measure. This is done since the distinction between different types of alternative fuels can be made in the production process. After the comparison between the different systems, a conclusion can be drawn on the improvements made on the basis of modularity and emission reduction.

This report is structured in the following manner. First, the literature review of modularity, propulsion systems and performance indicators is given in chapter 2. Secondly, in chapter 3 the method of generating the model to calculate the power requirements and energy expenditure is described. Next the results of the model and the reference vessel are given in chapter 4, where the conclusion is drawn for the selection of the propulsor. In chapter 5 the concept design generation process of the modular propulsion system is given including the way of representing the model for modularity analyses. The results are given and compared of the concept designs in chapter 6. Lastly, in chapter 7 the discussion and recommendations are given and in chapter 8 the conclusion is drawn.

2

Literature Review

In this chapter, the literature review regarding the mid-speed vessel's propulsion system and modularity will be described. Firstly, the definition of modularity will be discussed and how to quantify modularity. Next, the propulsion system architecture will be discussed. Subsequently, current energy conversion, storage and future solutions will be discussed. Followed by the different types of propulsors. Lastly, the different performance indicators, that will be used to evaluate different propulsion systems will be explained.

2.1. Modularity

Modularity in ship propulsion design has gained significant attention in recent research. This section aims to provide a comprehensive review of the existing literature on the inclusion of modularity in ship propulsion design, focusing on the definition of modularity, quantification methods, and the application of the Design Structure Matrix (DSM) in assessing modularity. The ultimate goal is to establish a framework for evaluating and improving modularity in ship propulsion systems.

The definition of modularity in design has been explored from various perspectives. Hölttä-Otto and de Weck (2007) describe modularity as using the same module in multiple products, enabling a wide variety of products without altering the overall product or platform. The advantages of modularity include managing complexity, organizing parallel work, and facilitating changes and improvements to individual modules over time (Baldwin & Clark, 2006). In the context of ship design, Erikstad (2019) defines modularity as decisions made during the ship's design stage to decompose and encapsulate ship system elements, leading to improved design and manufacturing efficiency, as well as enhanced ship operational performance.

Different types of modularity have been identified, although their applicability to ship propulsion design varies. While Salvador et al. (2002) outline four different types of modular systems in their research, it is important to note that not all types are equally applicable to the design of a propulsion system due to the interrelations between different functions and systems (Hans Klein Wout & Douwe Stapersma, 2002).

Quantifying modularity is a crucial aspect of assessing and improving ship propulsion design. Various modularity indices have been developed, many of which are based on the Design Structure Matrix (DSM) (Eppinger & Browning, 2012). The DSM serves as a network modelling tool, representing the components and their interactions within a system. The DSM modularity metrics are well defined for product design, but for conceptual system design the quantification is complex due to the lack of detail within modules, but the application of DSM in ship propulsion system analysis provides valuable insights into the decomposition and assessment of modularity. As proposed by Eppinger and Browning (2012), the Product Architecture DSM model is suitable for ship propulsion systems, as it focuses on components working together to perform their functions, which can give valuable insight in the decomposition of the ship's propulsion system. To assist the decomposition, Lagemann et al. (2021) has proposed a method of decomposing the ship's requirements to functions to actual modules, which can give a framework for developing a modular architecture.

In conclusion, modularity is a significant consideration in ship propulsion design, emphasizing its potential to improve design and manufacturing efficiency and operational performance. It highlights the need to define and quantify modularity, with a focus on the use of the Design Structure Matrix (DSM) as a valuable tool. Not all types of modularity are equally applicable in ship propulsion design due to the complex interrelations between functions and systems. Overall, the goal is to establish a framework for evaluating and enhancing modularity in ship propulsion systems to address these challenges effectively.

2.2. Propulsion System

The propulsion system of a ship plays a crucial role in its operation, enabling the vessel to move efficiently through the water. The main functions of a ship's propulsion system are energy storage, energy conversion, and propulsion. Energy conversion involves transforming chemical energy into rotational or electrical energy, which is then used to generate thrust. Energy storage is necessary to ensure a continuous power supply for propulsion and other onboard systems.

Section 2.3 examines the current and future solutions for energy conversion and storage in marine applications. It explores various methods of energy conversion, such as internal combustion engines (ICE), gas turbines (GT), and fuel cells (FC), considering their efficiency, emissions, and applicability to the maritime industry. Additionally, it delves into the different types of energy storage systems used in ships, including chemical, electrical, and kinetic storage. The evaluation of alternative fuels and advancements in battery technology are discussed, highlighting their potential to reduce greenhouse gas emissions and improve overall system efficiency.

Moving on to section 2.4, which investigates various options for vessel propulsion, considering their characteristics and applications. The propulsor types discussed include sub-cavitating propellers (such as fixed-pitch and controllable-pitch propellers), super-cavitating propellers, and pumpjets. The objective is to determine the most suitable propulsor type based on the vessel type and operational requirements. The evaluation considers studies that examine the performance of different propulsors under varying conditions, taking into account their strengths and limitations.

2.3. Energy Conversion and Storage

The conversion of fuel to thrust in ship propulsion systems requires the transformation of chemical energy to rotational or electrical energy. This section examines the current and future solutions for energy conversion and storage in marine applications, with a focus on propulsion systems. The goal is to evaluate different energy conversion methods and identify their applicability to this thesis.

2.3.1. Energy Conversion

The primary method of energy conversion in current propulsion systems is the internal combustion engine (ICE) fueled by fossil fuels (Stapersma, 2010a; Xing et al., 2021a). However, the production of greenhouse gases (GHG) associated with these fuels necessitates the exploration of alternative energy conversion methods to reduce emissions in line with the International Maritime Organization's (IMO) goal of cutting GHG by 50% in 2050 (IMO, 2021). One option to achieve emission reduction with ICE is the use of end-of-pipe solutions such as scrubbers and carbon capture systems. Scrubbers are already installed and proven to reduce sulfur oxides onboard, carbon capture systems however still have a long way to go to become practical onboard (H. Wang et al., 2017). Another approach is the utilization of alternative fuels, which will be discussed in Section 2.3.2. However, the high specific fuel consumption and lower efficiency of ICE make emissions reduction challenging without alternative fuels (Bae & Kim, 2017; Gohary & Seddiek, 2013; Shadidi et al., 2021). Gas turbines (GT) are another method of converting chemical energy to rotational energy, primarily suitable for high power density applications (Stapersma, 2010a). However, GTs have lower efficiency and specific fuel consumption compared to ICE. Due to their high specific fuel consumption and limited application in mid-speed vessels, GTs are not considered as prime movers in this thesis but may be relevant in hybrid systems for waste heat recovery (Bae & Kim, 2017; Shadidi et al., 2021). Fuel cells (FC) provide a relatively new technology for energy conversion, directly converting chemically stored fuel to electric energy through a redox reaction.

FCs offer several advantages, including high efficiency, low emissions, low noise and vibration levels, and high reliability (Luckose et al., 2009). Different types of FCs, such as Alkaline Fuel Cells (AFC), Proton Exchange Membrane Fuel Cell (PEMFC), High Temperature Proton Exchange Membrane Fuel Cell (HT-PEMFC), Phosphoric Acid Fuel Cell (PAFC), Direct Methanol Fuel Cell (DMFC), Molten Core Fuel Cell (MCFC), and Solid Oxide Fuel Cell (SOFC), exhibit varying characteristics in terms of fuel type, efficiency, power capacity, and operating temperature (see Table 2.1) (Xing et al., 2021b). While the technical feasibility of different types of FCs is established, their economic feasibility in the marine industry is a consideration. The suitability of specific FC types for marine purposes depends on various factors, and the application of FCs in ships requires coordination of multiple systems and compliance with relevant laws and standards (X. Wang et al., 2023). PEMFC will be best suited for the application of a ferry due to the fast start-up and shutdown time together with the high efficiency.

Type of FC	Fuel type	Efficiency	Power capacity	Operating temperature
AFC	H_2	50-60%	$\leq 500kW$	60-200 °C
PEMFC	H_2	50-60%	$\leq 120kW$	65-85 °C
HT-PEMFC	H_2	50-60%	-	160-220 °C
PAFC	H_2, LNG and methanol	40-55%	100-400kW	140-200 °C
DMFC	methanol	20-30%	$\leq 5kW$	75-120 °C
MCFC	H_2, methanol and hydrocarbons	50-55%	120kW - 10MW	650-700 °C
SOFC	H_2, methanol and hydrocarbons	50-60%	$\leq 10MW$	500-1000 °C

Table 2.1: Fuel cell characteristics (Xing et al., 2021a)

2.3.2. Energy Storage

Energy storage in ships can be classified into three categories: chemical, electrical, and kinetic. Chemical energy storage traditionally involves the use of conventional marine fuels, such as residual oils and diesel fuels. However, the emissions associated with these fuels necessitate the exploration of alternative fuels to reduce GHG emissions (Xing et al., 2021a). Alternative fuels, including renewable methanol (MeOH), ammonia, hydrogen, Renewable Natural Gas (RNG), bioethanol, BioDME (Di-Methyl Ether), and biodiesels, have been assessed and ranked based on technical availability, safety, infrastructure, fuel supply, investment and operational costs, climate change impact, and air pollution (see Figure 2.1) (Xing et al., 2021a). Electrical energy storage systems, such as batteries, have gained significant attention in recent years due to advancements in technology and decreasing costs. Lithium-ion batteries are the most common type of batteries used in marine applications due to their high energy density, long cycle life, and relatively low self-discharge rates. They are suitable for applications that require high power and energy density, such as hybrid propulsion systems and peak shaving (Bae & Kim, 2017; Inal, Charpentier, et al., 2021; Shadidi et al., 2021). Other types of batteries, such as solid-state batteries and flow batteries, are also being explored for marine applications. Solid-state batteries offer advantages such as improved safety, higher energy density, and faster charging rates compared to lithium-ion batteries, but they are still in the early stages of development and commercialization (Sun, 2020). Kinetic energy storage systems, such as flywheels, store energy in the form of rotational motion. They have high power density and can provide short-duration, high-power bursts, making them suitable for applications that require frequent load levelling and transient response, such as dynamic positioning systems and manoeuvring (Bae & Kim, 2017; Shadidi et al., 2021).

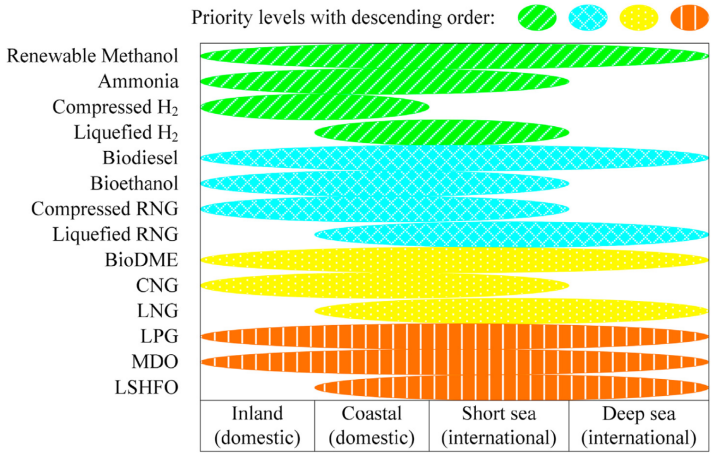

Figure 2.1: Priority levels and potential application of alternative fuels (Xing et al., 2021a)

In addition to standalone energy storage systems, hybrid energy systems that combine multiple energy storage technologies are also being explored. These systems aim to optimize energy utilization, improve overall system efficiency, and reduce emissions. For example, hybrid systems can combine batteries and fuel cells to provide a continuous power supply while maximizing the benefits of both technologies (Bae & Kim, 2017; Shadidi et al., 2021). It's worth noting that the selection of an appropriate energy conversion and storage system for a specific marine application depends on various factors, including power and energy requirements, vessel size and type, operational profiles, available space, cost considerations, and regulatory requirements. A comprehensive evaluation is necessary to identify the most suitable solution for a given scenario.

In conclusion, while ICE fueled by conventional marine fuels are currently the dominant method of energy conversion in marine propulsion systems, there is a growing need to explore alternative energy conversion methods to reduce greenhouse gas emissions. Fuel cells and advanced internal combustion engines are among the technologies being considered. Energy storage systems, including batteries, flywheels, and capacitors, are also gaining prominence, offering the potential to improve efficiency, reduce emissions, and enable hybrid propulsion systems. The selection of appropriate energy conversion and storage solutions depends on various factors and requires careful consideration of technical, economic, and regulatory aspects.

2.4. Propulsors

In this section, the focus is on discussing various options for vessel propulsion, their characteristics, and applications. The chapter aims to answer the question: "Which propulsor type can be applied for the chosen vessel type and operation profile?" Several propulsors commonly used in the marine industry are examined. These include:

- Sub-cavitating propellers (also called conventional propellers)
  - Fixed pitch propellers (FPP)
  - Controllable pitch propellers (CPP)
  - Cycloidal propellers
- Super cavitating propellers
  - Fully submerged
  - Surface piercing
- Pumpjet
  - Linear pumpjet
  - Waterjet
  - Centrifugal pumpjet

To determine the most suitable propulsor type for a given vessel type and operation profile, a comparison is made among the available options. One propulsor, the PJM (Pump Jet Module), can be ruled out unless a very shallow draft application is required, as its efficiency peaks before reaching the design speed of 25 knots. The remaining options are the sub and super cavitating propellers, the linear pumpjet, and the waterjet. The linear pump jet has to be split into two options one with an accelerating nozzle and one with a decellerating one. In Morrison (2018) it is stated that the decelerating nozzle is beneficial for military applications due to the good cavitation performance, not efficiency so that will be excluded in this thesis.Zhou et al. (2022) states that the design of a linear jet is complex due to the interaction between the stator, rotor and duct. For this propulsor, the consideration has to be made between modularity and efficiency, since it is possible to increase efficiency but it reduces modularity. When considering efficiency, a study by A. F. Molland et al. (2011) indicates that the sub-cavitating propeller outperforms the super cavitating propeller around the speed of 25 knots. Another study by Kamal et al. (2015) compares FPP and waterjet for mid-speed wave-piercing catamarans, concluding that the propeller-driven catamaran has higher overall propulsive and transport efficiency compared to the waterjet-driven catamaran. However, it's worth noting that the tested speed range in the study does not exactly match the application in this thesis. Comparing a pumpjet to a conventional waterjet, Giles et al. (2010) conducted a study on a 41m test vessel for the US Navy, evaluating the efficiencies of an advanced submerged waterjet (AWJ), which resembles a pumpjet. The study shows that the AWJ performs relatively lower in terms of required power at lower speeds (18% more power required at 10 knots) but closes the efficiency gap as the speed increases towards 30 knots. The efficiency difference at the design speed in this thesis is only 5%, but the low efficiency at manoeuvring speed might make it an unsuitable option for ferry operations that involve frequent port stops. Morrison (2018) also highlight that the efficiency of pumpjets decreases as the vessel speed approaches zero, which can be disadvantageous for ferry operations that often involve low-speed manoeuvres. Regarding the sub-cavitating propellers, the cycloidal propeller is not considered due to its higher complexity and lower efficiency, as mentioned in A. F. Molland et al. (2011). Therefore, the propulsors taken into account for evaluating the propulsion system's efficiency are FPP, waterjet, and linear pumpjet (with an accelerating duct). The CPP is excluded due to the basis of the calculation where axial impulse balance is used, which excludes the pitch of the propeller.

2.5. Performance Indicators

This section focuses on the performance indicators for evaluating different propulsion systems. de Vos (2018) mentioned that main drivers for energy distribution systems are operational feasibility and performance, costs, weight and space requirements, safety considerations and operability. For this thesis the focus will not be on safety and operability but on feasibility, costs, weight and space requirements. In addition to these drivers, the driver of modularity and emissions are added. To evaluate the propulsion systems qualitatively, these drivers are translated to performance indicators. The indicators are weight, volume, Life Cycle Costing (LCC), emissions, and modularity. From the performance indicators identified, modularity is the one that will be difficult to directly measure. In the first instance, modularity indexes will be the solution. The issue is the level of detail required as mentioned in 2.1. Modularity will not only be evaluated on the number of connections, but the architecture used and the distribution of the connections within the DSM will be taken into account when comparing propulsion solutions to one other. The performance indicators of weight and volume will be evaluated via parameters found in the literature or data analysis that link the weight and volume to a specific characteristic of the component, e.g. power of an internal combustion engine. For LCC the NPV calculation will be used based on parameters from literature and data analysis as well. Emission comparison will be done based on the carbon dioxide equivalent parameter that directly links the amount of fuel (alternative fuels included) to an amount of carbon dioxide equivalent in grams.

3

Model

3.1. Introduction

In this chapter, the model for the calculation of the power requirement will be described. The model for power requirement will result in an energy expenditure per trip and subsequently emission levels. This will be then the input for the design and sizing of the new modular concepts. The model requires a resistance curve and an operational profile as input. Firstly, the resistance calculation based on regression analysis will be discussed. Secondly, the operational profile will be defined in three different stages. Lastly, the efficiency calculation for the propulsor and energy converter will be explained. The result of the model will be a comparison of the reference vessel's propulsion system with the different propulsors named in section 2.4. The model then can be altered to calculate the emissions of the concept designs that will be created in chapter 5.

To start the model the reference case of the propulsion system has to be determined. In the case of the reference vessel, the propulsion system is a direct-driven waterjet via a diesel engine with a gearbox. To model the modules, the operational profile has to be further determined. Furthermore, the reference case hull shape is not optimized for propeller propulsion, but for waterjets. So an alteration has to be made to the hull shape to facilitate a propeller. Lastly, the resistance curve and the propulsor hull interaction have to be determined as an input for the model.

3.2. System description

The propulsion system consists of multiple components. To achieve the goal of power and energy requirement calculation the efficiency of the components needs to be determined. Two propulsive architectures will be given that describe the components required to create the different direct and hybrid propulsion architectures. In figure 3.1 the energy flow diagram of the direct drive architecture is given. This architecture will be taken as the reference architecture installed in the reference vessel. The efficiencies in the figure are given in Tupper (2013) and Hans Klein Wout and Douwe Stapersma (2002). In the following sections, the variable efficiencies will be determined. In figure 3.1, the second line represents the electrical architecture or serial hybrid architecture, which differs from the direct drive after the gearbox. These efficiencies are determined by a digital twin model of a battery-driven vessel via Wärtsilä. The battery in the flow diagram could be exchanged by an electrical generator (efficiency modelled as electric motor) combined with an ICE or a fuel cell, which has variable efficiency dependent on load as well.

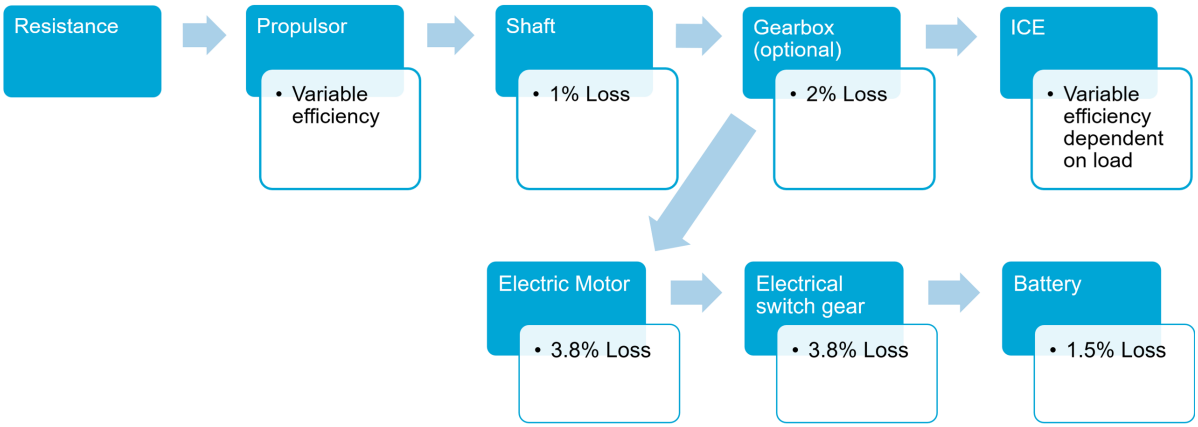

Figure 3.1: Flow diagram including efficiencies of components direct drive architecture

3.3. Operational profile

The operational profile will consist of three different manoeuvres. The manoeuvres will be crabbing to move away from the dock, then a turning manoeuvre to head in the correct direction, transit sailing at 25 kn and lastly, a crabbing manoeuvre to dock the vessel. The transit sailing condition will be evaluated based on resistance data. The crabbing manoeuvre will be evaluated via the transverse force balance. In Brix (1993) the forces acting on the vessel are stated as the hydrodynamic and the wind forces. Formula 3.3 will be used to evaluate the force acting on the vessel during the crabbing manoeuvre, where Y is the resulting lateral force acting on the vessel, which is constructed from the hydrodynamic force Y" and the wind force Y_w In this case, the wind resistance will not be taken into account.

$$Y" = C_y"(\beta) \cdot \rho \cdot \frac{V_s^2}{2} \cdot L_{pp} \cdot T \tag{3.1}$$

$$Y_w = C_{yw}(\epsilon) \cdot \frac{V_w^2}{2} \cdot \rho_w \cdot A_{lat} \tag{3.2}$$

$$Y = Y" + Y_w \tag{3.3}$$

- $C_y"(\beta)$ - Lateral resistance coefficient dependant of drift angle
- $C_{yw}(\epsilon)$ - Wind resistance coefficient dependant of wind angle
- ρ - Density of medium (water or air)
- V_s - Ship speed
- V_w - Wind speed
- L_{pp} - Length between perpendicular
- T - Depth of the vessel
- A_{lat} - Lateral area of the vessel above waterline

The transverse force on the crabbing manoeuvre will be delivered by the two waterjet thrusters. The reference vessel does not have a bow thruster to compensate for the yaw moment so the thrust force has to cross the lateral underwater area center. For a vessel with propellers and rudders, the yaw moment generated has to be compensated, where a bow thruster is required.

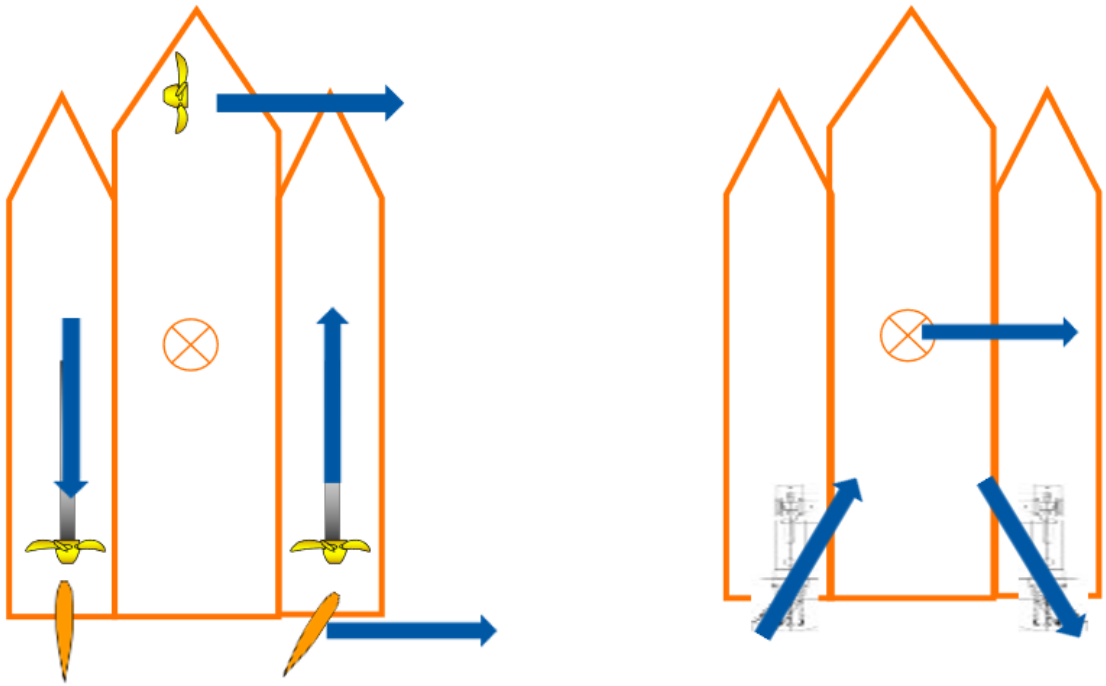

Figure 3.2: Crabbing lateral force generation

The turning moment that has to be overwon to turn the vessel is also described by Brix (1993), where it is mentioned as the hydrodynamic damping moment. This can be calculated by the rotational speed that is required. Described in Brix (1993) turning speed ($\dot{\psi}$) is given by formula 3.4 dependant on the thruster force (Y_0), which is defined by the turning moment divided by the length of the vessel, and overall vessel dimensions. In this formula the corresponding value of k = 160°.

$$\dot{\psi} = k \cdot \sqrt{\frac{Y_0}{\rho \cdot L_{pp}^3 \cdot T}} \tag{3.4}$$

When evaluating the power required for these manoeuvres, the turning speed and crabbing velocity need to be set which will result in the required thrust per thruster which results in the power per thruster. In this reference case, a crabbing speed of 0.3 m/s is chosen and a turning rate of 0.1 rad/sec.

3.4. Ship resistance moddeling

The original hull shape was made for waterjets. To facilitate a propeller, an additional boundary condition has been stated, the propeller cannot be lower than the baseline of the vessel. To facilitate a propeller of decent size for acceptable propulsive performance the distance between the transom and the baseline of the vessel needs to be increased. This does have an impact on the resistance of the vessel. Mainly on the transom resistance since that part of the vessel will be adjusted. The analytical analysis of the resistance of a catamaran is described in Geurts (2009). The resistance is divided into the following components represented in figure 3.3.

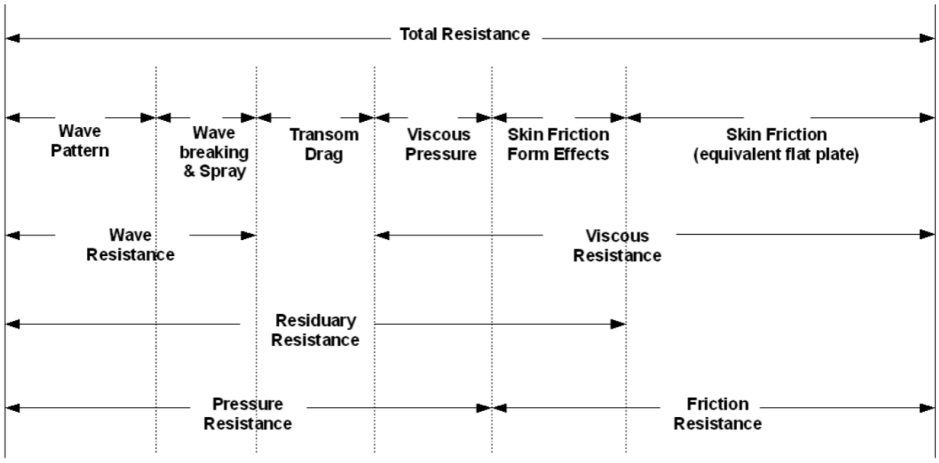

Figure 3.3: Hull resistance decomposition

To estimate the resistance of the vessel the NPL-Molland (A. Molland et al., 1994) regression for the residual resistance is used. In Geurts (2009) multiple regression models for estimating resistance are mentioned. The NPL-Molland regression is chosen since the reference vessel is outside the perimeters of the Sahoo 2004 regression, outside the speed range of the Sahoo 2002 regression, and the Müller-Graf regression is made for planing vessels so it will overestimate the resistance of the semi-planing speed range. The following hull shape was used for the regression, although the shape does not accurately represent the TrAM hull, the parameters correspond with the given parameter range from the regression.

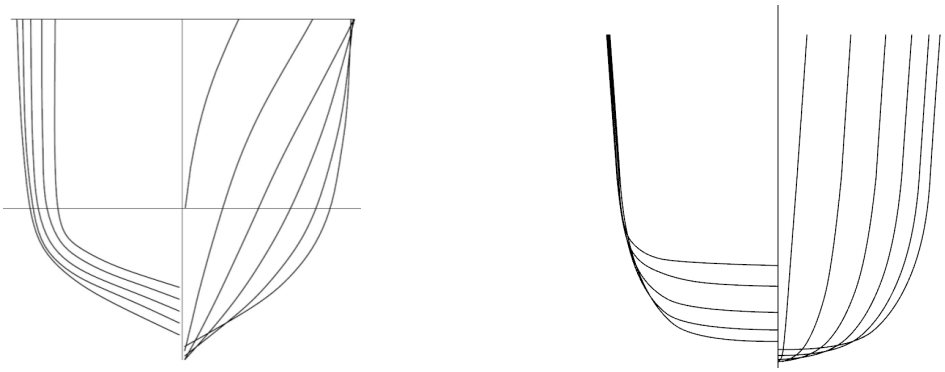

(a) NPL hull form **(b)** TrAM base hull

Figure 3.4: Hull shape comparison

The resistance is calculated via the way of residuary resistance and frictional resistance (figure 3.3). The residuary resistance is calculated via a regression formula obtained via towing tank tests varying different aspects of the catamaran hull form. The coefficients are given in appendix B. The result is a residual resistant coefficient (C_R) which can be used to calculate the actual coefficient via formula 3.6. A note has to be made that some coefficients are based on one demi-hull. This is due to the method of testing used to obtain the regression, where one demi-hull is tested alongside a wall of the tank.

$$C_R = \left(a_1 + a_2 \cdot \frac{LCB}{L_{WL}} + a_3 \cdot \frac{B}{L_{WL}} + a_4 \cdot \frac{B}{T} + a_5 \cdot \frac{s}{L_{WL}}\right) \cdot \frac{\nabla^{\frac{1}{3}}}{L_{WL}} \tag{3.5}$$

- LCB - Length position of buoyancy point
- L_{wl} - Length of waterline
- B - Width of the vessel
- s - Separation distance of the demi-hulls

- ∇ - Water displacement of one demi-hull

$$R = \frac{1}{2} \cdot \rho \cdot g \cdot C_R \cdot S \cdot V_s^2 \tag{3.6}$$

- g - Gravitational acceleration
- S - Wet surface area demi-hull

The frictional resistance coefficient is calculated via the ITTC'57 equation also given in Geurts (2009). This can also be used to calculate the actual frictional resistance using formula 3.6 with the resistance coefficient from formula 3.7.

$$C_{f0} = \frac{0.075}{(\log_{10}(Re) - 2)^2} \tag{3.7}$$

Additionally, the appendage resistance has to be included in the total resistance. In Geurts (2009) a method of skin friction resistance including a form factor for specific appendage drag is given. The appendage form factors can be found in appendix B. Formula 3.8 is used for the appendage resistance. To evaluate the appendages present the assumption has been made that the rudder size is 1.4-1.7 % of $L_{WL} \cdot T$ (Müller-Graf et al., 1989), the bracket size has been estimated via the contour of the TrAM project presented in Strobel et al. (2020). For the rudder shape the NACA 0015 has been chosen since it has been mentioned in Liu and Hekkenberg (2017) that is most widely used shape for the rudder. The duct shape of the 19A duct is used to estimate the wet surface area of the duct. Visualization of this is given in appendix A.

$$R_{AP} = \frac{1}{2} \cdot \rho \cdot V_s^2 \cdot S_{AP} \cdot (1 + k_2)_{eq} \cdot C_{f0} \tag{3.8}$$

- S_{AP} - Appendage wet surface area
- $(1 + k_2)_{eq}$ - Appendage form factor

Furthermore, the shape of the vessel's transom will be adjusted to provide a propeller and a larger waterjet. This will have an impact on the resistance of the transom. To take this into account, the transom resistance will be calculated separately. As can be seen in figure 3.3 the transom resistance is included in the residual resistance. To include the transom resistance in more detail a method of calculating it individually is introduced by Doctors et al. (2007). This method is based on regression data that describes the transom ventilation of the vessel. This regression is based on the Froude number based on the transom depth (Fr_T), the breadth over depth ratio of the transom (B/T) and the transom Reynolds number (Re_{NT}). Doctors et al. (2007) has given multiple regressions based on different sensors and variables. Doctors et al. (2007) concludes that the transom Reynolds number has little to no effect on the ventilation so that part will be neglected. Formula 3.9 results in the transom ventilation ratio which is described by equation 3.10. It has to be noted that the vessel's transom can be clear of water at some stage in the speed range. This results in a lower wetted surface area. This has an effect on the skin friction of the vessel so should not be neglected.

$$\eta_{dry} = C1 \cdot Fr_T^{C2} \cdot \left(\frac{B}{T}\right)^{C3} \cdot Re_{NT}^{C4} \tag{3.9}$$

$$\eta_{dry} = 1 - \frac{S_{TR,dyn}}{S_{TR,static}} \tag{3.10}$$

To calculate the transom resistance, equation 3.11 is given by Doctors et al. (2007). The definitions of the variables are defined in figure 3.5. In

$$R_{TR} = \rho g \int_{-T^*}^{\zeta^*} b(x^*, z)(z - \zeta^*) dz \tag{3.11}$$

- T^* - Dynamic draft at the transom
- ζ^* - Elevation of the stagnant water in the hollow immediately behind the transom

- $b(x^*, z)$ - Local beam at x^*

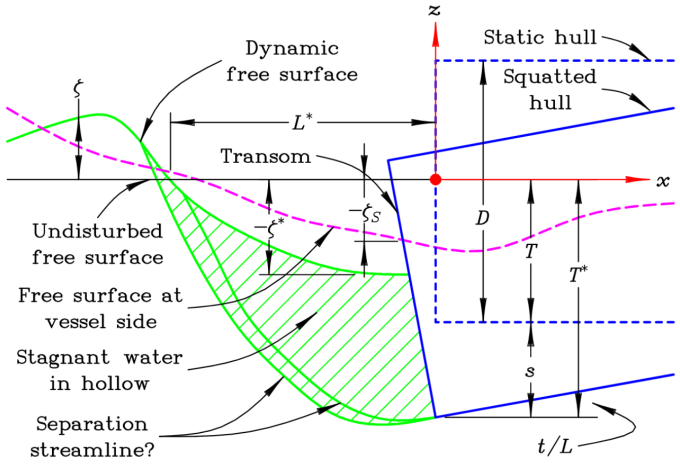

Figure 3.5: Variables in stern ventilation and transom resistance calculation (Doctors et al., 2007)

To obtain the correct variables the shape of the transom has to be known to calculate ζ^* via the definition of η_{dry}, in combination with the pitch to get the sinkage of the vessel which is indicated by s in figure 3.5. The pitch angle can be determined by the regression also described by the NPL-Molland regression given by Geurts (2009). To calculate the trim angle, equation 3.12 is used with the regression coefficients given in appendix B.

$$\tau = \left(a_1 + a_2 \cdot \frac{LCB}{L_{WL}} + a_3 \cdot \frac{B}{L_{WL}} + a_4 \cdot \frac{B}{T} + a_5 \cdot \frac{s}{L_{WL}}\right) \cdot \frac{\nabla^{\frac{1}{3}}}{L_{WL}} \tag{3.12}$$

To result in the total resistance the residuary, skin friction and appendage resistance are added together. The same is done for the adapted hull shapes for the propeller and larger waterjet. Subsequently, the transom resistance calculated from the baseline vessel is subtracted from the adapted hull shapes' total resistance and the transom resistance calculated specifically for the adapted hull shapes is added. For the calculation of the vessel's resistance, the reference hull shape has the following values.

Constant	Value
L_{WL}	33.8 m
B	9.685 m
T	1.26 m
s	7.22 m
S	112.68 m^2
LCB	15.01 m

Table 3.1: Ship constants

To accommodate the propeller the aft buttock is lifted to create more space to the baseline of the vessel. The comparison between the two vessels can be seen in figure 3.6.

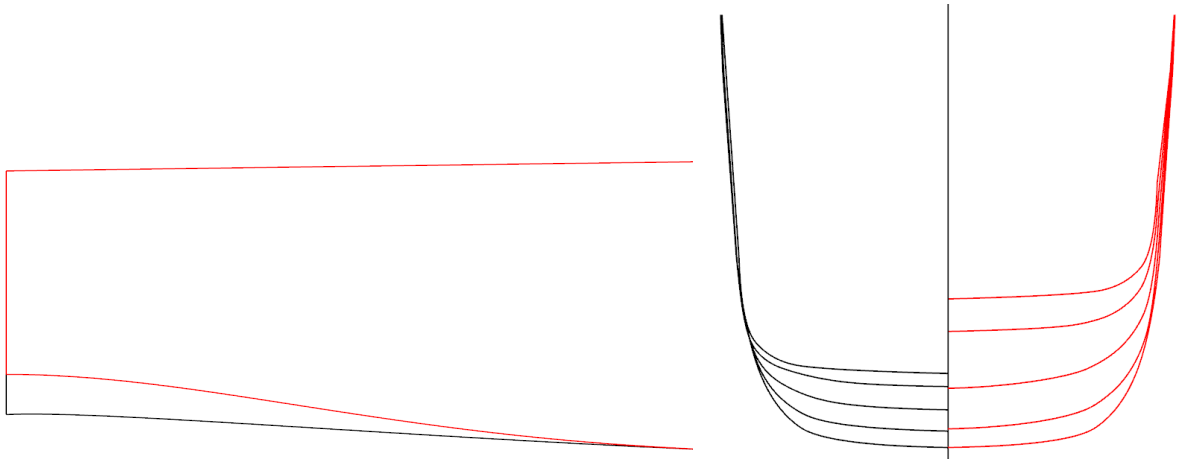

(a) Aft buttock shape propeller **(b)** Aft frame lines propeller

Figure 3.6: Aft hull shape comparison

To analyse the difference in resistance between the two different hull shapes the parameters that have changed have to be evaluated. The choice has been made to keep the displacement the same to evaluate both hulls. This means that the depth of the vessel will change including the wet surface area and the length centre of buoyancy position (LCB). Which will be the following values.

Constant	Value
T	1.32 m
LCB	15.65 m
S	113.12 m^2

Table 3.2: Adjusted parameters

To include a bigger waterjet than the vessel is designed for the transom area needs to be larger to accommodate the waterjet. The central axis of the pump needs to be below the waterline otherwise while starting the jet will run dry and can potentially damage the waterjet.

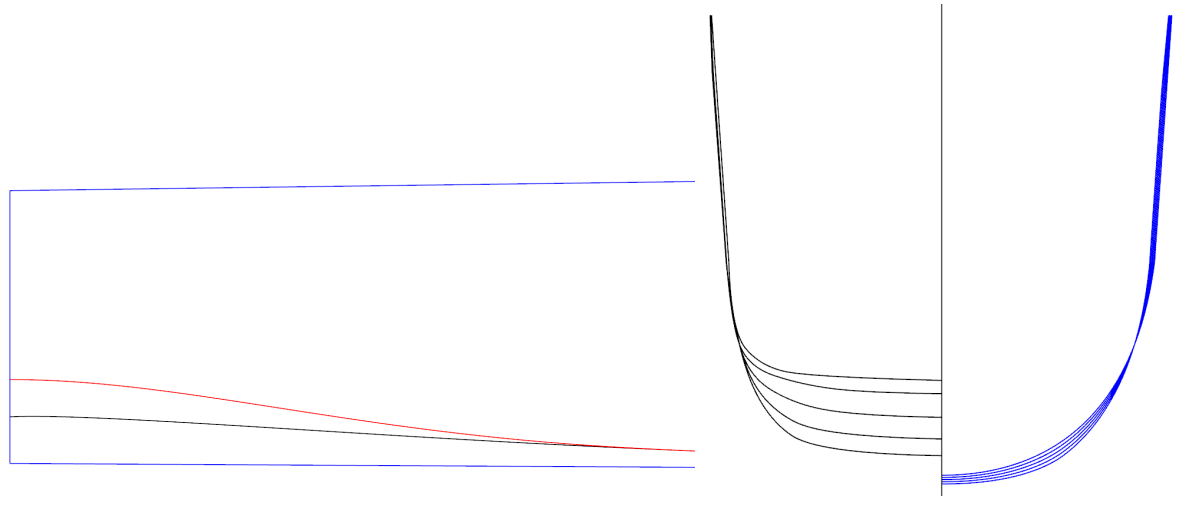

(a) Aft buttock shape waterjet **(b)** Aft frame lines waterjet

Figure 3.7: Aft hull shape comparison

Constant	Value
T	1.21 m
LCB	14.33 m
S	111.5 m^2

Table 3.3: Adjusted parameters for larger waterjet

To compare the three hulls the three resistance curves are plotted in one figure, including the points where the transom clears and the operating point of the reference vessel. By introducing the transom resistance separate from the residual resistance it can be seen that the transom resistance has a bigger role at lower speeds when the transom is not clear of water. In figure 3.8a it can be seen that the three hulls are similar when the transoms are all clear but will differ slightly more at higher speeds. This difference is presented in more detail in figure 3.8b. When an operational profile is defined in a different way where slower speeds are required this could have a large effect on the propulsor selection. Since the operational profile is defined as a steady-state operation the lower-speed region is not taken into account. The difference in resistance is so close that it could be taken as inaccuracy due to the regression models. So a propulsor selection sole based on the resistance should be treated carefully.

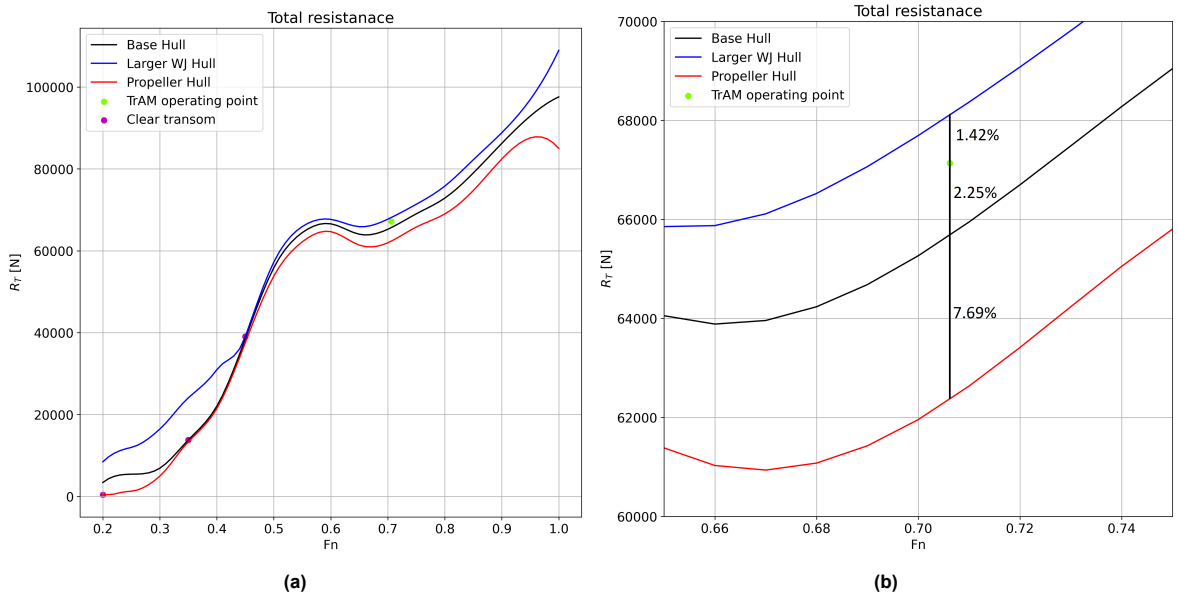

Figure 3.8: Total resistance curve three hulls

3.4.1. Hull propulsor interaction

The propulsor hull interaction factors have to be determined for both the waterjet and the open and ducted propeller. These factors will have an influence on the inflow velocity of the water to the propulsor and the interaction of the accelerated flow of water with the hull in the form of thrust deduction, which will directly influence the open water efficiency.

Waterjet

The wake fraction dependent on the Froude number for a flush intake waterjet is mentioned in Duerr and Von Ellenrieder (2015), where the dependency can be seen in figure 3.9. This value describes the deceleration of the inflow to the propulsor.

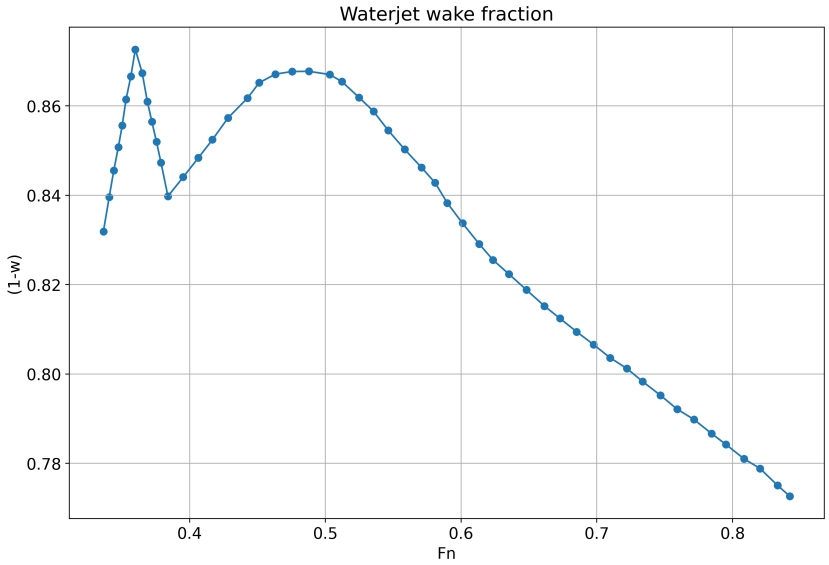

Figure 3.9: Wake fraction for flush intake waterjet Duerr and Von Ellenrieder (2015)

The thrust deduction factor has been investigated by Eslamdoost et al. (2018) as a dependency of the Froude number as well the results can be seen in figure 3.10.

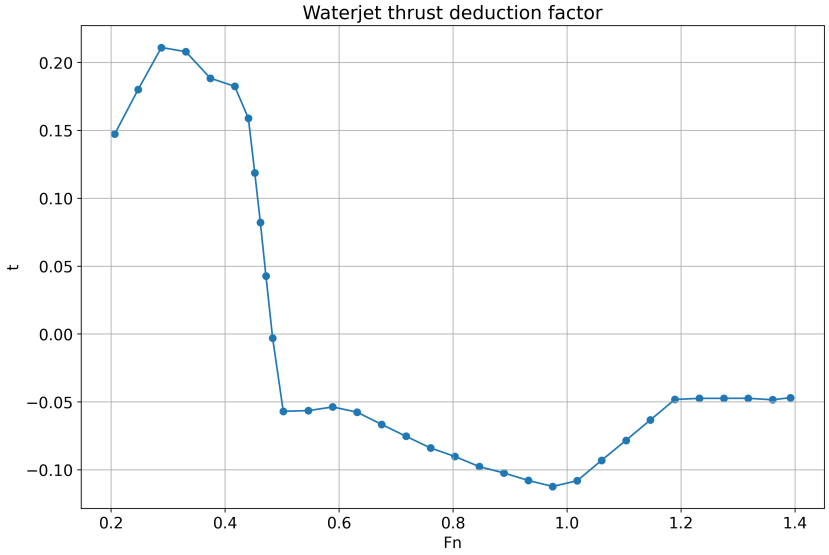

Figure 3.10: Thrust deduction factor for flush intake waterjet Eslamdoost et al. (2018)

The operating range for the vessel will be at Froude number of 0.706 which results in a wake fraction (w) of 0.195 and a thrust deduction factor (t) of -0.073.

Propeller

For the propeller hull interaction values the starting values are given by Papanikolaou et al. (2020), which are t = 0.045 and w = 0.029 which are values of the latest and actual hull design. The design of the TrAM project aft shape has a propeller tunnel and a low shaft angle, which can influence the thrust deduction value and wake fraction.

The propeller tunnel included in the vessel's hull lines has an impact on the form factor of the vessel. This results in a difference in the form factor of 1.080 with a tunnel to 1.101 without a tunnel. This is an increase of 2.1% that acts on the frictional resistance.

The shaft angle of the vessel has an impact on the propulsive factors as well. This has to do with the placement of the motor onboard the vessel. The first assumption for this will be that the same shaft angle (which is 5°) will be possible with the current vessel shape. If that is not the case this value can be adjusted in the manner that is presented in Müller-Graf et al. (1989). This can be done by the following formula, where ψ the shaft angle represents with respect to the baseline of the vessel. If a duct is added to the propeller for the ducted propulsor or the linear jet, the propulsive factors will not be influenced by this (Bhattacharyya & Steen, 2014). It has to be noted that the duct will increase the frictional resistance of the hull in the form of appendage resistance.

$$t = 1 - \frac{R_t}{T \cdot \cos\psi} \tag{3.13}$$

3.5. Waterjet

In the following section, the efficiency and rotational velocity of the waterjet will be determined and validated. The efficiency will be determined by adding loss components of the inlet, outlet and pump. These factors are given in figure 3.11 which gives a schematic representation of the waterjet propulsor.

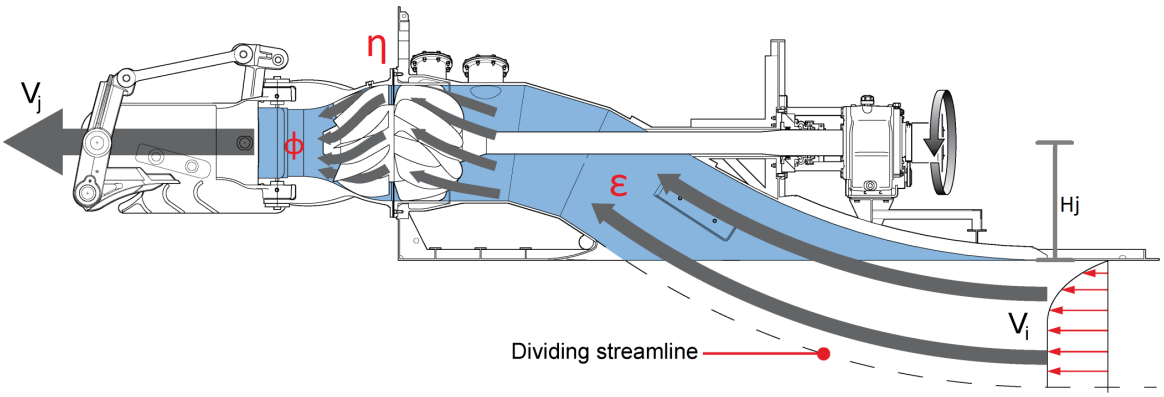

Figure 3.11: Waterjet variable definition for loss coefficients (“Waterjets Product Guide”, 2017)

The number of waterjets installed depends on the sizing of the waterjets and the power capabilities. In the product guide of the Wärtsila waterjets (“Waterjets Product Guide”, 2017) a method of selection of the jet diameter is given. For the base hull vessel, the smallest size of 510 is sufficient if 4 and 2 jets are selected since it is capable of handling 900 kW per jet.

3.5.1. Transit sailing

The waterjet can be modelled by first principle models based on the conservation of momentum and cavitation limits. This is well described by Bulten (2006). The waterjet open water efficiency can be determined by formula 3.14, where ϕ is the nozzle loss coefficient and ϵ is the inlet loss coefficient these are 0.02 and 0.2 respectively (van Terwisga, 1997). In formula 3.14, μ is defined as the ratio between the inflow and jet velocity ($\frac{V_i}{V_j}$).

$$\eta_{wj} = \eta_{pump} \cdot \frac{2\mu(1-\mu)}{(1+\phi) - \mu^2(1-\epsilon)} \tag{3.14}$$

In formula 3.14 the pump efficiency can be determined by an empirical formula. This has to be empirical due to the unknown shaft torque that is needed for the required flow rate since not a specific unit will be chosen for this application. The formula stated in Bulten (2006) is given in formula 3.15.

$$\eta_{pump} = 0.95 - \frac{0.05}{Q/Q_{ref}} - 0.125(log(n_\omega)) \tag{3.15}$$

This formula is dependent on the flow rate (Q) and the specific speed constant (n_ω). This value can be calculated with formula 3.16, where Ω (rotational speed) can be determined with cavitation limits as described in Verbeek (1992).

$$n_\omega = \frac{\Omega\sqrt{Q}}{(g \cdot H)^{\frac{3}{4}}} \tag{3.16}$$

With the required system head defined by.

$$H = \frac{V_j^2}{2g}(1+\phi) - \frac{V_i^2}{2g}(1-\epsilon) + h_j \tag{3.17}$$

- V_j - Jet velocity of the water
- V_i - Inflow velocity of the water
- h_j - Physical head of the waterjet

Verbeek (1992) describes a formula to determine the maximum rotational speed that can be achieved without cavitation. This can be calculated by formula 3.18. This will give a maximum rotational speed, which means that the rotational speed will differ depending on the waterjet's specific design for the required flow rate. In this formula N_{ss} is taken as 3.5 as a starting point since in Verbeek (1992) it is stated that for design purposes this value can be taken.

$$\Omega \leq N_{ss}(g \cdot NPSH_a)^{\frac{3}{4}} \cdot \sqrt{\frac{\rho V_i(1-\mu)}{T\mu}} \tag{3.18}$$

The evaluation of the waterjet power requirement starts with the definition of the thrust that has to be delivered per individual unit. This is defined by formula 3.19. The value for t which is the thrust deduction factor can be estimated based on the Froude number as can be seen in Eslamdoost et al. (2018) and given in section 3.4.1.

$$T = \frac{R_s}{(1-t)} \tag{3.19}$$

The required thrust can then be the input for the flow rate (Q) required to provide the thrust via formula 3.20. In this formula, the introduction of the different velocities that are present in the waterjet design are introduced. In this formula, there are two unknowns, the flow rate and the jet velocity which can be connected via the definition of the jet area, which is $Q = V_j \cdot A_j$.

$$T = \rho Q(V_j - V_i) \tag{3.20}$$

When the relation between the jet area and the flow rate is implemented in formula 3.20, the following formula has to be solved for the jet velocity to obtain the value for the required flow rate. In this instance, the jet area is also unknown. This value can be taken as a variable to be able to solve for maximum efficiency.

$$V_j - V_i V_j - \frac{T}{\rho A_j} = 0 \tag{3.21}$$

When the jet velocity is obtained the velocity ratio μ can be calculated and implemented in formula 3.14. In combination with 3.15 the open water efficiency for the water jet at a given speed can be calculated.

To validate this method a reference case was selected from the Wärtsilä portfolio. This case was the Tiger ferry operating between Harlingen and Terschelling. The operating point of the vessel was also 25 kn. This resulted in an efficiency that is 0.3% lower than the actual value. With an N_{ss} value of 3.5 which was recommended by Verbeek (1992), the jet rpm resulted in a lower value than the design value of the Tiger. When a value of 5 is used for the N_{ss} value the rpm results in 0.8% lower rpm. The change of the N_{ss} was suggested by Verbeek (1992). This proves that the method will result in an accurate estimation of the open water efficiency and the operating rotational velocity of the vessel.

3.5.2. Bollard pull for manoeuvring

For the bollard pull condition formula 3.14 for the efficiency can not be used due to the fact that the inflow velocity becomes zero, this will result in μ also being zero. So the power requirement has to be done in a separate way. In Denny and Feller (1979) the power requirement for the bollard pull condition of a waterjet is described. So via the thrust required to achieve the certain manoeuvre speed requirement and the flow rate identity, the required jet velocity is calculated which is given below.

$$T_B = \rho Q_B V_{jB} \tag{3.22}$$
$$Q_B = A_j V_{jB} \tag{3.23}$$
$$\tag{3.24}$$

To calculate the output power required, formula 3.25 is used.

$$P_{jB} = \frac{1}{2} T_B V_{jB} \tag{3.25}$$

This then can be related to the input power via data regression where the equation 3.26 hold true. in formula 3.26 the value for F is 1146.77 for SI unites. The resulting power is given in kW

$$T_B V_{jB} = F \cdot P^{1.0566} \tag{3.26}$$

3.6. Propeller

The following section will explain the method of calculating the efficiency of the propeller on the basis of impulse balance. This is done so that the method for the waterjet rests on the same principle for the propeller. This method is described in an internal document from Wärtsilä, so a shortened version will be represented here. For the definitions of the different velocities, figure 3.12 will give the definitions of the different locations of the velocity.

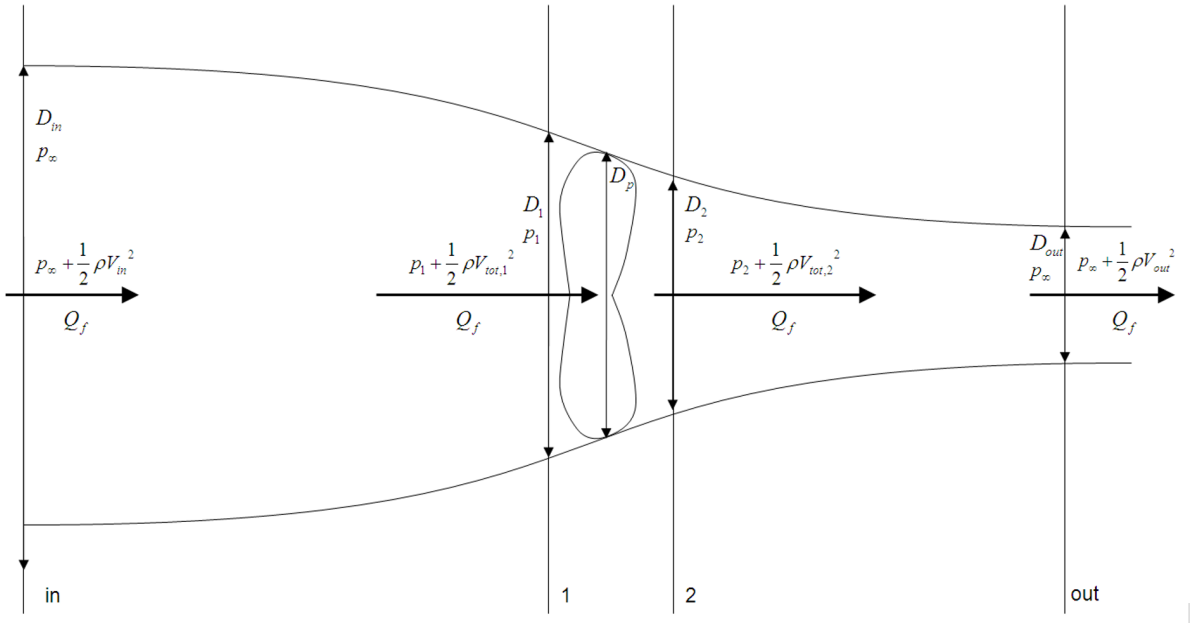

Figure 3.12: Velocity definitions of the open propeller calculations

3.6.1. Transit sailing

For the transit condition, the efficiency is determined by the ideal efficiency, which accounts for axial losses, and the effective efficiency, which describes the amount of energy used by the propeller so this includes frictional and rotational losses in the actuator disc. The open water efficiency is then defined

by formula 3.27. In the following logic, the jet efficiency is given by the ideal efficiency. This holds only for the open propeller, the jet velocity is defined differently for the ducted propeller.

$$\eta_{ow} = \eta_{jet} \cdot \eta_{effective} = \frac{R_{ship} V_{ship}}{P_{ow}} \tag{3.27}$$

$$\eta_j = \eta_i = \frac{2}{1 + \sqrt{1 + C_T}} \tag{3.28}$$

$$C_T = \frac{T}{\frac{1}{2}\rho V_i^2 A_p} \tag{3.29}$$

$$\tag{3.30}$$

In formula 3.27, $\eta_{effective}$ is defined as follows.

$$\eta_{effective} = \frac{\frac{1}{2}\rho(V_{ax,j}^2 - V_{ax,i}^2)Q_f}{2\pi n Q} = \frac{\frac{1}{2}\rho(V_{ax,j}^2 - V_{ax,i}^2)Q_f}{P_{ow}} \tag{3.31}$$

This is thus the effective energy used by the propeller to get the power required to reach the required speed. The following equation is used to calculate the required delivered power. Eventually, the delivered power can be used in formula 3.27, where $V_{p,ax}$ is the velocity of the water at the propeller.

$$P_{ow} = \frac{E_{effective}}{\eta_i} \tag{3.32}$$

$$E_{effective} = \frac{1}{2}\rho(V_{ax,j}^2 - V_{ax,i}^2)Q_f \tag{3.33}$$

$$Q_f = A_p \cdot V_{p,ax} \tag{3.34}$$

$$V_{p,ax} = \frac{V_{ax,j} + V_{ax,i}}{2} \tag{3.35}$$

To calculate the open water power required, the ratio between inflow and outflow velocity has to be calculated. This is done in the same manner as described for the waterjet. Where the following equation is solved for μ.

$$T = \rho A_p \frac{\frac{V_{ax,i}}{\mu} + V_{ax,i}}{2}\left(\frac{V_{ax,i}}{\mu} - V_{ax,i}\right) \tag{3.36}$$

For further evaluation of the performance of the propeller, the rotational speed has to be calculated to eventually estimate the required gearbox ratio. To calculate the propeller rotational speed the cavitation limits will be used. As described in A. F. Molland et al. (2011) the limit for merchant vessels can be determined via the Burrill diagram that connects the non-dimensional value τ_c to the cavitation number σ.

$$\tau_c = \frac{T}{0.5\rho A_p V_r^2} \tag{3.37}$$

$$\sigma = \frac{P_{atm} + \rho g h - P_v}{0.5\rho V_r} \tag{3.38}$$

$$\tau_c = 0.43(\sigma - 0.02)^{0.71} \tag{3.39}$$

- τ_c - Non-dimensional thrust
- σ - Cavitaion number
- h - Propeller depth
- P_{atm} - Atmospheric pressure
- P_v - Vapour pressure

The result from equation 3.39 is the V_r which is a reference velocity at 70% of the radius of the propeller. Which can be used to calculate the rotational speed of the propeller via formula 3.41.

$$V_r = \sqrt{V_a^2 + (0.7\pi n D)^2} \tag{3.40}$$

$$n = \sqrt{\frac{V_r^2 - V_a^2}{0.49\pi^2 D^2}} \tag{3.41}$$

To verify the method of efficiency and rotational speed calculation, a case from Wärtsilä has been used. The reference vessel is a 130 m catamaran vessel designed by Incat that sails at 25 kn. Via the method used and described in this thesis, the open water efficiency and advance ratio for the rpm differ by 1.9% and 0.8% respectively. The difference is marginal but it can be seen that the efficiency will be overestimated slightly, which has to be taken into account when selecting the propulsor.

3.6.2. Bollard pull for manoeuvring

For the bollard pull, the efficiency is, by definition, zero with zero inflow speed. So the power required will be calculated via the ratio of thrust and delivered power to the propeller. This is described by formula 3.42.

$$\frac{T}{P_d} = \frac{2}{V_{ax,j} + V_{ax,i}} \eta_{effective} \tag{3.42}$$

To get to the required velocities, mainly the axial outflow velocity, the definition of thrust has to be used to calculate this since the required thrust is known. Since the inflow speed is equal to zero and the flow rate Q_f can be substituted with formula 3.44

$$T = \rho Q_f (V_{ax,j} - V_{ax,i}) \tag{3.43}$$

$$Q_f = A_p \cdot V_{p,ax} \tag{3.44}$$

If the formula's 3.43, 3.44 and 3.35 are combined the resulting ratio is described by formula 3.45. The $eta_{effective}$ can be calculated via the transit condition results.

$$\frac{T}{P_d} = \frac{\eta_{effective}}{V_{p,ax}} \tag{3.45}$$

$$\eta_{effective} = \frac{E_{effective}}{P_d} \tag{3.46}$$

3.7. Ducted propeller

For the propeller in a duct analysis, the same theory of the impulse balance will be used but the velocities in the flow stream of the propeller will be different. In the analysis, a pumpjet is also mentioned as an option for mid-speed vessels. Stators can increase efficiency by rectifying the inflow or regain energy of the outflow of the propeller. The direct efficiency increase can not be taken into account in the low-fidelity model like the impulse balance used in this thesis since radial and tangential velocities are not taken into account. For the pumpjet the efficiency gains are minimal, it has to be evaluated if the efficiency gains mentioned in the literature are sufficient to facilitate efficient operation (Oosterveld, 1970). The design of the addition of the stator is complex and requires a model that includes radial and tangential velocities. If the results suggest that it will be beneficial to add a stator to the propulsor to increase the open water efficiency it will be taken into account in the conclusion.

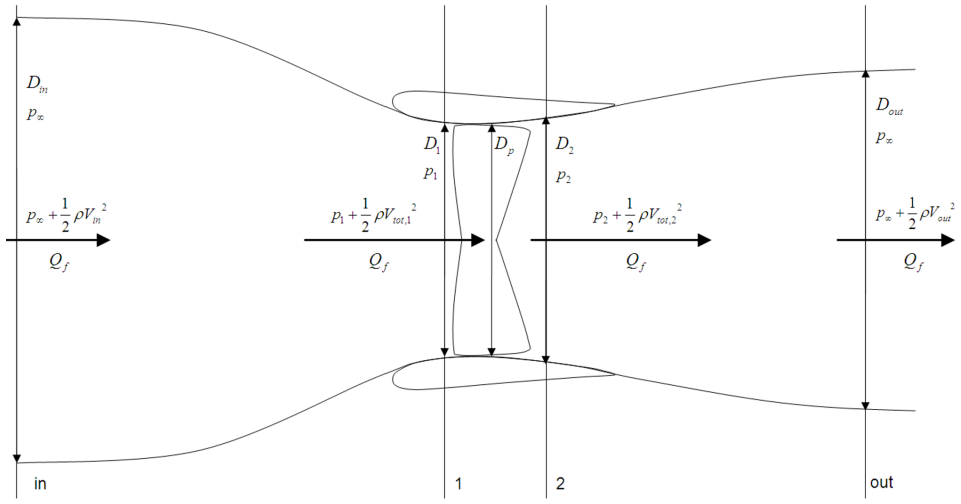

Figure 3.13: Velocity flow of a propeller in a duct

3.7.1. Transit sailing

In transit condition, the open water efficiency of a propeller in a duct is defined by formula 3.47. In formula 3.47, $\eta_{effective}$ is defined in the same way as in formula 3.31.

$$\eta_{ow} = \frac{2\mu}{\mu + 1}\eta_{effective} \tag{3.47}$$

For the effective energy calculation, formula's 3.33 and 3.44 are used. The velocity of the water at the propeller is described as in figure 3.13. In formula 3.48 the λ represents the amount of diffusion in the selected duct profile.

$$\lambda = V_{ax,out}/V_{ax,p} \tag{3.48}$$

To result in a solution for the open water efficiency, equation 3.49 has to be solved for μ. The equation cannot be solved due to the additional parameter λ. μ can be made dependent of λ but it requires the thrust loading coefficient which makes the equations dependent of each other, which results in no solutions. For the first estimate, a value of 1 for λ has been selected which represents a straight duct. The larger the diffuser ratio becomes, the better the efficiency in this model. In practice, this will not hold due to the flow around the duct that is not taken into account here.

$$T_{total} = \rho\lambda\frac{V_{ax,in}}{\mu}A_p\left(\frac{V_{ax,in}}{\mu} - V_{ax,in}\right) \tag{3.49}$$

When the variable of μ is known by solving equation 3.49 the efficiency can be calculated as stated in formula 3.27

To calculate the rotational speed of the propeller inside a duct, the following equation given by Weir (1987) can be used.

$$\frac{1}{2}wr = \frac{\frac{1}{2}T_pV_a}{2r\Omega\rho V_aA} \tag{3.50}$$

- w - Velocity difference between inflow and jet velocity
- r - Propeller radius from hub end until propeller tip
- A - Blade swept area

The propeller thrust given in equation 3.50 is solely the thrust of the propeller, not the duct. This can be estimated by the method described by Oosterveld (1970) where the thrust coefficient is related to the area ratio of the duct. It has to be noted that the radius used in equation 3.50 is the radius of the hub to the propeller tip. In Carlton (2019) it is mentioned that the hub diameter is 0.16-0.25 of the overall

propeller diameter, in this thesis a value of 0.2 is assumed.

To validate this method the program PropCalc, which is a propeller optimization program with the open water characteristics from Wageningen B-series propellers. Using the required thrust and propeller hull interaction coefficients the optimal efficiency can be calculated, by using a K4-70 propeller within a 19A nozzle. This results in an efficiency of 60.9% with an advance coefficient of 0.775. Compared to the result of the first principle model, which is 64.4% with an advance coefficient of 0.742, the first principle model overestimates the efficiency with 3.5% and the advance coefficient is underestimated with less than a percent difference. The rotational velocity is accurately estimated, but for the energy expenditure calculation and selection of the propulsor the overestimation of the efficiency has to be taken into account.

3.7.2. Bollard pull for manoeuvring

For the bollard pull, the following relation holds between the propulsive power and the thrust given. When the value for λ is known or estimated.

$$\frac{T}{P_D} = \frac{2\lambda}{V_{ax,p}} \eta_{effective} \tag{3.51}$$

In formula 3.51 the effective efficiency can be calculated with formula 3.31, 3.48 and 3.44 together with the results of the transit condition.

3.8. Energy converters

To calculate the power requirement and the energy required to perform the operational profile the efficiency of the energy converter is required. For the efficiency of the internal combustion engine, a constant value can not be taken. To calculate the efficiency at part load, specific fuel consumption data at part load can be used. In Abdel-Rahman et al. (1994), engine data of the SFC in part load conditions are given. The efficiency can be calculated from the SFC as described in Stapersma (2010a). The efficiency is then normalized and multiplied by a more recent value of a diesel engine efficiency stated in Stapersma (2010a) as well. This results in efficiency for part load conditions of the internal combustion engine, as can be seen in figure 3.14.

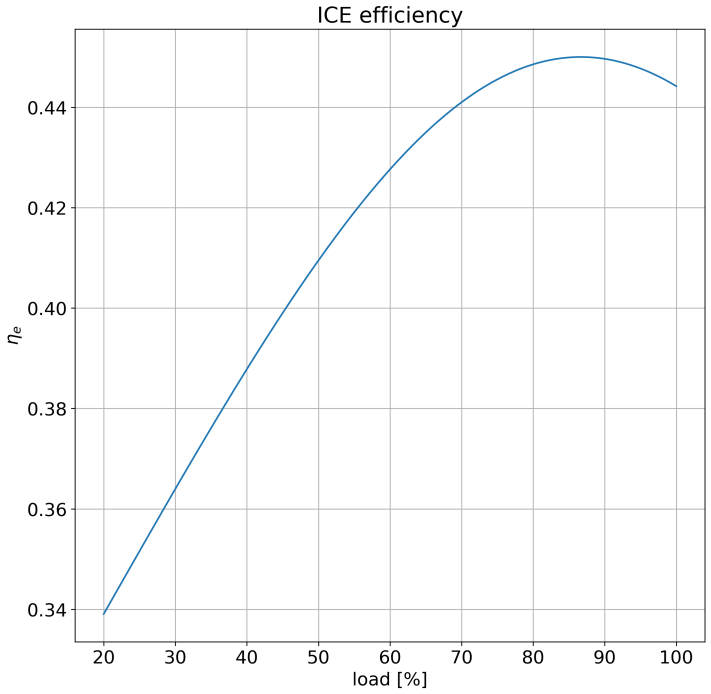

Figure 3.14: Part load efficiency ICE

To add a fuel cell to the chain of components, the efficiency should be determined and implemented at different levels of load. In Kistner et al. (2023), the efficiency by part load of a PEMFC is given and represented in figure 3.15. The objective of the article was to create a fuel cell model that possesses adaptability in terms of size, achieved through the capture of dynamic responses and their corresponding efficiencies. In figure 3.15, the efficiency of a PEMFC stack at part load conditions can be seen.

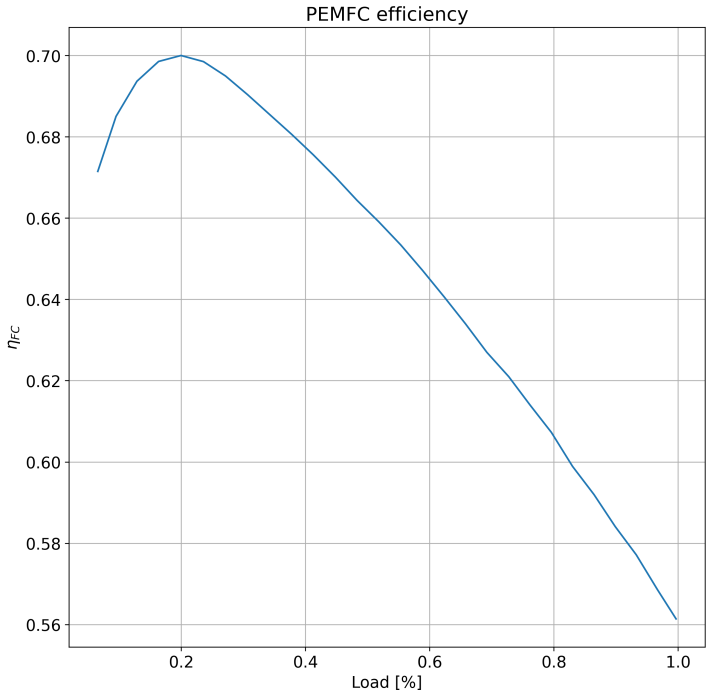

Figure 3.15: PEMFC efficiency at part load conditions

3.9. Fuel consumption and emissions

To calculate the fuel consumption from the required power requirement, the power required has to be calculated by dividing the effective power (which is the resistance multiplied by the speed) by the propulsor efficiency and the gearbox efficiency if installed. The power required per time unit (depending on the definition in the operational profile) is firstly divided by the engine efficiency at the specified loading. Secondly, it is integrated over time to result in the total amount of energy. To result in the amount of fuel required, the energy expenditure has to be divided by the lower heating value to obtain the total weight of fuel required.

For the evaluation of the emissions, the carbon dioxide equivalent index will be used. This value is a weighted average of the different emissions related to different fuels. This is done to be able to compare the different concept designs directly with each other. Different fuels emit different amounts of emissions when produced and used for energy creation. In Methanol Institute (2021), the $CO_2 - eq$ values are given and represented in table 3.4. It has to be noted that in the case of renewable fuels, the values do not incorporate emissions regarding renewable energy generation. The values that have to be added in the different cases are also given in table 3.4

Fuel	$CO_2 - eq$ [g/kWh]
MDO	344 “Lijst emissiefactoren” (2023)
EU-Grid	71
Methanol	80
Renewable Methanol	4
Hydrogen (NG basis)	104
Hydrogen (NG + CCS)	8
Renewable Hydrogen	0.8
Ammonia (NG basis)	188
Renewable Ammonia	0
Solar electric	4
Wind electric	7
Hydro electric	19

Table 3.4: $CO_2 - eq$ for each fuel and renewable energy creation

3.10. Conclusions

To conclude, this chapter has introduced the first principle models to calculate resistance, define the operational profile and calculate the efficiency of the propulsion system’s components resulting in the required power, energy expenditure and emissions. The chaining of the models can describe the energy flow and losses at different stages of the propulsion system. The accuracy of the first principle propulsor models has been benchmarked to CFD and propulsive test data and resulted in an accurate description of the reality, but the ducted propeller model overestimated the efficiency by a larger portion than the open propeller or waterjet.

4

Baseline Results and Propulsor selection

In this chapter, the results of the model described in chapter 3 of the different propulsors will be represented as power requirements for the different stages of a trip. This chapter will also include the energy and fuel (MDO) requirement, which results in the emissions represented in CO_{2eq}. The three propulsors that will be evaluated are waterjets, open propellers, and ducted propellers. In the following sections, the results of each propulsor in combination with the shaft, gearbox and ICE.

4.1. Waterjet

In this section, the reference vessel propulsion systems' power and energy requirements will be given for the waterjet-propelled vessel. In figure 4.1 one trip with the required power in kW is given. The first two minutes is the crabbing manoeuvre followed by the turning manoeuvre and the transit phase, finished with a crabbing manoeuvre. The sizing of the waterjet itself is needed together with the main engine. A Sea Margin (SM) of 10% is chosen for the main engine to get the optimal efficiency of the diesel engine, which means that the maximal power required is multiplied by 1.1 to get the installed power. To come to the most energy-efficient solution a propulsion system with two waterjets in total is selected with a diameter of 720 mm.

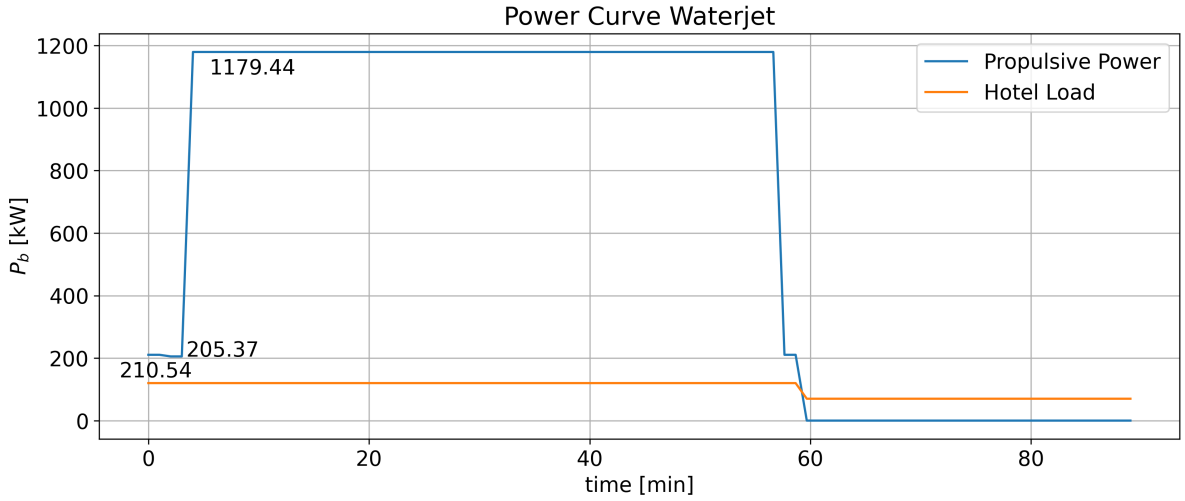

Figure 4.1: Waterjet propelled vessel power requirement

Result	Value	Unit
Energy requirement	2745.3	kWh
MDO required	231.46	kg
MDO required	0.2571	m^3
Emissions	944.38	kg CO_{2eq}

Table 4.1: Results WJ

4.2. Propeller

Graph 4.2 represents the results for the propeller-propelled vessel. The propeller-propelled vessel has a decrease in energy expenditure of 2.6% with respect to the waterjet-propelled vessel. The propeller-propelled vessel requires a tip clearance of 25% of the diameter which results in a maximum propeller diameter of 0.815 m.

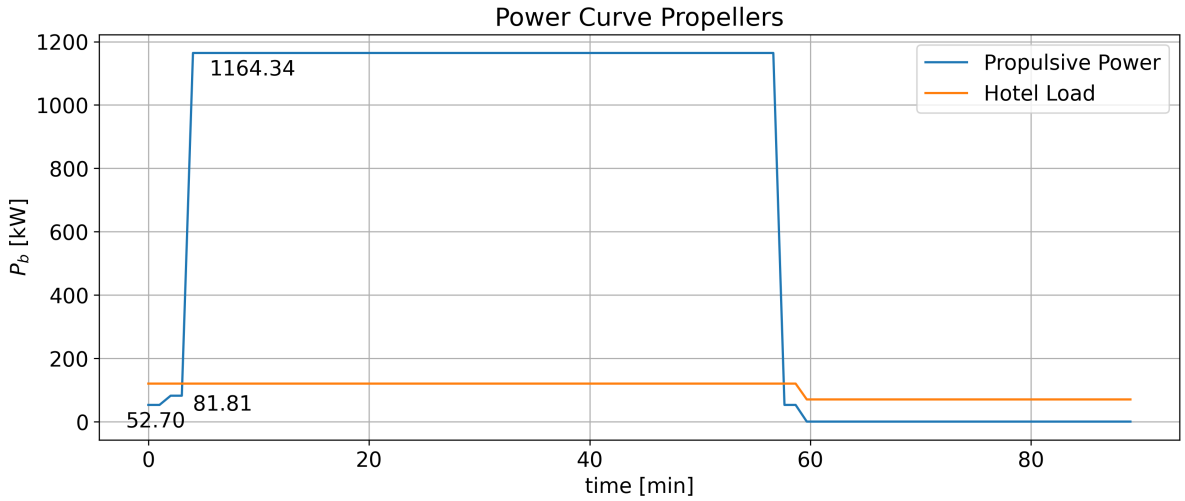

Figure 4.2: Propeller propelled vessel power requirement

Result	Value	Unit
Energy requirement	2673.2	kWh
MDO required	225.38	kg
MDO required	0.2504	m^3
Emissions	919.58	kg CO_{2eq}

Table 4.2: Results Propeller

4.3. Ducted propeller

Graph 4.3 represents the results for the ducted propeller-propelled vessel. The ducted propeller-propelled vessel has an increase in energy expenditure of 4.2%. The duct has been taken as a 19A shape nozzle to estimate the propeller's diameter and surface area for added resistance. The diameter of the propeller results in a diameter of 0.65 m.

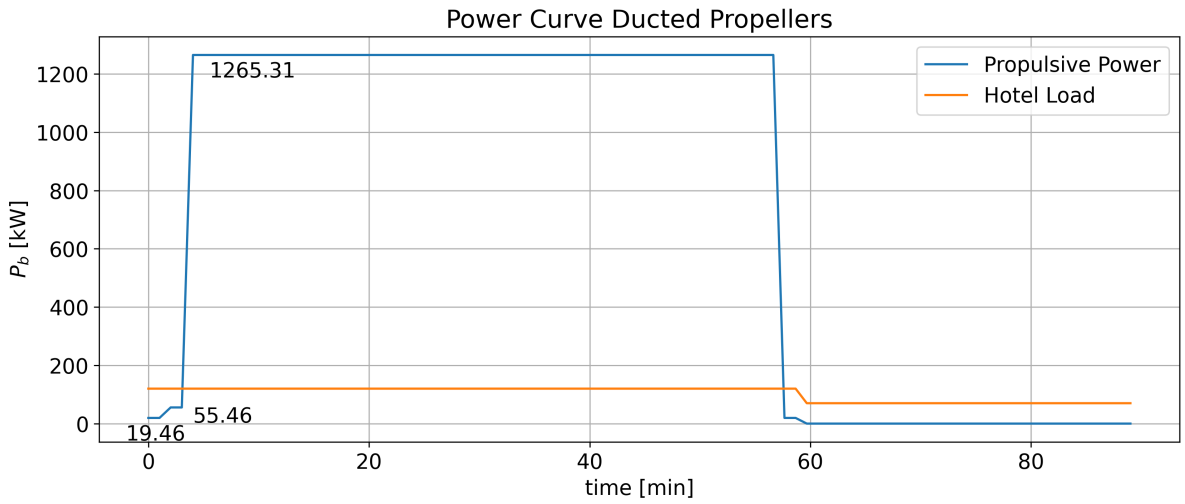

Figure 4.3: Ducted propeller propelled vessel power requirement

Result	Value	Unit
Energy requirement	2861.5	kWh
MDO required	241.25	kg
MDO required	0.2681	m^3
Emissions	984.36	kg CO_{2eq}

Table 4.3: Results Ducted propeller

4.4. Conclusion

When looking at the different energy expenditures, the most efficient solution is the propeller. The ducted propeller performs the worst of the three propulsors defined, the difference is 7.0%. This difference is significant which will rule out the ducted propeller as an efficient solution. To make the ducted propeller an option a stator has to be added to increase the open water efficiency. The increase required is higher than mentioned possible in the literature (Oosterveld (1970); Zhou et al. (2021)). Additionally, Zhao et al. (2022) has mentioned that the addition of a stator is complex which does not benefit modularity. Between the open propeller and the waterjet, the difference is too small to conclude which is more efficient due to the inaccuracies of the resistance calculation methods due to its nature of regression and the inaccuracies in the first principle models of the propulsors. Additionally, it has to be noted that the propeller efficiency calculation overestimates the efficiency. This does prove however that the mid-speed range is a grey area for the propulsor selection detailed analysis has to be done to be more certain of the most efficient selection of propulsor. The calculation method does not result in a clear best propulsor based on efficiency. Based on modularity the waterjet can be more isolated as a propulsor module due to the nature of the flush intake and the skid installation into the vessel, additionally, waterjet-propelled vessels tend to be more manoeuvrable than propeller vessels. Since the efficiency does not result in a clear best propulsor the selection will be made based on modularity which will be the waterjet moving onwards.

5

Concept design generation

In this chapter, the concept design generation for the propulsion system will be discussed. The generation will be done via a logical modularization framework discussed by Lagemann et al. (2021), where he describes a way to represent the components within the hull. Additionally, a SLD will be used to visualize the connections including those from the auxiliary systems which can then be transformed into a DSM.

5.1. Modularity framework

Lagemann et al. (2021) describes that the generation of a modular platform is done in three phases. The first phase is described as requirements. During the requirements phase, all the necessary information for the development of the ship class is collected and organized. In the case of the reference vessel type, which is a mid-speed 30 m ferry-type vessel, the following requirements have been deducted.

- Achieve 25 kn in transit condition
- Be able to produce low power for manoeuvring
- Produce power with as little emissions as possible
- Strive to store enough energy for one day

The second phase of the logical modularization framework is the functions phase. This phase uses the requirements as inputs and translates them into functions that the vessel needs to perform. In this case, the whole vessel modular redesign is not the goal of this thesis. So the functions will be formulated for the propulsion system itself. This will exclude payload, structure and hull requirements. This will be included in the evaluation of the feasibility of the concept designs, where the space and weight available onboard the vessel will be evaluated. The functions developed specifically for the propulsion system are the following:

- Produce 1180 kW for the transit condition
- Strive to store 27450 kWh of energy
- Convert stored energy to usable energy for the propulsor

Lastly, the third phase will be the phase where the modules will be defined. These modules will be composed of multiple components but will fulfil the functions in combination with each other. The following modules have been defined to fulfil the function determined above.

- Energy storage
- Energy conversion
- Energy distribution
- Propulsion
- Auxiliary (cooling, lubrication oil, fuel and control)

5.2. Modularity representation

To compare the different designs (current and concept designs), modularity needs to be assessed. A method that can result in a direct comparison via a modularity metric was the DSM method described in Eppinger and Browning (2012) with the metrics described in Hölttä-Otto et al. (2012). The metrics rely on the definition of modules and components that build up those modules. When the design remains on a conceptual design level, the metrics will not be able to identify the modularity in design, due to the lack of decomposition within modules. The DSM, however, can give valuable insight into the different connections between modules. In Eppinger and Browning (2012), an example is given of a DSM where multiple connection types are defined. In the example, the connection types are physical, energy, information and matter. With the combination of SLD and DSM representation, modularity can be visualised by the combination of the weight and the number of connections within the system. The significance of the connections in the system can also be implemented in the DSM. This is done by adding weight to the different connections. The weight for the four different connection types will be the following:

- Physical - 4
- Matter - 3
- Energy - 2
- Information - 1

5.2.1. Reference vessel

The visual and DSM representation of the propulsion system is done for the reference vessel described in the introduction. The reference vessel described operated at its optimum with two waterjets. To keep an organized overview of the system, only one side of the propulsion system installed in one demi hull will be drawn. For this vessel, detailed design data is not available so the cooling and control systems have been assumed. The assumptions are based on the following two articles that describe the cooling and control systems on a conceptual level. In Geertsma et al. (2017), the control scheme for a mechanically driven FPP with feedback control is taken as the control scheme for this vessel, including an extra output to the waterjet for the steering control. For the cooling solution, an overall schematic drawing of the vessel's centralized cooling arrangements is given in Fang et al. (2018). This is taken as an assumption of how it is arranged in the reference vessel. These assumptions together with the actual propulsion arrangement of the vessel, which is a mechanically driven waterjet via a gearbox by an ICE, are given and represented in figure 5.1 including all the connections with the corresponding DSM in figure 5.2.

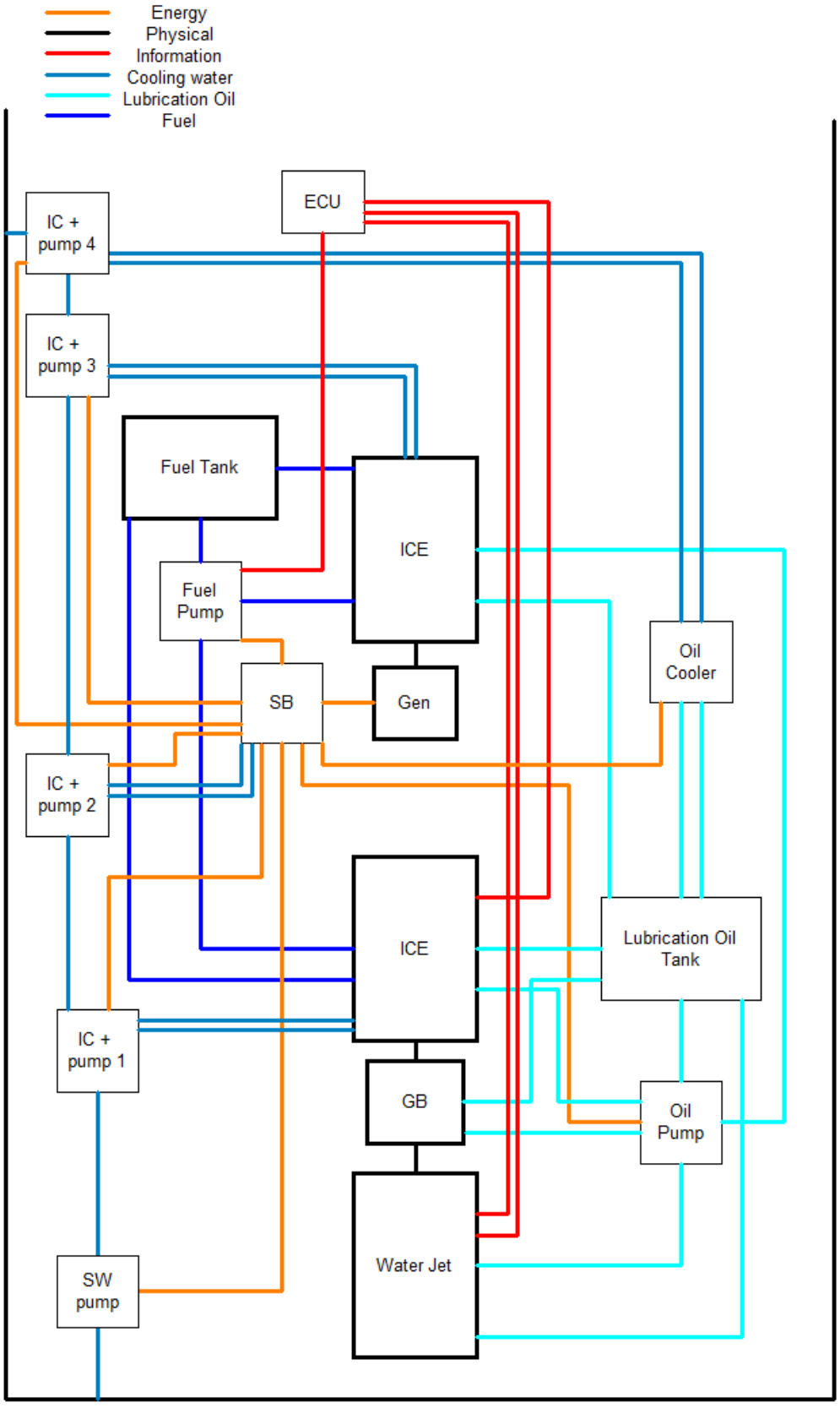

Figure 5.1: Propulsion layout and connections

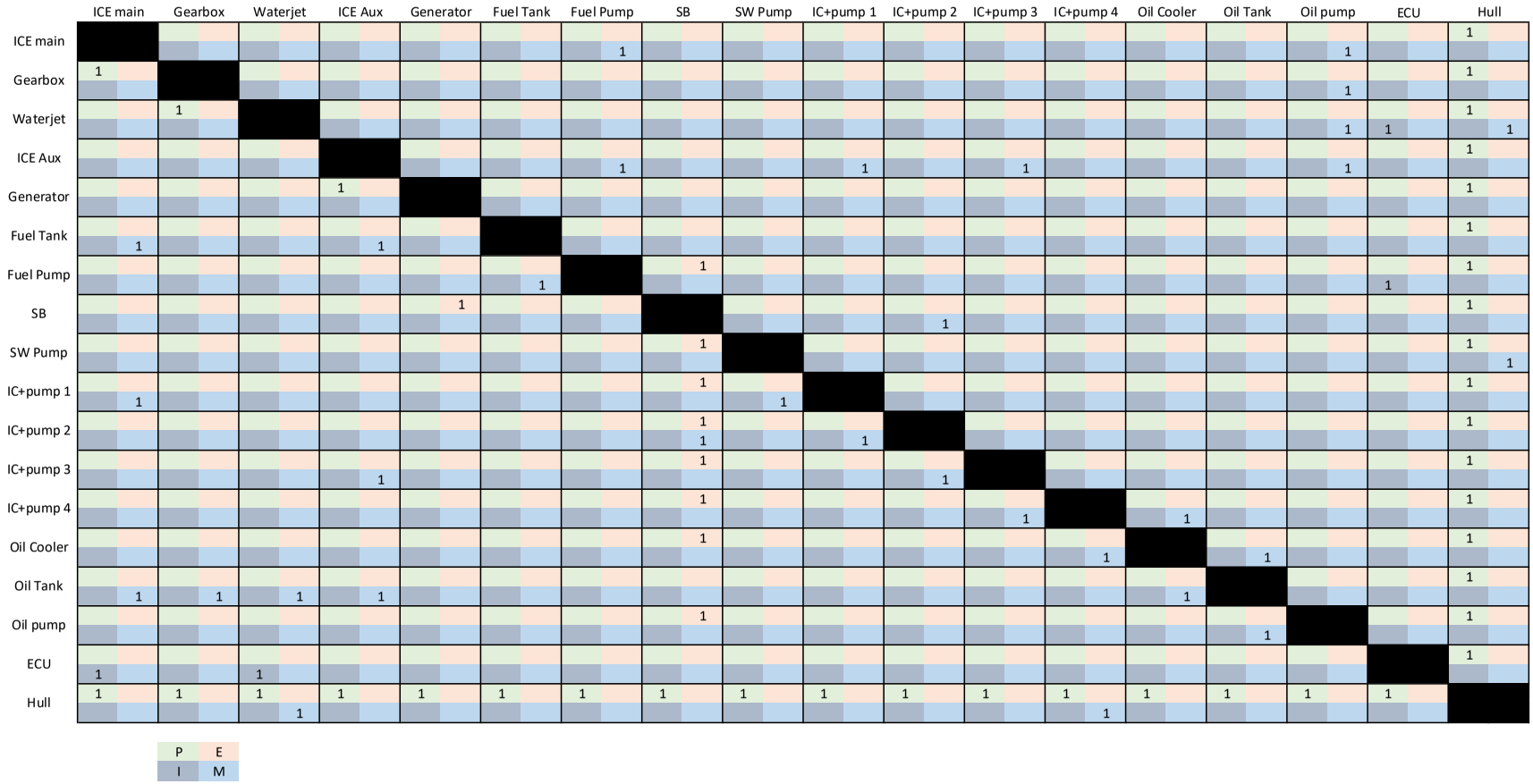

Figure 5.2: DSM for the directly driven reference vessel

5.3. New concepts

For the creation of the new concept designs a few steps have to be taken. Firstly a decision on the architecture has to be made to create a modular system. Secondly, the type of energy conversion has to be chosen in combination with the type of fuel. This depends on the technical feasibility and maturity of the different combinations of energy converter and fuel.

5.3.1. Architecture selection

For the beginning of new concept generation, a modular architecture is needed to be created. The different types of architecture need to be compared to see where the most gain is to achieve a modular system. For ship propulsion, a few types of architectures are used in ship design.

- Direct drive architecture

- Direct geared drive architecture

- Serial or Electric architecture

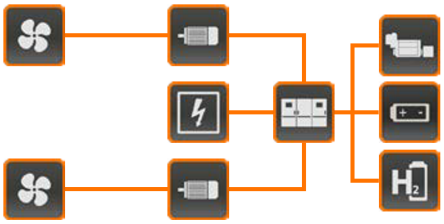

- Parallel architecture

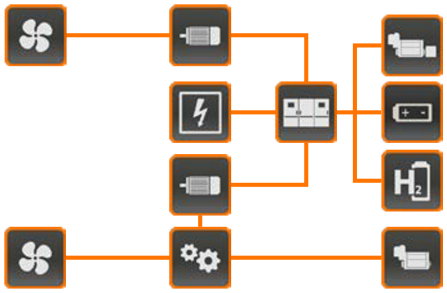

- Serial-Parallel architecture

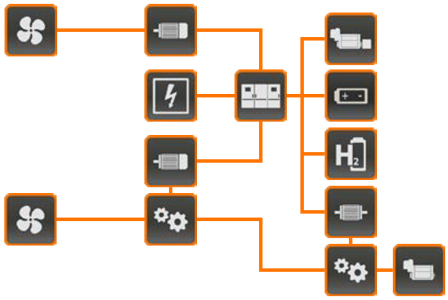

Figure 5.3: Propulsion architectures

When selecting an architecture for the new modular concepts, the objective is to reduce the number of connections or use a different type of modularity. Salvador et al. (2002) has given an overview of the different types of modularity. In figure 5.4 the different modularity types are given. It can be concluded that electrical propulsion architecture is set up as bus modularity. This type of modularity can facilitate multiple types of energy converters and storage systems and can facilitate the required electrical load without an additional energy converter. This will reduce the number of connections required. For future and hybrid solutions, the electrical architecture can facilitate modularity in design due to the nature of direct electricity conversion by FC and direct electricity from batteries.

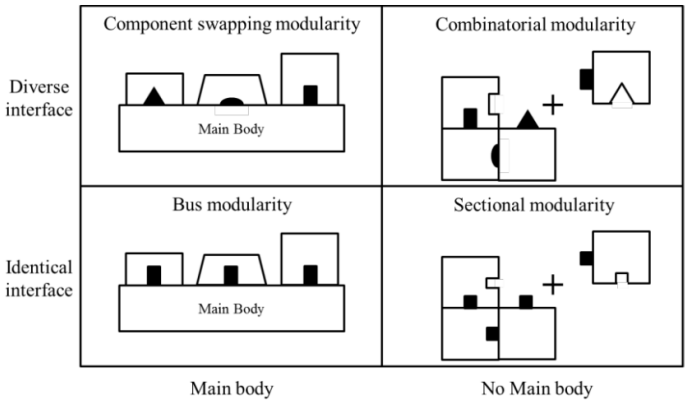

Figure 5.4: Modularity Type (Salvador et al., 2002)

Fully electric propulsion in the case of an ICE can be seen in figure 5.5, with the corresponding DSM in figure 5.6. In the figure, it can be seen that the number of connections and modules is less. The thing that has to be noted is that the efficiency is overall less than a directly driven vessel due to the extra energy conversion steps. This is why a parallel architecture could facilitate better performance. The serial-parallel architecture can facilitate good dynamic behaviour but adds additional components and connections which are not necessary due to the nature of electrical induction machines that can operate both in generator and motor conditions. This reduces the components with an electrical machine and a gearbox. Both the serial/electrical architecture and the parallel hybrid architecture are created and compared based on modularity.

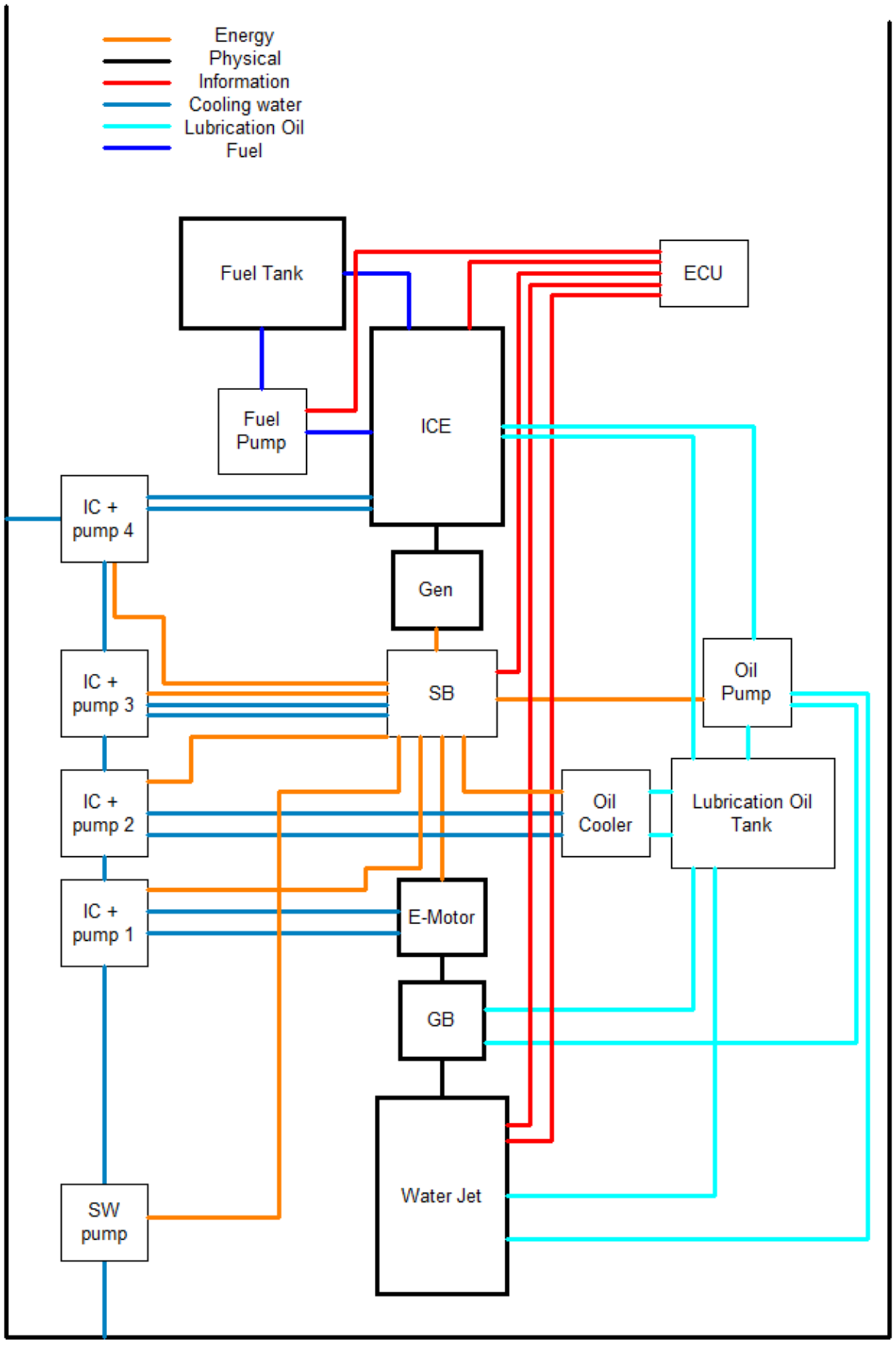

Figure 5.5: Electrical architecture with an ICE

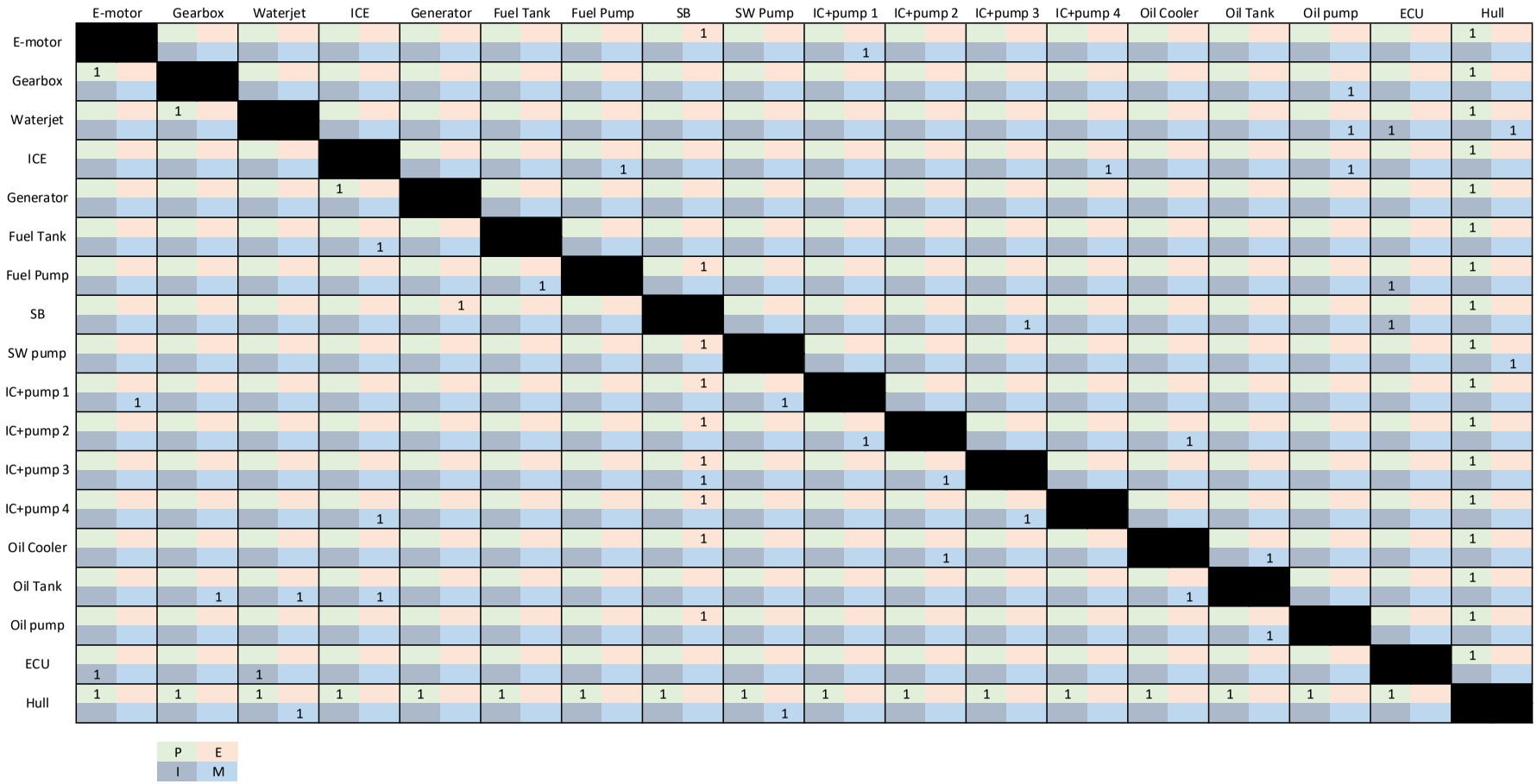

Figure 5.6: DSM for the electrically driven reference vessel

When comparing the geared direct drive architecture with the electrical architecture, it can be seen that the number of connections in total are more with the electrical architecture, but the weighted connections are less due to the fact that most connections will be electrical and less physical connections (table 5.1). Mainly the fuel and lubrication are also reduced due to the fact that an additional ICE for electrical energy generation is needed. Additionally, it can be noticed that the bus modularity nature of the lubrication oil system and the cooling water system is still in place. The energy distribution is redesigned to take advantage of the bus modularity due to the electrical propulsion architecture. The direct substitution of a FC in the design of the propulsion system is possible. The only thing that should be altered in the design is the fuel supply to the FC. In the case of a PEMFC the fuel should be pure hydrogen which can be either stored or created from a hydrogen carrier like ammonia. A SOFC has more options regarding alternative fuels, but start-up and shutdown times are long and are more prone to thermal cracking. Looking at the hybrid solution, the propulsion system can be represented in the following way, with the electrical storage system being a battery pack. The SLD is given in figure 5.7 and the corresponding DSM in 5.8.

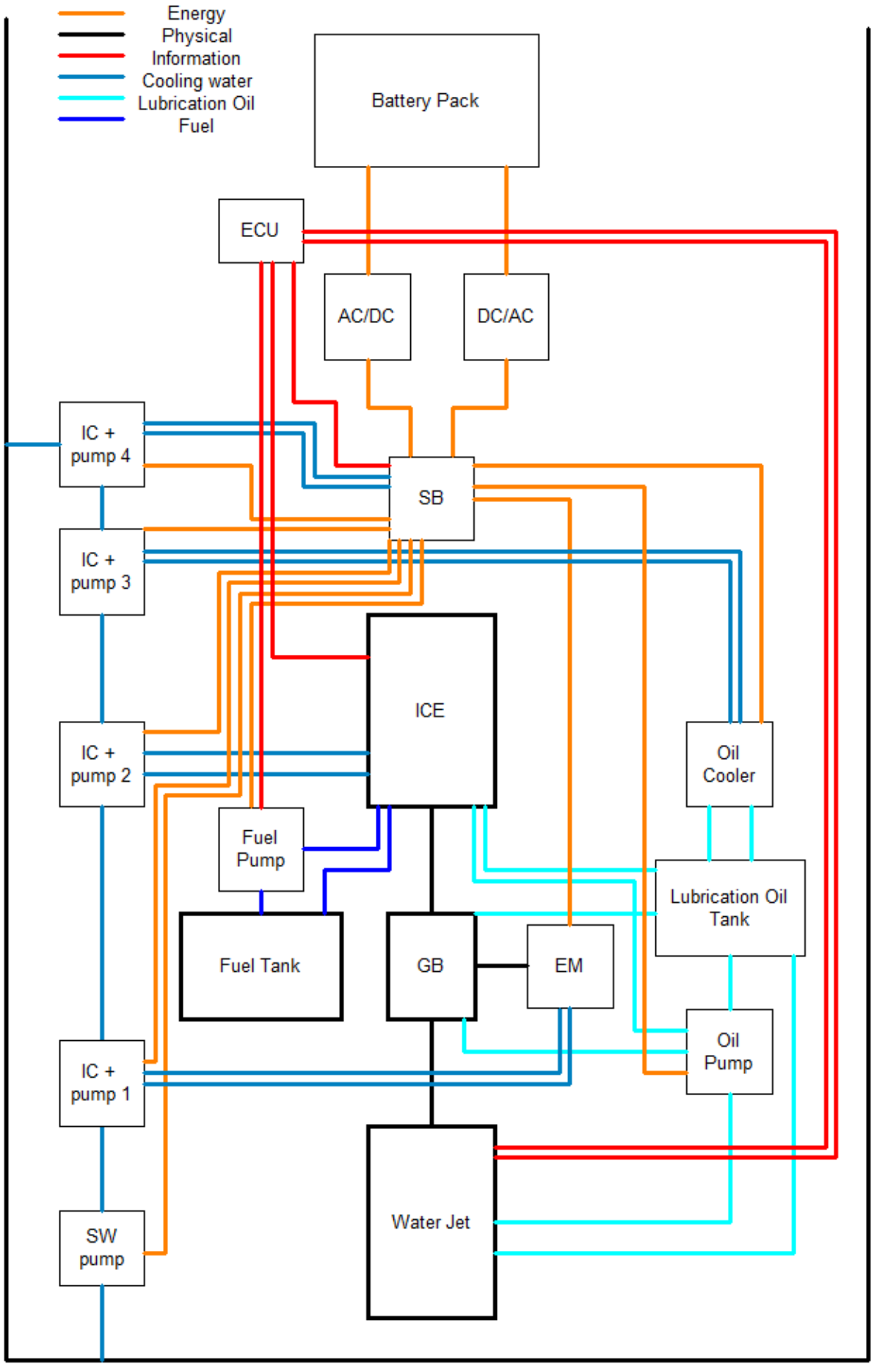

Figure 5.7: Parallel Hybrid Propulsion System

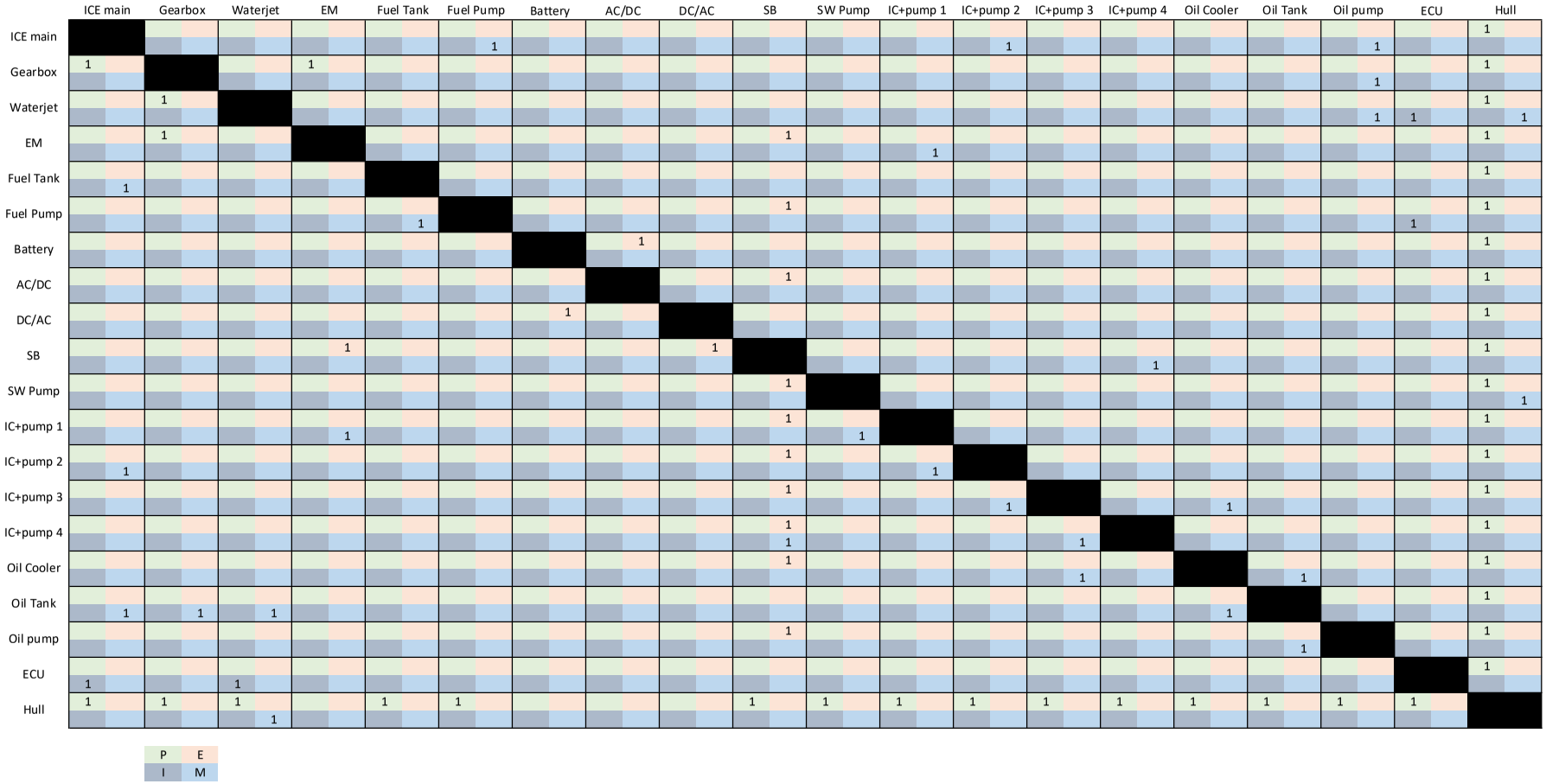

Figure 5.8: Hybrid system DSM

To compare the three architecture types the DSM and the visual connections can be evaluated. An indication of modularity can be given by the number of connections and the corresponding sum of the weighted connections. To compare the three architectures the number of connections are given in table 5.1.

Architecture	Connections	Weighted connections	Average connection weight
Direct drive	82	266	3.244
Electrical drive	80	257	3.213
Hybrid drive	83	252	3.036

Table 5.1: DSM Connection

When assessing the three architectures it can be seen that there will be a trade-off between the weighted sum of connections and the actual number of connections, based on these numbers the best performing are either the electrical or hybrid drive (Serial or Parallel hybrid). When visually comparing the DSM's and line diagrams of the electrical and hybrid system, it can be seen that the different defined modules are more distinctively decoupled at the electrical architecture. The increase in connections around the diagonal would also indicate higher levels of modularity (Jung & Simpson, 2017). What can be taken away from this comparison is that the second ICE for electrical power generation will increase the number of connections in the system. Both electric and parallel system architectures can be used to achieve a modular system with reduced emissions. The issue that can arise is the scalability of the propulsion system. The most efficient solution of the propulsor was a system that contained two waterjets (one for each demi hull). In the parallel hybrid architecture, if an extra propulsor is added an extra ICE is also required, while in the fully electrical architecture, only an extra electric motor is required, which can result in a negative impact on modularity. When analysing the scalability of the two systems the following trend was seen. The SLD are shown in appendix C. Due to the large increase in connections if an additional propulsor is added it does not benefit modularity. So the most modular propulsion architecture is the electrical propulsion (serial hybrid) architecture.

Architecture	One propulsor connections	Two propulsors connections	Difference
Hybrid	252	409	+62%
Electric	257	321	+25%

Table 5.2: Scalability of architectures

5.3.2. Energy conversion and storage

The energy conversion options for the most modular architecture have to result in electrical energy. The most efficient way is to store electrical energy directly in batteries since it will reduce the conversion step from chemical to electrical. The issue with batteries is that the energy density is limited so it has to be investigated if the solution will be feasible onboard the vessel. Secondly, the electrical architecture does add an additional conversion step to generate electric power but the addition of the possibility to add batteries for peak shaving and manoeuvring, together with the possibility for alternative fuels the reduction in emission will be possible. The scope of the concept design generation will be on implementing batteries, alternatively fuelled ICE and FC to an electrical architecture to facilitate modularity in design.

5.4. Performance indicator evaluation

To evaluate the different options onboard the vessel the performance indicators that have been selected are volume, weight, life cycle costing, modularity and emissions. Modularity and emission evaluation have been described earlier. In this section, the method of calculating the volume, weight, and life cycle costing will be presented. These factors will be evaluated via indices referencing to a particular weight or volume to the characterized variable of the component. As an example, kW for a fuel cell and engine and kWh for batteries. In the following sections, the weight, volume and LCC parameters will be presented of the main components. The main components are the components that characterise the system and that have the highest influence on the performance indicators. The following components

are taken into account for the comparison. In the following sections, parameters are based on the literature or data analysis. These plots are given in appendix D.

- Waterjet
- ICE
- FC
- Gearbox
- EM
- Fuel
- Batteries

5.4.1. Weight parameters

The weight parameters are related to the characteristic parameter of the component. In table 5.3 the parameters link the characteristic value of the component with the weight of the component. For the internal combustion engine, the reference fuel is MDO and the future fuel will be methanol since it has the highest potential as an alternative fuel (Xing et al., 2021b). The performance of methanol-fuelled ICE is comparable with a diesel-fuelled ICE, so the same performance indicator parameters will be used (Tunér et al., 2018). For the liquid hydrogen storage, an energy penalty of 30% has to be taken into account for keeping the hydrogen liquid (Tarhan & Çil, 2021). Formula 5.1 and 5.2 are based on data analysis of product catalogues.

Component	Value	Unit	Reference
Waterjet	formula 5.1	kg	(Wärtsilä modular waterjet)
ICE	58.25	W/kg	Wu et al. (2022)
FC	0.2	kW/kg	Ballard Power Systems (2021)
Gearbox	2.0	kg/kW	Hekkenberg (2014)
EM	formula 5.2	kg	(VEM catalogue)
Batteries	111	Wh/kg	“Marine Battery Sizing - Spear Power Systems Trident” (2019)
MDO	42.7	MJ/kg	Stapersma (2010a)
Methanol	19.9	MJ/kg	Van Lieshout et al. (2020)
Hydrogen	120	MJ/kg	Bae and Kim (2017)

Table 5.3: Weight parameters

$$M = 1.994 \times 10^{-6} D_j^3 + 5.979 \times 10^{-3} D_j^2 - 4.513 D_j + 1.265 \times 10^3 \tag{5.1}$$

With D_j in mm and resulting weight in kg, with a R^2 value of 0.999

$$M = (3.490 \times 10^2) + (-3.004 \times 10^{-1}) \cdot n + (8.158) \cdot P + (6.149 \times 10^{-5}) \cdot n^2 + (-2.158 \times 10^{-3}) \cdot P^2 + (-6.325 \times 10^{-4}) \cdot n \cdot P \tag{5.2}$$

With P in kW and n in rpm and the resulting weight in kg, with an R^2 value of 0.9649.

5.4.2. Volume parameters

The following parameters will be used to estimate the size of the following components. Stapersma and Vos (2015) have created first principle models to estimate the sizing of the ICE, EM and the GB.

Component	Length [m]	Height [m]	Width [m]	Volume	Reference
Waterjet	In: $4.085 + 245.73 \cdot D_{jet}$ Out: $2.689 \cdot D_{jet}$	$1.279 \cdot D_{jet}$	$1.279 \cdot D_{jet}$	11.081 $\cdot D_{jet}^3$	(Wärtsilä modular waterjet)
ICE	$4.286 \cdot L_s$	$2 \cdot L_s$	$1 \cdot L_s$	43.75 kW/m^3	Kistner et al., 2021 Stapersma and Vos, 2015
FC	0.896 kW/m^2			101 kW/m^3	Ballard Power Systems, 2021
Gearbox	$i_{GB} \cdot D_w$	$\left(1 + \frac{1}{i_{GB}}\right) \cdot D_w$	$1 \cdot D_w$	Formula 5.3	Wärtsilä, Stapersma and Vos, 2015
EM	$3.75 \cdot D_r$	$\frac{D_r}{0.5}$	$\frac{D_r}{0.5}$	Formula 5.9	Stapersma and Vos, 2015
Batteries	variable			95 Wh/L	"Marine Battery Sizing - Spear Power Systems Trident", 2019
MDO	variable			900 kg/m^3	Stapersma, 2010b
Methanol	variable			784.5 kg/m^3	Engineering Toolbox, 2018
Hydrogen	variable			0.09 kg/m^3 (0 °C and 1 atm)	Bae and Kim (2017)
Hydrogen	variable			23.3 kg/m^3 (350 bar)	Inal, Dere, et al. (2021)
Hydrogen	variable			39.3 kg/m^3 (700 bar)	Inal, Dere, et al. (2021)
Hydrogen	variable			70 kg/m^3 (Liquid)	Inal, Dere, et al. (2021)

Table 5.4: Size parameters

The dimensions of the ICE have been assumed via the ratio of width and height of the diesel engine mentioned by Stapersma and Vos (2015), also mentioned was that the length is scaled by the number of cylinders times the bore diameter, with the ratio between the stroke length and bore diameter being assumed to be 1.4 as mentioned in Stapersma (2010a) as a representable value for mid-speed engines. The assumption for the number of cylinders is 6.

$$V = 0.00082978 \cdot M - 0.33384366 \tag{5.3}$$

V in m^3 and M in kg

For the electric motor, the following reasoning behind the volume determination is used. With σ being equal to 35 kPa. This value is chosen since there is a large spread of values and the data referring to the electromotor without additional components was the data of 3GBM in Stapersma and Vos (2015), so that data is used, where the clustering is around 35 kPa.

$$P = \omega_m Q \tag{5.4}$$
$$P = \omega_m \cdot r \cdot F \tag{5.5}$$
$$F = 2\pi \cdot r \cdot l \cdot \sigma \tag{5.6}$$
$$P = 2\pi \cdot r^2 \cdot l \cdot \omega_m \cdot \sigma \tag{5.7}$$
$$V = \pi \cdot r^2 \cdot l \tag{5.8}$$
$$V = \frac{60 \cdot P}{2\pi \cdot n \cdot \sigma} \tag{5.9}$$

5.4.3. LCC parameters

For the life cycle cost assessment, two types of costs will be considered, Capital Expenses (CAPEX) and operational expenses (OPEX). CAPEX is the initial investment cost for each component when the vessel is being built. OPEX are the costs that are required to keep the component and system running, such as maintenance costs and fuel expenses which are defined by each year of operation. The following components are required to calculate the Net Present Value (NPV) to compare the LCC of propulsion systems. In the following two tables, the parameters for each component are given. Additionally, the method of calculating NPV will be given.

Component	Price	Unit	Reference
Waterjet	0.6625·D_{jet} - 205.654	k€	Wärtsilä internal
ICE	MDO: 251.2, MeOH: 276.1	€/kW	Kistner et al. (2023)
FC	1410	€/kW	Taljegard et al. (2014)
Gearbox	40	€/kW	Hekkenberg (2014)
EM	Appendix D	€/kW	VEM (2023)
Batteries	800	€/kWh	Kistner et al. (2021)
Hydrogen Storage	78	€/kg (300 bar)	Inal, Dere, et al. (2021)
Hydrogen Storage	658	€/kg (700 bar)	Inal, Dere, et al. (2021)
Hydrogen Storage	1290	€/MWh (liquid)	Kistner et al. (2023)
MDO storage	158	€/MWh	Kistner et al. (2023)
Methanol Storage	120	€/MWh	Kistner et al. (2023)

Table 5.5: CAPEX Parameters

Component	Price	Unit	Reference
Waterjet	61	€/mm/year	(Wärtsila internal)
ICE	Diesel: 4.7, MeOH: 5.64	€/MWh	Hansson et al. (2019)
FC	11	€/MWh	Hansson et al. (2019)
Gearbox	2.75	€/kW/year	Neary et al. (2014)
EM	0.04832 $\cdot CAPEX$	€/year	Neary et al. (2014)
MDO	Appendix E	€/ton	Horton et al. (2022)
Methanol	Appendix E	€/ton	Horton et al. (2022)
Hydrogen	Appendix E	€/ton	Horton et al. (2022)
Electricity	104.02	€/MWh	"European power price tracker" (2023)*

Table 5.6: OPEX Parameters

The price of electricity in the EU is quite uncertain due to the volatility of the electricity market. Forecasting the price cannot be done accurately so a constant electricity price is taken as constant. The OPEX parameters for the gearbox and electric machine are based on failure data of marine energy conversion technologies.

To use these values the following method will be used for the calculation of the costs. The future value of the payments will be calculated by taking into account the inflation rate. The expected cash flows in this case will be the costs related to operating the propulsion system. Each operating year the OPEX will be summed and used in formula 5.10. Summing these values including the CAPEX will result in the total cost for the operating system.

$$NPV = \sum FV \cdot (1+i)^t \tag{5.10}$$

- FV - Future Value
- i - Inflation rate (taken as 5% (IMF, 2023))
- t - Number of years in operation

6

Performace indicator evaluation comparison

In this chapter, the results of the performance indicators (PI) of the concept propulsion systems are given. They will be compared to the reference system in a few different ways. First, the sizing of the components onboard will be given. Next, the block render of the components onboard will be presented to visualize the propulsion system onboard. Subsequently, the Single Line Diagram (SLD) of the system with the linked DSM will be presented to be able to compare the systems based on modularity. Afterwards, the LCC will be calculated to compare the economic costs related to the system. Lastly, the emissions related to operating the system in the previously defined operational profile will be presented. The emissions for alternative fuels will be given based on the grey production process, additional emission reduction is possible by using blue or green options. In chapter 5, the conclusion was drawn that the electrical architecture would be most modular. The choice has been made to use this architecture to connect different energy storage and energy converters which are seen to be the most potent solutions for reducing emissions which were explored in chapter 2. That is why the following systems are chosen to be explored for solutions to reducing or eliminating emissions. For the energy storage determination, a sea margin of 10 percent will be used to calculate the required energy storage size.

6.1. Reference system

In this section, the results of the reference vessel's propulsion system are given. This system is a directly driven waterjet via a gearbox by an ICE with an additional auxiliary engine to provide electrical energy to the vessel. Only the main drive components are represented to keep a better overview of the system onboard the vessel. In table 6.1 the characteristic size, weight and volume of the components are given, based on the parameters given in section 5.4. These values will be the benchmark for the concept designs to be compared against. Following the weight and volume results, the render of the propulsion system onboard the vessel is represented by figure 6.1. Subsequently, the corresponding single line diagram is given in figure 6.2, the DSM is given in figure 5.2 and lastly the LCC calculation is given in table 6.2 calculated as described in 5.4.3.

Component	Size	Weight [kg]	Volume [m^3]
Waterjet	2x 720 mm	3719	8.272
ICE	2x 655 kW @ i_{gb} = 1.04	22489	29.943
ICE aux	133 kW	2283	3.040
Gearbox	2x 655 kW	2620	1.506
EM	133 kW	1142	0.048
MDO	2.83 m^3	2546	2.829
Total		34799	45.638

Table 6.1: Weight and volume direct drive propulsion system

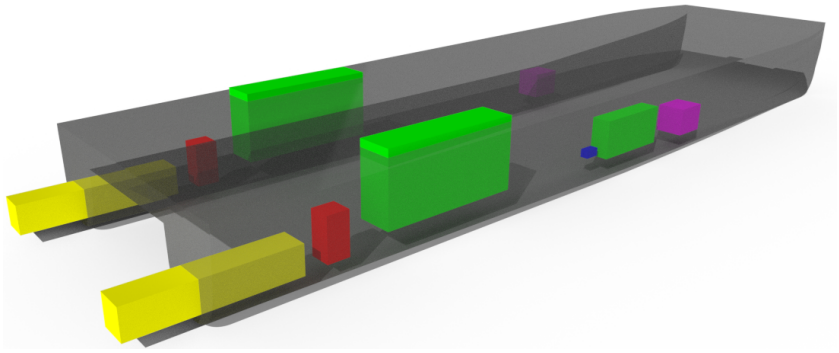

Figure 6.1: Graphic representation of the baseline propulsion system

Waterjet:	Yellow	ICE:	Green
Gearbox:	Red	Fuel storage:	Magenta
Electric generator:	Blue		

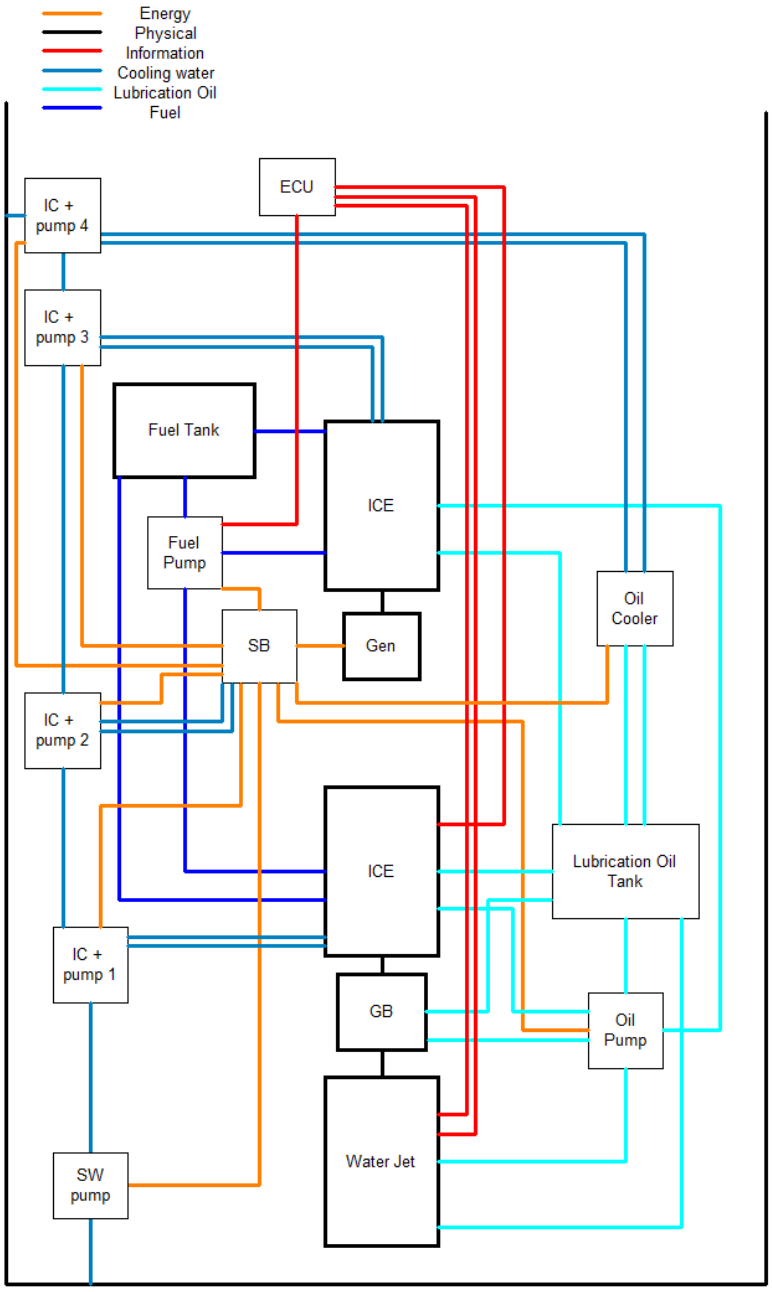

Figure 6.2: Propulsion layout and connections of reference vessel

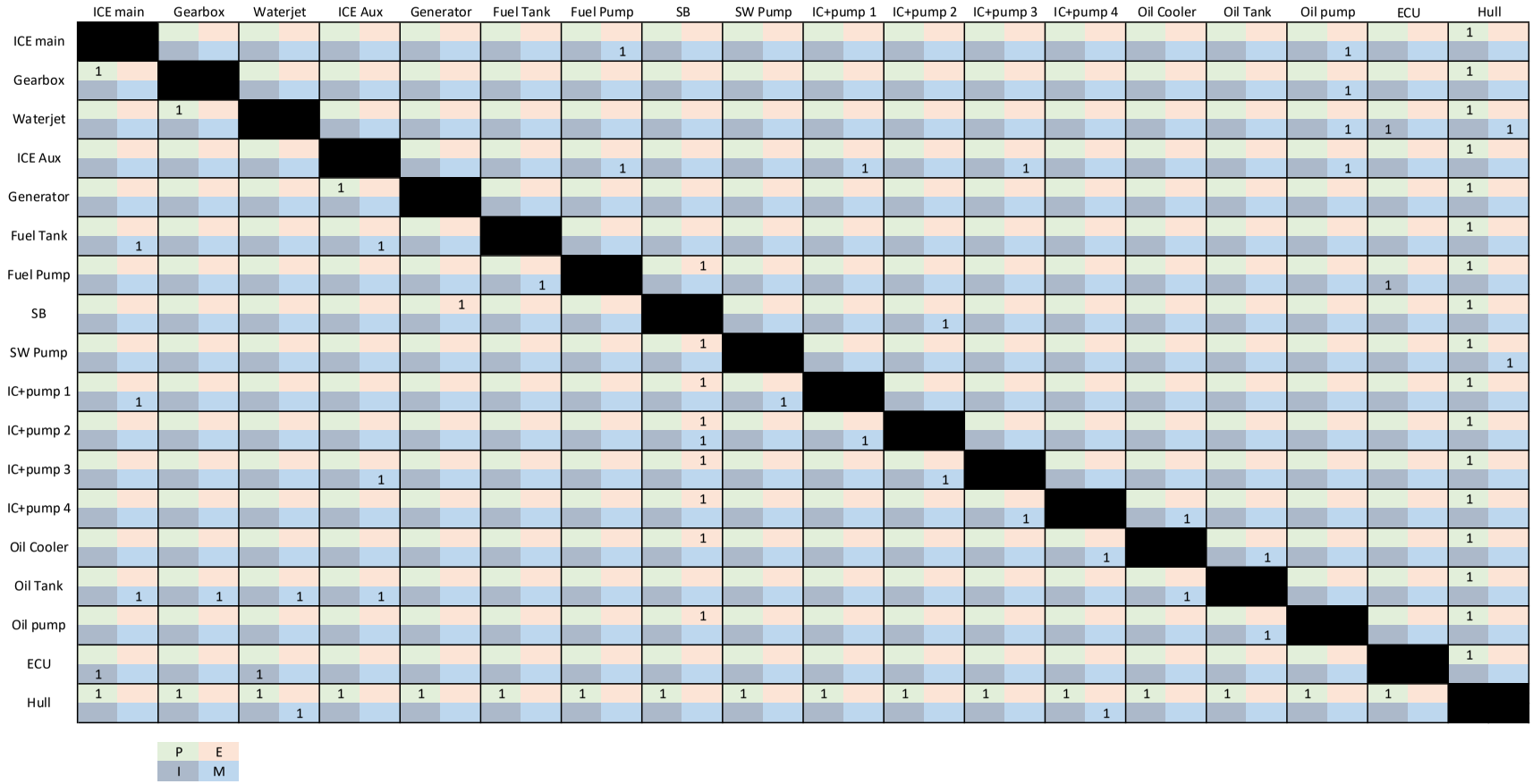

Figure 6.3: DSM for the directly driven reference vessel, with a total number of connections of 82, weighted connections of 266 and an average connection weight of 3.244

Year	Waterjet	ICE + ICE aux	Gearbox	EM	Fuel	Total	NPV
2023	€542 756	€813 852	€51 200	€42 827	€2 506	€1 453 142	€1 453 142
2024	€87 840	€47 090	€3 603	€2 069	€443 430	€584 032	€613 234
2025	€87 840	€47 090	€3 603	€2 069	€440 265	€580 867	€640 406
2026	€87 840	€47 090	€3 603	€2 069	€438 438	€579 040	€670 311
2027	€87 840	€47 090	€3 603	€2 069	€437 973	€578 575	€703 261
2028	€87 840	€47 090	€3 603	€2 069	€438 315	€578 917	€738 862
2029	€87 840	€47 090	€3 603	€2 069	€440 047	€580 649	€778 125
2030	€87 840	€47 090	€3 603	€2 069	€442 670	€583 273	€820 723
2031	€87 840	€47 090	€3 603	€2 069	€445 921	€586 523	€866 562
2032	€87 840	€47 090	€3 603	€2 069	€449 119	€589 722	€914 852
2033	€87 840	€47 090	€3 603	€2 069	€451 000	€591 602	€963 657
2034	€87 840	€47 090	€3 603	€2 069	€451 252	€591 854	€1 012 271
2035	€87 840	€47 090	€3 603	€2 069	€448 964	€589 566	€1 058 777
2036	€87 840	€47 090	€3 603	€2 069	€446 806	€587 408	€1 107 646
2037	€87 840	€47 090	€3 603	€2 069	€444 118	€584 720	€1 157 706
2038	€87 840	€47 090	€3 603	€2 069	€441 947	€582 549	€1 211 077
2039	€87 840	€47 090	€3 603	€2 069	€438 199	€578 801	€1 263 450
2040	€87 840	€47 090	€3 603	€2 069	€433 708	€574 310	€1 316 329
2041	€87 840	€47 090	€3 603	€2 069	€427 886	€568 488	€1 368 134
2042	€87 840	€47 090	€3 603	€2 069	€423 782	€564 385	€1 426 172
2043	€87 840	€47 090	€3 603	€2 069	€420 067	€560 669	€1 487 623
2044	€87 840	€47 090	€3 603	€2 069	€415 757	€556 359	€1 549 996
2045	€87 840	€47 090	€3 603	€2 069	€412 016	€552 618	€1 616 552
2046	€87 840	€47 090	€3 603	€2 069	€407 925	€548 528	€1 684 816
2047	€87 840	€47 090	€3 603	€2 069	€403 693	€544 295	€1 755 406
2048	€87 840	€47 090	€3 603	€2 069	€399 997	€540 599	€1 830 660
Total						€15 811 492	€30 009 751

Table 6.2: LCC of the direct drive propulsion system

The results are summarized in table 6.3. These values will be taken as a benchmark to compare the concept design's performance indicators. The weight of the propulsion system is taken as a reference to calculate the increase in displacement required of the vessel which will result in a higher resistance. The higher resistance leads to an increase in power requirement and energy expenditure. The volume parameter will have more lenient boundaries since the vessel's space onboard is not maximized. The cost, modularity and emissions are included to compare the improvements made on the two main drivers for the redesign of the propulsion system, modularity and emissions. The NPV calculation is added to compare the cost of the improvements made based on the concept propulsion systems.

System	Volume [m^3]	Weight [kg]	NPV	Modularity	Emissions
MDO direct drive	45.638	34799	€30 009 751	266	944.38

Table 6.3: Results reference system

6.2. Battery system

For the battery drive propulsion system, the capacity of the battery pack has to be determined. This is done as mentioned in Al-Falahi et al. (2018), where a figure is given which relates the depth of discharge (DoD) to the number of cycles before it needs to be replaced. In the situation of designing the propulsion system, a return trip will be used to determine the energy requirement. This is done to limit the required infrastructure to one port of the ferry operation. The pure energy requirement for one trip results in 1293 kWh. To account for waves and current, a sea margin of 10% is used. So the energy requirement total before recharging is 2845 kWh. For a design life of 10 years which will be 18250 cycles, results to a depth of discharge value of 75%. Depth of discharge is the amount of charge of the battery that can be drained during one cycle. Which results in an installed battery energy of 3792.8 kWh. Which results in the following characteristic values of the components installed. The rotational velocity of the waterjet and that of the design points of the electric motor catalogue match (less than 1% difference), so a gearbox is not needed. To reduce the weight of the electric motor the rotational velocity can be increased, but the weight increase of the addition of a gearbox does not counteract the weight savings of the electric motor so no gearbox is selected.

Component	Size	Weight [kg]	Volume [m^3]
Waterjet	2x 720 mm	3719	8.272
EM	2x 570 kW	7674	0.415
Battery Pack	3793 kWh	34171	39.916
Total		45564	48.603
Difference		+10765	+2.965

Table 6.4: Weight and volume of the battery propulsion system

Looking at the sizing of the components the following results were evaluated. The additional weight introduced by the propulsion system increases the draft of the vessel by 0.089 m which increases the resistance by 14.8%, which increases the energy requirement by 156 kWh. This extra resistance increases the power required to 650 kW per jet, which increases the weight by 10.8%. When multiple iterations are established, the solution will be stated as converged when the weight increase is less than 1% which results in the following size, weight and volume of the components

Component	Size	Weight [kg]	Volume [m^3]
Waterjet	2x 720 mm	3719	8.272
EM	2x 709 kW	9042	0.516
Batteries	4538 kWh	41225	48.168
Total		53986	56.956
Difference		+19187	+11.318

Table 6.5: Weight and volume of the battery propulsion system

Year	Waterjet	EM	Battery	Electricity	Total	NPV
2023	€542 756	€438 339	€3 660 800		€4 641 895	€4 641 895
2024	€87 840	€21 181		€1 184 580	€1 293 600	€1 358 280
2025	€87 840	€21 181		€1 184 580	€1 293 600	€1 426 194
2026	€87 840	€21 181		€1 184 580	€1 293 600	€1 497 504
2027	€87 840	€21 181		€1 184 580	€1 293 600	€1 572 379
2028	€87 840	€21 181		€1 184 580	€1 293 600	€1 650 998
2029	€87 840	€21 181		€1 184 580	€1 293 600	€1 733 548
2030	€87 840	€21 181		€1 184 580	€1 293 600	€1 820 226
2031	€87 840	€21 181		€1 184 580	€1 293 600	€1 911 237
2032	€87 840	€21 181		€1 184 580	€1 293 600	€2 006 799
2033	€87 840	€21 181	€3 660 800	€1 184 580	€4 954 400	€8 070 196
2034	€87 840	€21 181		€1 184 580	€1 293 600	€2 212 496
2035	€87 840	€21 181		€1 184 580	€1 293 600	€2 323 120
2036	€87 840	€21 181		€1 184 580	€1 293 600	€2 439 276
2037	€87 840	€21 181		€1 184 580	€1 293 600	€2 561 240
2038	€87 840	€21 181		€1 184 580	€1 293 600	€2 689 302
2039	€87 840	€21 181		€1 184 580	€1 293 600	€2 823 767
2040	€87 840	€21 181		€1 184 580	€1 293 600	€2 964 956
2041	€87 840	€21 181		€1 184 580	€1 293 600	€3 113 203
2042	€87 840	€21 181		€1 184 580	€1 293 600	€3 268 864
2043	€87 840	€21 181	€3 660 800	€1 184 580	€4 954 400	€13 145 499
2044	€87 840	€21 181		€1 184 580	€1 293 600	€3 603 922
2045	€87 840	€21 181		€1 184 580	€1 293 600	€3 784 118
2046	€87 840	€21 181		€1 184 580	€1 293 600	€3 973 324
2047	€87 840	€21 181		€1 184 580	€1 293 600	€4 171 990
2048	€87 840	€21 181		€1 184 580	€1 293 600	€4 380 590
Total					€44 303 503	€85 144 924

Table 6.6: LCC of the battery-driven vessel with the energy storage for two trips

Evaluating the LCC (which is given in table 6.6) it can be seen that the cost has increased tremendously. It has increased by 184%. To see if other propulsors can end in a cheaper solution the trend in resistance when the weight increases has to be investigated. When looking at the two other hulls' resistance, the base hull has an increase in resistance of 14.1% and the propeller hull 15.1%. This difference is 1% which is negligible when looking at the resistance trend with increasing weight. Additionally, a change in propulsor for weight-saving purposes will not result in a solution either, since the weight of the propulsor is a small part of the weight of the overall propulsion system. To result in an economically feasible solution the trip will be reduced to just one trip instead of a return. The following sizing is the result of that, one trip requires 1293 kWh at the original weight including sea margin and depth of discharge the battery requires 1897 kWh of storage capacity. The resulting weight is 28483 kg, which is lower than the reference case, so the resistance will not increase, making it a feasible solution. The resulting propulsion system render, SLD, DSM and LCC are given in figures 6.4, 6.5, 6.6 and table 6.7 respectively.

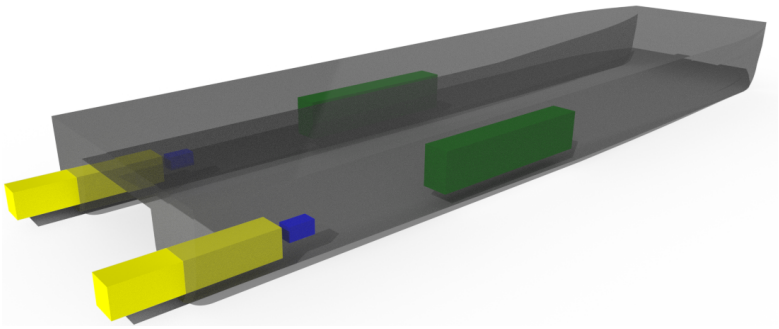

Figure 6.4: Render of the block representation of the battery-powered vessel
Waterjet: Yellow Battery Pack: Dark Green
Electric motor: Blue

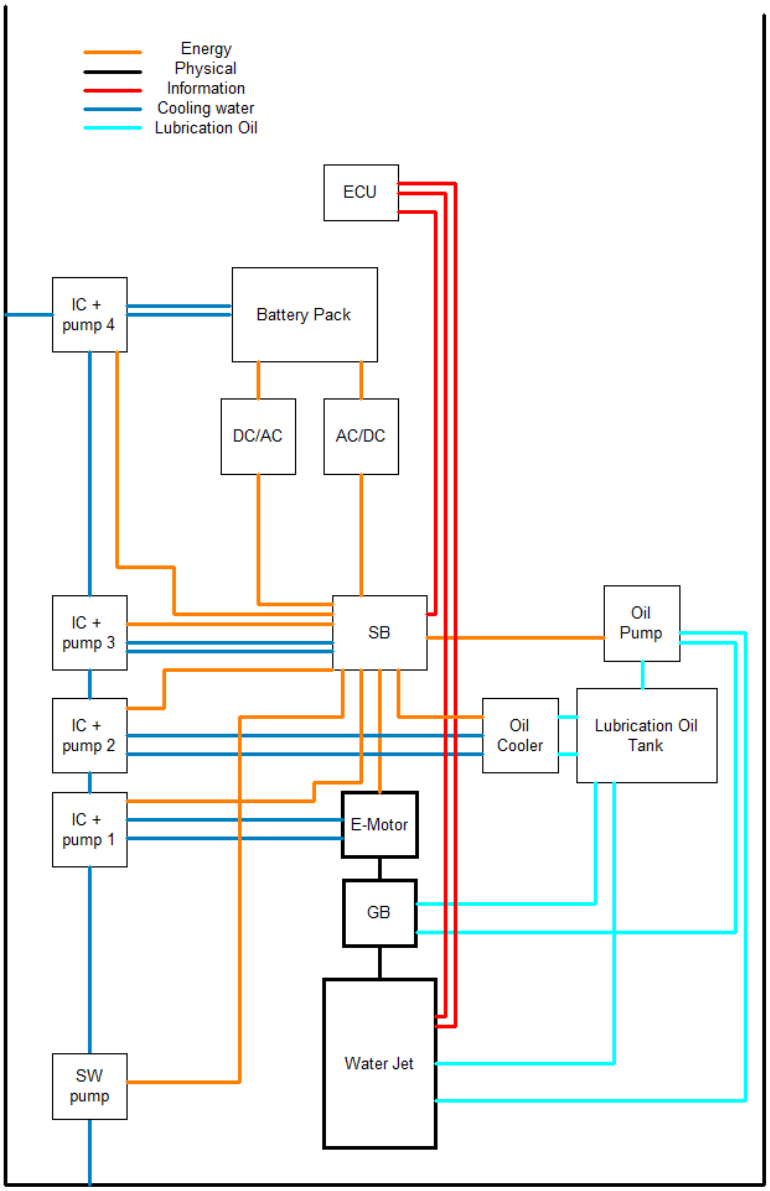

Figure 6.5: Battery driven electrical architecture

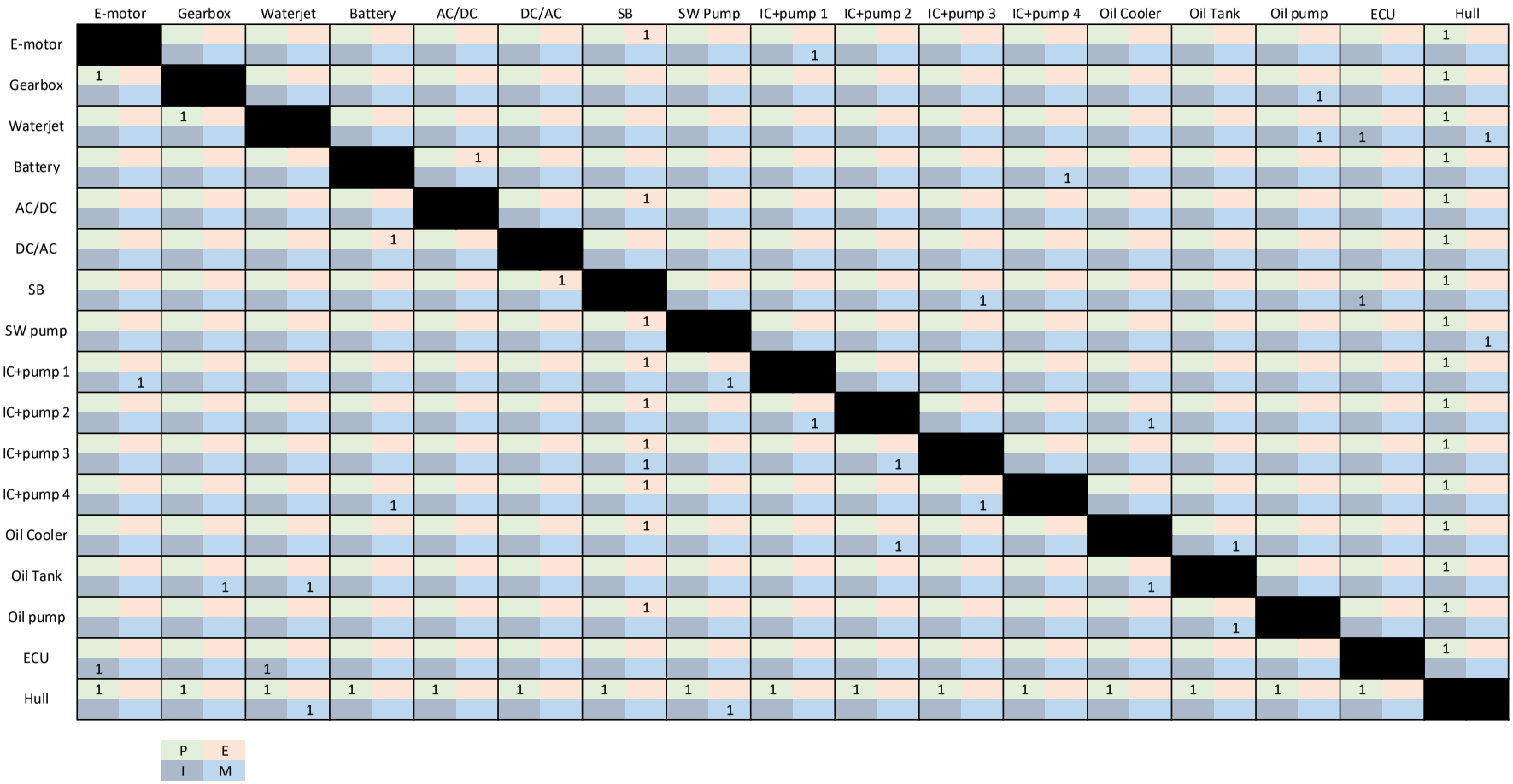

Figure 6.6: Battery driven vessel DSM, resulting in 73 connections with a total weight of 233 with an average connection weight of 3.19.

Year	Waterjet	EM	Battery	Electricity	Total	NPV
2023	€542 756	€353 230	€1 517 600		€2 413 586	€2 413 586
2024	€87 840	€17 068		€491 073	€595 981	€625 780
2025	€87 840	€17 068		€491 073	€595 981	€657 069
2026	€87 840	€17 068		€491 073	€595 981	€689 922
2027	€87 840	€17 068		€491 073	€595 981	€724 418
2028	€87 840	€17 068		€491 073	€595 981	€760 639
2029	€87 840	€17 068		€491 073	€595 981	€798 671
2030	€87 840	€17 068		€491 073	€595 981	€838 604
2031	€87 840	€17 068		€491 073	€595 981	€880 535
2032	€87 840	€17 068		€491 073	€595 981	€924 561
2033	€87 840	€17 068	€1 517 600	€491 073	€2 113 581	€3 442 800
2034	€87 840	€17 068		€491 073	€595 981	€1 019 329
2035	€87 840	€17 068		€491 073	€595 981	€1 070 295
2036	€87 840	€17 068		€491 073	€595 981	€1 123 810
2037	€87 840	€17 068		€491 073	€595 981	€1 180 001
2038	€87 840	€17 068		€491 073	€595 981	€1 239 001
2039	€87 840	€17 068		€491 073	€595 981	€1 300 951
2040	€87 840	€17 068		€491 073	€595 981	€1 365 998
2041	€87 840	€17 068		€491 073	€595 981	€1 434 298
2042	€87 840	€17 068		€491 073	€595 981	€1 506 013
2043	€87 840	€17 068	€1 517 600	€491 073	€2 113 581	€5 607 958
2044	€87 840	€17 068		€491 073	€595 981	€1 660 380
2045	€87 840	€17 068		€491 073	€595 981	€1 743 399
2046	€87 840	€17 068		€491 073	€595 981	€1 830 568
2047	€87 840	€17 068		€491 073	€595 981	€1 922 097
2048	€87 840	€17 068		€491 073	€595 981	€2 018 202
Total					€20 348 300	€38 778 885

Table 6.7: LCC of the electric battery drive propulsion system

To summarize the battery-powered vessel's result, the values of the performance indicators are given in table 6.8. Two concept propulsion systems are given. One system with the battery pack size based on a return trip operation, and the second system based on one trip operation before recharging. The vessel with the battery pack for a return trip is not feasible due to the enormous costs related to the oversizing of the battery pack and electric motors. When the number of trips is reduced to a single trip the solution will be feasible based on all performance indicators.

System	Volume [m^3]	Weight [kg]	NPV	Modularity	Emissions
Battery drive 2 trips	56.956	53986	€85 144 924		
Battery drive 1 trip	28.655	28483	€38 778 885	233	96.9

Table 6.8: Results battery driven system

6.3. Methanol fuelled ICE

For the methanol-fueled ICE concept, one ICE connected to a generator per demi-hull is installed and connected to the electrical architecture. The following values of the sizing, weight and volume are given in table 6.9

Component	Size	Weight [kg]	Volume [m^3]
Waterjet	2x 720 mm	3719	8.272
ICE	2x 780 kW	26781	35.657
E-Motor	2x 570 kW	7674	0.414
Electric generator	2x 780 kW	9677	0.568
Methanol	6.6 m^3	5178	6.600
Total		53029	51.511
Difference		+18230	+5.873

Table 6.9: Weight and volume of the methanol-driven electrical architecture

The additional weight has an impact on the resistance and the power required. The weight increase is 52.4%, which increases the resistance by 24.6%. Since the increase in resistance is lower than the increase in weight, the solution will converge. After another iteration, the weight increase was 9.1% and the resistance increase was 7.7%. Due to the low difference, the solution will converge, however, the energy expenditure will be excessive. This will not be the desired results regarding emissions. Additionally, after the second iteration, the LCC had increased by over 100%. Due to the excessive fuel requirements and costs this concept design will not be feasible.

To still take advantage of the most promising alternative fuel the direct drive architecture shown in figure 6.2 with a methanol-fuelled ICE can give a solution. Due to the efficiency increase of a methanol-fueled ICE (maximum of 51%), the energy expenditure is 2491 kWh. When the solution has converged with a maximum weight increase of 1%, table 6.12 gives the result of the size of the components including the weight and volume. Subsequently, in table 6.11 the LCC of the direct drive methanol propulsion system is given.

Component	Size	Weight [kg]	Volume [m^3]
Waterjet	2x 720 mm	3719	8.272
ICE	2x 691 kW	23725	31.589
ICE aux	133 kW	2283	3.040
Gearbox	2x 691 kW	2764	1.626
Generator	133 kW	1142	0.048
Methanol		5180	6.603
Total		38813	51.178
Difference		+4014	+3.490

Table 6.10: Weight and volume of the direct drive methanol system

Year	Waterjet	ICE + ICE aux	Gearbox	EM	Fuel	Total	NPV
2023	€542 756	€813 852	€51 200	€42 827	€2 506	€1 453 142	€1 453 142
2024	€87 840	€44 654	€3 801	€2 069	€902 260	€1 040 624	€1 092 656
2025	€87 840	€44 654	€3 801	€2 069	€895 819	€1 034 184	€1 140 188
2026	€87 840	€44 654	€3 801	€2 069	€892 102	€1 030 467	€1 192 894
2027	€87 840	€44 654	€3 801	€2 069	€891 156	€1 029 520	€1 251 388
2028	€87 840	€44 654	€3 801	€2 069	€891 852	€1 030 217	€1 314 847
2029	€87 840	€44 654	€3 801	€2 069	€895 376	€1 033 740	€1 385 311
2030	€87 840	€44 654	€3 801	€2 069	€900 714	€1 039 079	€1 462 088
2031	€87 840	€44 654	€3 801	€2 069	€907 328	€1 045 692	€1 544 963
2032	€87 840	€44 654	€3 801	€2 069	€913 836	€1 052 200	€1 632 308
2033	€87 840	€44 654	€3 801	€2 069	€917 662	€1 056 026	€1 720 156
2034	€87 840	€44 654	€3 801	€2 069	€918 175	€1 056 539	€1 807 040
2035	€87 840	€44 654	€3 801	€2 069	€913 520	€1 051 885	€1 889 034
2036	€87 840	€44 654	€3 801	€2 069	€909 129	€1 047 493	€1 975 205
2037	€87 840	€44 654	€3 801	€2 069	€903 659	€1 042 024	€2 063 136
2038	€87 840	€44 654	€3 801	€2 069	€899 242	€1 037 606	€2 157 108
2039	€87 840	€44 654	€3 801	€2 069	€891 616	€1 029 980	€2 248 317
2040	€87 840	€44 654	€3 801	€2 069	€882 478	€1 020 842	€2 339 789
2041	€87 840	€44 654	€3 801	€2 069	€870 632	€1 008 996	€2 428 269
2042	€87 840	€44 654	€3 801	€2 069	€862 283	€1 000 647	€2 528 585
2043	€87 840	€44 654	€3 801	€2 069	€854 722	€993 087	€2 634 955
2044	€87 840	€44 654	€3 801	€2 069	€845 953	€984 317	€2 742 271
2045	€87 840	€44 654	€3 801	€2 069	€838 340	€976 704	€2 857 115
2046	€87 840	€44 654	€3 801	€2 069	€830 017	€968 382	€2 974 408
2047	€87 840	€44 654	€3 801	€2 069	€821 405	€959 770	€3 095 354
2048	€87 840	€44 654	€3 801	€2 069	€813 885	€952 249	€3 224 654
Total						€26 975 412	€52 155 179

Table 6.11: LCC of the direct MeOH drive propulsion system

To summarize the methanol drive results the values are given in table 6.12. As can be seen, the more modular propulsion system due to the electrical architecture is not feasible due to the weight required to facilitate the architecture, these results are after two iterations so a technically feasible solution was not yet achieved. The weight increase results in a resistance increase that will increase the energy and power required. This circle results in oversized components which will result in high cost, which makes it not feasible. To take advantage of the most promising alternative fuel methanol a direct drive architecture has to be selected to come to a feasible solution.

System	Volume [m^3]	Weight [kg]	NPV	Modularity	Emissions
Electric drive MeOH	64.561	66293	€69 148 893	257	
Direct drive MeOH	51.178	38813	€52 155 179	266	208.24 kg

Table 6.12: Results battery driven system

6.4. Hydrogen PEMFC

To start the PEMFC hydrogen system the components needs to be sized. Preferably, to maximize the efficiency of the FC, it has to be operated at a constant power output (Maleki Bagherabadi et al., 2022). To facilitate the power fluctuations in the operational profile an additional battery pack is added to the system. To size the fuel cell an average power output required is calculated which comes down to 963 kW. The difference in energy required and delivered energy by the fuel cell is calculated summed and used to size the battery pack. When the energy requirement is higher than the delivered energy of the FC, the battery pack will deliver that energy. When the energy requirement is lower the FC will charge the batteries. Due to the sum of the differences the size of the battery pack can be determined. For the FC a sea margin of 10% is taken, and the same for the battery including the extra power to come to a DoD of 75%. To fully take advantage of the FC's high efficiency, the operational load will be set to operate at an efficiency of 60%, which is at 80% load. The choice has been made to store compressed hydrogen at 350 bar since the limiting factor is not the volume onboard this particular vessel.

Component	Size	Weight [kg]	Volume [m^3]
Waterjet	2x 720 mm	3719	8.272
FC	2x 600 kW	6000	11.881
EM	2x 570 kW	7674	0.414
Batteries	642 kWh	5910	6.905
Hydrogen		432	18.541
Total		23735	46.013
Difference		-11064	+0.375

Table 6.13: Weight and volume FC powered propulsion system

The resulting system is significantly lighter which makes it a feasible solution. To visualize the system the following render is made with the single-line diagram, corresponding DSM and LCC calculation.

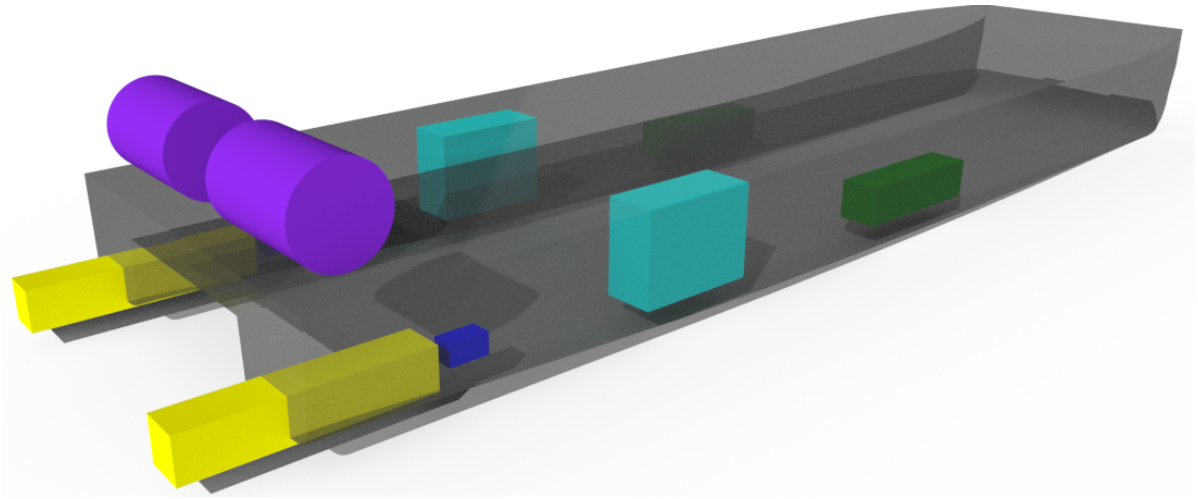

Figure 6.7: Representation of the FC system onboard

Waterjet:	Yellow	Battery Pack:	Dark Green
Electric motor:	Blue	Fuel Cell:	Cyan
Hydrogen storage:	Magenta		

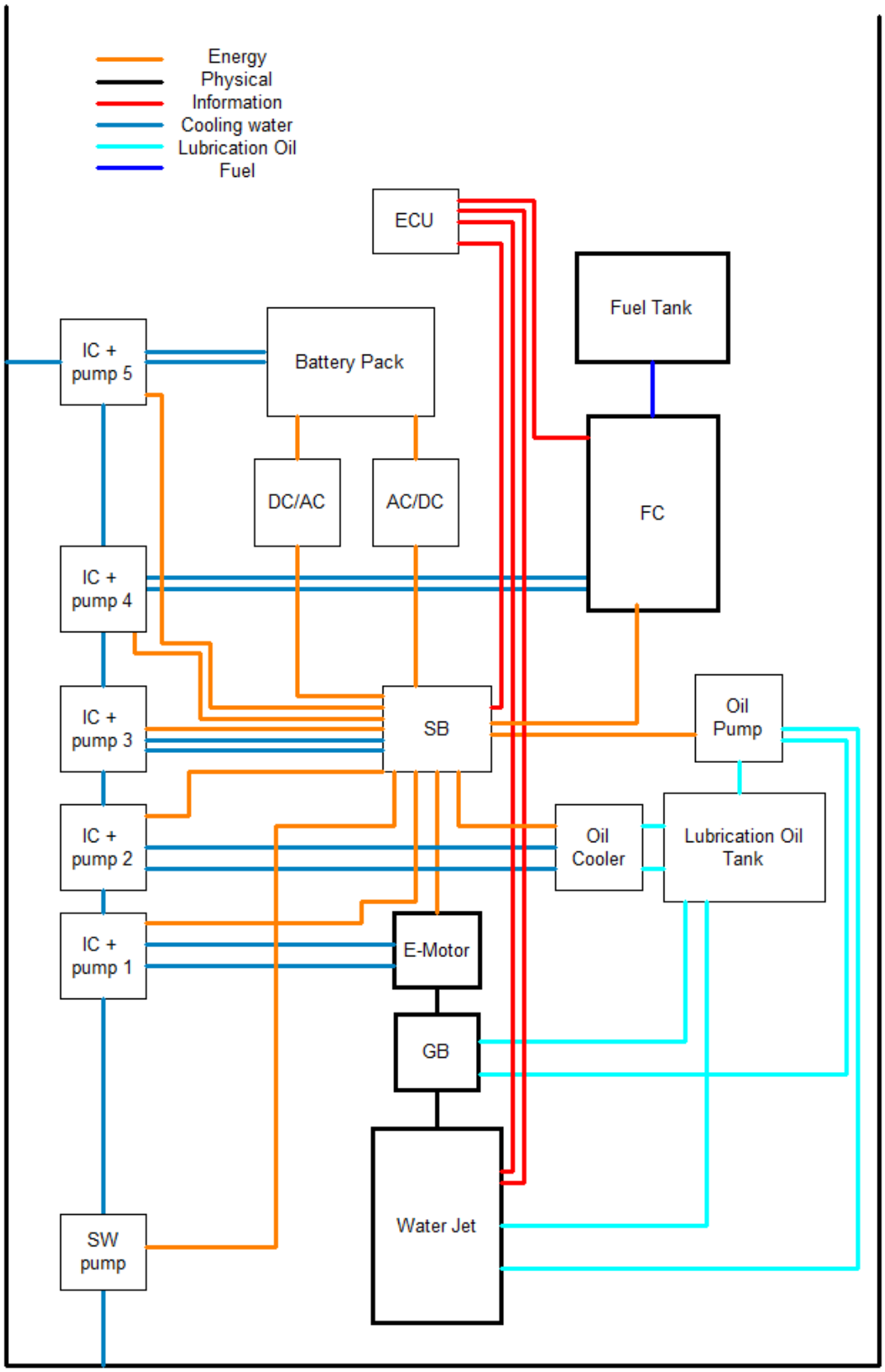

Figure 6.8: Electrical architecture with PEMFC and battery pack single-line diagram

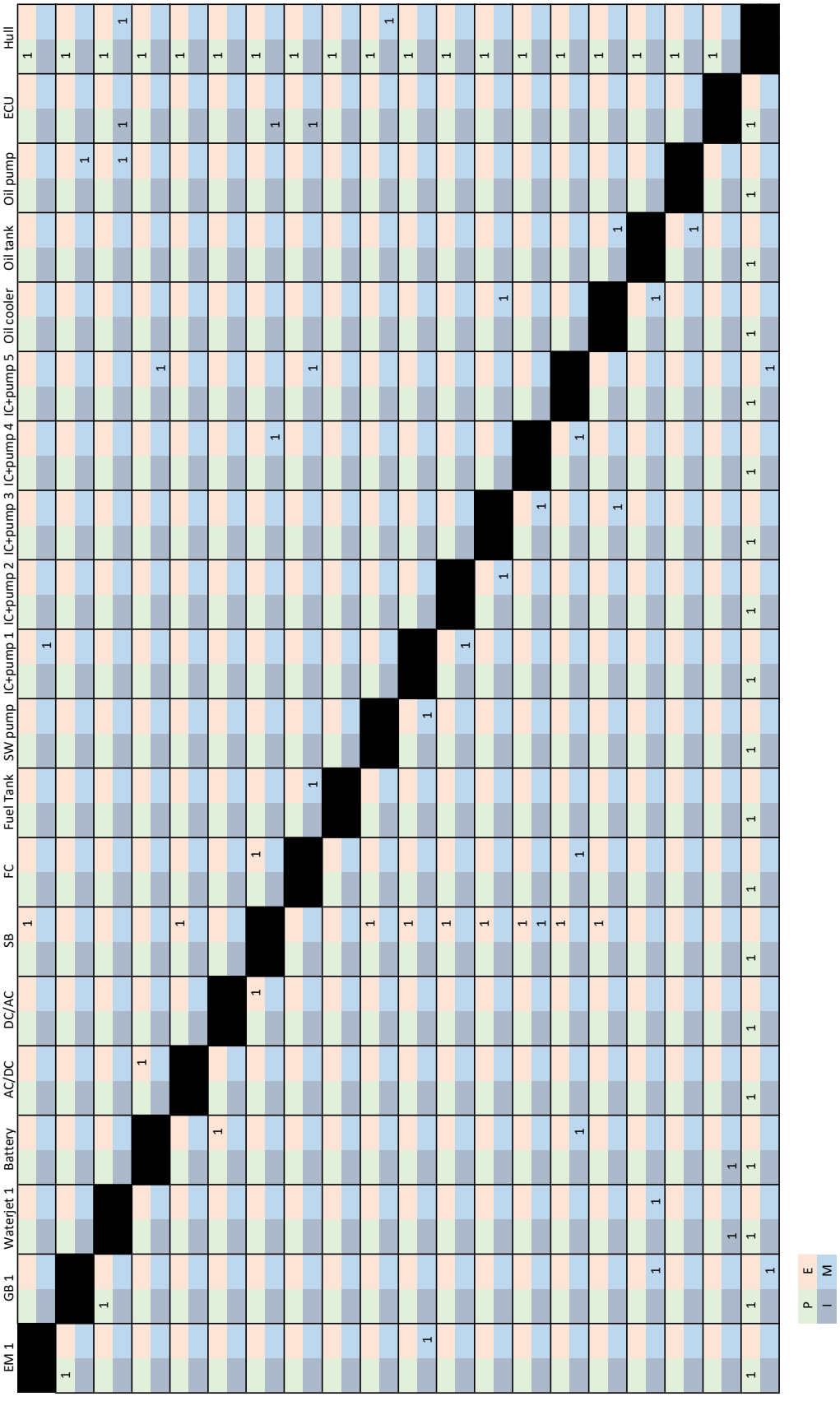

Figure 6.9: Fuel cell driven hybrid drive, with the total connections being 85, with 272 as the weighted connections resulting in 3.2 as the average connection weight.

For the lifecycle costing the FC needs to be replaced as well. In Taljegard et al. (2014) it is mentioned that for every 5^{th} or 6^{th} year an additional investment of 33% of the original investment cost needs to be made.

Year	Waterjet	EM	Battery	FC	Hydrogen	Total	NPV
2023	€542 756	€353 230	€1 517 600	€1 692 000	€25 084.80	€4 105 586	€4 105 586
2024	€87 840	€17 068		€115 632	€136 785.25	€357 325	€375 192
2025	€87 840	€17 068		€115 632	€137 664.34	€358 204	€394 920
2026	€87 840	€17 068		€115 632	€138 549.10	€359 089	€415 691
2027	€87 840	€17 068		€115 632	€139 382.93	€359 923	€437 489
2028	€87 840	€17 068		€673 992	€140 658.06	€919 558	€1 173 615
2029	€87 840	€17 068		€115 632	€143 740.85	€364 281	€488 171
2030	€87 840	€17 068		€115 632	€146 970.75	€367 511	€517 125
2031	€87 840	€17 068		€115 632	€150 704.18	€371 244	€548 497
2032	€87 840	€17 068		€115 632	€154 683.79	€375 224	€582 095
2033	€87 840	€17 068	€1 517 600	€673 992	€157 523.23	€2 454 023	€3 997 345
2034	€87 840	€17 068		€115 632	€159 097.42	€379 637	€649 309
2035	€87 840	€17 068		€115 632	€160 911.82	€381 452	€685 033
2036	€87 840	€17 068		€115 632	€162 949.79	€383 490	€723 127
2037	€87 840	€17 068		€115 632	€164 753.93	€385 294	€762 856
2038	€87 840	€17 068		€673 992	€166 501.48	€945 402	€1 965 422
2039	€87 840	€17 068		€115 632	€168 246.22	€388 786	€848 672
2040	€87 840	€17 068		€115 632	€169 979.63	€390 520	€895 078
2041	€87 840	€17 068		€115 632	€171 730.02	€392 270	€944 045
2042	€87 840	€17 068		€115 632	€173 503.04	€394 043	€995 727
2043	€87 840	€17 068	€1 517 600	€673 992	€175 103.50	€2 471 604	€6 557 900
2044	€87 840	€17 068		€115 632	€175 317.80	€395 858	€1 102 845
2045	€87 840	€17 068		€115 632	€175 311.45	€395 852	€1 157 969
2046	€87 840	€17 068		€115 632	€175 305.11	€395 845	€1 215 848
2047	€87 840	€17 068		€115 632	€175 298.76	€395 839	€1 276 620
2048	€87 840	€17 068		€115 632	€175 292.42	€395 832	€1 340 429
Total						€18 883 692	€34 156 604

Table 6.14: LLC of the FC-powered propulsion system

To summarize the results of the PEMFC-powered vessel, table 6.15 represents the performance indicators. What can be derived from these values is that the weight is significantly reduced which has a positive effect on the resistance. Additionally, the emission reduction with grey hydrogen is already 73.6%, to further achieve the goal of 80% reduction a solution solution will be blue and green hydrogen. This will have an impact on the LCC. When blue hydrogen is taken the LCC will rise by 8.6%, but the goal of 80% emission reduction will be achieved.

System	Volume [m^3]	Weight [kg]	NPV	Modularity	Emissions
H2 PEMFC	46.013	23735	€34 156 604	272	249.6

Table 6.15: Performance indicators PEMFC powered propulsion system

6.5. Comparison

The comparison will be done on the basis of feasibility, LCC, modularity and emissions. Each of the individual solutions will be compared to the baseline solution. In the table below each concept propulsion system is listed and compared. When the system is coloured red the system does not converge to a feasible solution.

System	Volume [m^3]	Weight [kg]	NPV	Modularity	Emissions
MDO direct drive	45.638	34799	€30 009 751	266	944.38
Battery drive 2 trips	56.956	53986	€85 144 924	233	
Battery drive 1 trip	28.655	28483	€38 778 885	233	96.9
MeOH Electric	64.562	66293	€69 148 893	257	
MeOH Direct	51.178	38813	€52 155 179	266	208.24
H2 PEMFC	46.013	23735	€34 156 604	272	249.6

Table 6.16: Comparison of the performance indicators of the different systems

Looking at the comparison of the different concept types, the best solution regarding weight and costs is H^2 PEMFC with battery solutions. The best performing on modularity would be the battery system purely based on the number of weighted connections, if the bus modularity is taken it can be seen that the SB onboard would function as the bus so the addition of the FC system has a low impact on the overall architecture of the system, which is exactly the advantage of modularity onboard. The costs related to the PEMFC propulsion system are 13.8% higher than the reference vessel, but the best solution to reduce the emissions by >80%, since the option to use blue or green hydrogen is possible to be used without changes to the system. The difference in technology readiness is also in favour of the hydrogen-fuelled FC (Law et al., 2021). For the battery-type vessel, the onshore requirements are more significant to realize than the hydrogen. The power required to charge the vessel in its port time is 2.59 MW, which is required on both ends of the operation. The H^2 fuel cell operation will need to be fuelled once per day of operating which will reduce the investment costs for the fuelling equipment. To further give a comparison of the different propulsion systems the following spider chart is made. In figure 6.10 it can be seen that the reduction of emissions is a success for all three feasible propulsion systems. The drawback is that the systems are all more expensive, but on the other hand lighter and more modular. Modularity can not be accurately seen in this figure due to the nature of measuring modularity. It can be seen that on the most limiting performance indicators which are weight, emissions and costs, the H2 PEMFC system performs the best.

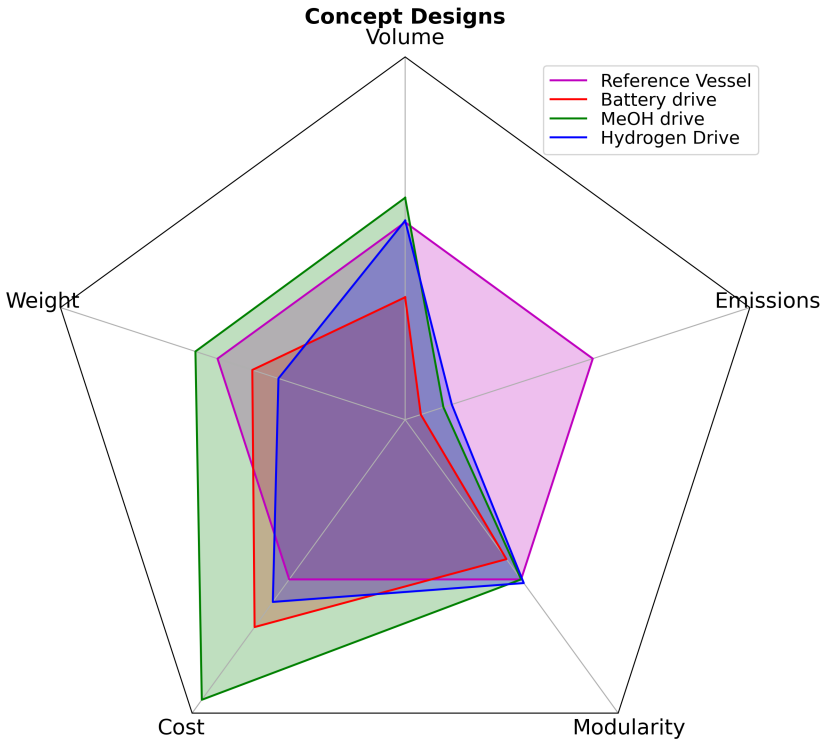

Figure 6.10: Direct comparison of propulsion systems

7

Discussion and recommendations

Looking at the results the best solution for this application is electrical architecture powered by a PEMFC and a battery pack. The limitation is the alternative fuel infrastructure. The more technologically-ready solution is the battery drive solution. The limitation of that is that it requires two charging facilities at both ends of the ferry operation. The objective to both increase modularity in design and decrease emissions was concluded to be difficult due to the limiting factor being weight.

Relating to the previous findings in the literature can be seen that the most promising alternative fuel was methanol. The issue relating is the combination with the electrical architecture. When the direct drive is used in combination with the methanol-fuelled ICE the cost related to the propulsion system is quite some margin higher (52.4% higher) than the reference case. On the contrary, the installation costs of the hydrogen-fuelled FC is higher but the total LCC costs are relatively low increase of 15.1%.

The advantages and the novelty of this thesis are the combination of multiple first principle models already defined and the addition of first principle models based on data to fully understand the energy chain and sizing of the individual components in a vessel's propulsion system. The application of this method is tested on a mid-speed vessel with a ferry-type operational profile. The method is not limited to this type of vessel, the modular nature of the method gives the opportunity to use other first principle models to suit the vessel type. That mostly applies to the resistance calculation.

The method used has its limitations as first principle models are used. Therefore, the results do not completely represent the real value. In this study, however, these values are used to compare different designs, therefore the results are still valid. To get more detailed results individual components need to be chosen (such as waterjet type and propeller type). This is done to bridge the gap between concept design and detail design.

Future research recommendations can be to verify the different components of the model to test results to see what the level of accuracy is and if it can be increased by differing values that are assumed based on literature. To see if the framework can also work on different types of vessels and different operational profiles, different test cases can be done to verify the method of performance indicator analysis and evaluate the accuracy of the different parameters given.

8

Conclusion

This thesis aims to create a framework to design and evaluate propulsion systems in a modular fashion, thereby taking the vessel's requirements and operational profile dependencies into account. To take full benefit of the state-of-the-art technologies the goal is to create these solutions with the lowest emissions possible. To encapture all the goals of this thesis the following main research question was made: "How can a propulsion system for mid-speed ferries be made modular and be made to lower or eliminate emissions?". Supporting this main question the sub-questions are stated as follows:

- What propulsor would be best for mid-speed vessels regarding modularity and emissions?
- What propulsion architecture would facilitate modularity in design and emissions reduction?
- Which future technologies would be feasible and best suited for mid-speed vessels?

Looking at the different results, the best propulsor type is the waterjet for the mid-speed ferry-type vessel due to the high open water efficiency and the best option to create a propulsive module. This can be done by combining the electric motor on the skid to create a propulsor module. Regarding the propulsion architecture, the electrical architecture enables multiple energy converters and energy storage methods increasing the modularity of the system. The issue with the electrical architecture is the weight. Looking at combining a gen-set to the electrical system the weight required is too large to come to a feasible solution. The alternative energy storage of converters such as a FC and batteries comes to a feasible solution with a reduction in emissions >80% with the combination of blue or green hydrogen. To take advantage of the ICE in the mid-speed vessel range the direct drive architecture needs to be used to achieve a feasible solution. The parallel hybrid drive can be used as well, but looking at modularity it is not the best solution due to the lack of scalability within the architecture. Including alternative fuels in the system is not an issue since volume and area are not the limiting factor, weight onboard is. For the mid-speed range the increase in depth and wet surface area results in a large increase in resistance that will be detrimental to the propulsion system.

The framework created combines different first principle models to swiftly evaluate different options for propulsion systems. The first step of the framework is to define the resistance of the vessel via a regression model that only requires a few hull parameters. Secondly, define the operational profile and use the first principle models to evaluate the power required. Furthermore, the framework defines a method to calculate the energy required which will lead to the emissions. Lastly, the framework defines a method to estimate the volume, weight and LCC for the propulsion system. For this thesis, the focus was on mid-speed ferry operation. The framework created can be seen as a modular framework. For different vessel types and different operational profiles, the same framework can be used but with a different model suited for that vessel type and operational profile. To bridge the gap from conceptual design to detailed design, each individual step can be further worked out in detail. The resistance assumption can be more detailed with CFD or towing tank tests. For the efficiency estimation of the propulsor CFD can be done as well when a specific unit is selected. For the performance indicators, the specific weight size and cost can be included when a unit is selected after it is sized in the conceptual design phase.

Looking at future technologies it seems that the hydrogen PEMFC is the most promising technology since it is the lightest solution and the least expensive solution to reduce emissions. To eliminate

emissions the possibility is there to include blue or green hydrogen to reduce the emissions further. This would require that the vessel be supplied with compressed hydrogen which is not readily available.

References

Abdel-Rahman, A. A., Ibrahim, M. K., & Said, A. A. (1994). *An improvement of part load performance of diesel engines operating at constant speed conditions* (tech. rep.). Alexandria University Egypt. Alexandria. https://doi.org/10.1243/PIME_PROC_1994_208_005_02

Al-Falahi, M. D., Coleiro, J., Jayasinghe, S., Enshaei, H., Garaniya, V., Baguley, C., & Madawala, U. (2018). *Techno-Economic Feasibility Study of Battery-Powered Ferries* (tech. rep.).

Bae, C., & Kim, J. (2017). Alternative fuels for internal combustion engines. *Proceedings of the Combustion Institute*, *36*(3), 3389–3413. https://doi.org/10.1016/j.proci.2016.09.009

Baldwin, C. Y., & Clark, K. B. (2006). *"Modularity in the Design of Complex Engineering Systems" in Complex Engineered Systems* (D. Braha, A. A. Minai, & Y. Bar-Yam, Eds.; 1st ed.). Springer Berlin, Heidelberg. https://doi.org/https://doi.org/10.1007/3-540-32834-3

Ballard Power Systems. (2021). Fuel Cell Power for Marine Applications. https://www.ballard.com/docs/default-source/spec-sheets/fcwavetm-specification-sheet.pdf?sfvrsn=6e44dd80_16

Bhattacharyya, A., & Steen, S. (2014). Propulsive factors in waves: A comparative experimental study for an open and a ducted propeller. *Ocean Engineering*, *91*, 263–272. https://doi.org/10.1016/j.oceaneng.2014.09.020

Brix, J. E. (1993). *Manoeuvring technical manual*. Seehafen-Verl.

Bulten, N. (2006). *Numerical Analysis of a Waterjet Propulsion System* (tech. rep.).

Carlton, J. (2019). *Marine Propellers and Propulsion* (C. Bolger, Ed.; 4th ed.). Elsevier. https://doi.org/10.1016/C2014-0-01177-X

Denny, S. B., & Feller, A. R. (1979). *Waterjet Propulsor Performance Prediction in Planing Craft Application* (tech. rep.). David W. Taylor Naval Ship Research and Development Center. https://apps.dtic.mil/sti/pdfs/ADA075690.pdf

de Vos, P. (2018). *On early-stage design of vital distribution systems on board ships* (Doctoral dissertation). Delft University of Technology. Delft. https://doi.org/10.4233/uuid:eb604971-30b7-4668-ace0-4c4b60cd61bd

Doctors, L. J., Macfarlane, G. J., & Young, R. (2007). *A Study of Transom-Stern Ventilation* (tech. rep.). The University of New South Wales. Sydney. https://www.researchgate.net/publication/285534839

Duerr, P., & Von Ellenrieder, K. D. (2015). Scaling and Numerical Analysis of Nonuniform Waterjet Pump Inflows. https://doi.org/10.1109/JOE.2014.2339395

Engineering Toolbox. (2018). Methanol - Density and Specific Weight vs. Temperature and Pressure. https://www.engineeringtoolbox.com/methanol-density-specific-weight-temperature-pressure-d_2091.html

Eppinger, S. D., & Browning, T. R. (2012). *Design Structure Matrix Methods and Applications*. The MIT Press. https://doi.org/10.7551/mitpress/8896.001.0001

Erikstad, S. O. (2019). Design for Modularity. In *A holistic approach to ship design* (pp. 329–356). Springer International Publishing. http://link.springer.com/10.1007/978-3-030-02810-7_10

Eslamdoost, A., Larsson, L., & Bensow, R. (2018). Analysis of the thrust deduction in waterjet propulsion – The Froude number dependence. *Ocean Engineering*, *152*, 100–112. https://doi.org/10.1016/j.oceaneng.2018.01.037

European power price tracker. (2023). https://ember-climate.org/data/data-tools/europe-power-prices/

Fang, C., Cai, B. H., Ma, S. H., & Li, B. (2018). Simulation and Experimental Study on Flow and Heat Transfer of Ship Central Cooling System. *MATEC Web of Conferences*, *213*. https://doi.org/10.1051/matecconf/201821304001

Geertsma, R. D., Negenborn, R. R., Visser, K., & Hopman, J. J. (2017). Design and control of hybrid power and propulsion systems for smart ships: A review of developments. https://doi.org/10.1016/j.apenergy.2017.02.060

Geurts, K. (2009). *Resistance Prediction of Cruising Motor Catamarans* (Doctoral dissertation). Delft University of Technology. Delft. https://www.researchgate.net/publication/205117931

Giles, W., Dinham-Peren, T., Amaratunga, S., Vrijdag, A., & Partridge, R. (2010). *The Advanced WaterJet: Propulsor Performance and Effect on Ship Design* (tech. rep.).

Gohary, M. M. E., & Seddiek, I. S. (2013). Utilization of alternative marine fuels for gas turbine power plant onboard ships. *International Journal of Naval Architecture and Ocean Engineering*, *5*(1), 21–32. https://doi.org/10.2478/ijnaoe-2013-0115

Hans Klein Wout & Douwe Stapersma. (2002). *Design of Propulsion and Electric Power Generation Systems*. IMarEST.

Hansson, J., Månsson, S., Brynolf, S., & Grahn, M. (2019). Alternative marine fuels: Prospects based on multi-criteria decision analysis involving Swedish stakeholders. *Biomass and Bioenergy*, *126*, 159–173. https://doi.org/10.1016/j.biombioe.2019.05.008

Hekkenberg, R. G. (2014). *European Inland Waterway Navigation Conference 10-12* (tech. rep.).

Hölttä-Otto, K., Chiriac, N. A., Lysy, D., & Suk Suh, E. (2012). Comparative analysis of coupling modularity metrics. https://doi.org/10.1080/09544828.2012.701728

Hölttä-Otto, K., & de Weck, O. (2007). Degree of modularity in engineering systems and products with technical and business constraints. *Concurrent Engineering Research and Applications*, *15*(2), 113–125. https://doi.org/10.1177/1063293X07078931

Horton, G., Finney, H., Fischer, S., Sikora, I., McQuillen, J., Ash, N., & Shakeel, H. (2022). *Technological, Operational and Energy Pathways for Maritime Transport to Reduce Emissions Towards 2050* (tech. rep.). Ricardo Energy & Environment.

IMF. (2023). Inflation rate, average consumer prices. https://www.imf.org/external/datamapper/PCPIPCH@WEO/OEMDC/ADVEC/WEOWORLD/NLD

IMO. (2021). IMO's work to cut GHG emissions from ships. https://www.imo.org/en/MediaCentre/HotTopics/Pages/Cutting-GHG-emissions.aspx

Inal, O. B., Charpentier, J. F., & Deniz, C. (2021). Hybrid power and propulsion systems for ships: Current status and future challenges. https://doi.org/10.1016/j.rser.2021.111965

Inal, O. B., Dere, C., & Deniz, C. (2021). Onboard Hydrogen Storage for Ships: An Overview. *5th International Hydrogen Technologies Congress*. https://www.researchgate.net/publication/351982637

Jung, S., & Simpson, T. W. (2017). New modularity indices for modularity assessment and clustering of product architecture. *Journal of Engineering Design*, *28*(1), 1–22. https://doi.org/10.1080/09544828.2016.1252835

Kamal, I. M., Zürcher, K., Bose, N., Binns, J., Chai, S., & Davidson, G. (2015). *Powering for Medium Speed Wave-Piercing Catamarans comparing Waterjet and Screw Propeller Performance using Model Testing* (tech. rep.).

Kistner, L., Bensmann, A., Minke, C., & Hanke-Rauschenbach, R. (2023). Comprehensive techno-economic assessment of power technologies and synthetic fuels under discussion for ship applications. *Renewable and Sustainable Energy Reviews*, *183*. https://doi.org/10.1016/j.rser.2023.113459

Kistner, L., Schubert, F. L., Minke, C., Bensmann, A., & Hanke-Rauschenbach, R. (2021). Techno-economic and Environmental Comparison of Internal Combustion Engines and Solid Oxide Fuel Cells for Ship Applications. *Journal of Power Sources*, *508*. https://doi.org/10.1016/j.jpowsour.2021.230328

Lagemann, B., Seidenberg, T., Jürgenhake, C., Ove Erikstad, S., & Dumitrescu, R. (2021). *System alternatives for modular, zero-emission high-speed ferries* (tech. rep.). https://onepetro.org/snamefast/proceedings/FAST21/2-FAST21/D021S003R005/470671

Law, L. C., Foscoli, B., Mastorakos, E., & Evans, S. (2021). A comparison of alternative fuels for shipping in terms of lifecycle energy and cost. *Energies*, *14*(24). https://doi.org/10.3390/en14248502

Lijst emissiefactoren. (2023). https://www.co2emissiefactoren.nl/lijst-emissiefactoren/

Liu, J., & Hekkenberg, R. (2017). Sixty years of research on ship rudders: effects of design choices on rudder performance. *Ships and Offshore Structures*, *12*(4), 495–512. https://doi.org/10.1080/17445302.2016.1178205

Luckose, L., Hess, H., & Johnson, B. (2009). Fuel cell propulsion system for marine applications. *2009 IEEE Electric Ship Technologies Symposium*, 574–580. https://doi.org/10.1109/ESTS.2009.4906569

Maleki Bagherabadi, K., Skjong, S., & Pedersen, E. (2022). Dynamic modelling of PEM fuel cell system for simulation and sizing of marine power systems. *International Journal of Hydrogen Energy*, *47*(40), 17699–17712. https://doi.org/10.1016/j.ijhydene.2022.03.247

Marine Battery Sizing - Spear Power Systems Trident. (2019).

Methanol Institute. (2021). *MEASURING MARITIME EMISSIONS - Policy recommendations regarding GHG accounting of the maritime industry* (tech. rep.). https://www.methanol.org/wp-content/uploads/2021/08/Methanol-Institute-Measuring-Maritime-Emissions-Policy-Paper-August-2021.pdf

Molland, A., Wellicome, J., & Couser, P. (1994). *Resistance experiments on a systematic series of high speed displacement catamaran forms: variation of length-displacement ratio and breadth-draught ratio* (tech. rep.). University of Southampton.

Molland, A. F. (2008). *The Maritime Engineering Reference Book*. Elsevier. https://doi.org/10.1016/B978-0-7506-8987-8.X0001-7

Molland, A. F., Turnock, S. R., & Hudson, D. A. (2011). *Ship Resistance and Propulsion - Practical Estimation of Ship Propulsive Power*. Cambridge University Press.

Morrison, A. (2018). *A comparison of pumpjets and propellers for non-nuclear submarine propulsion* (tech. rep.).

Müller-Graf, B., Radojčić, D., & Simić, A. (1989). *Resistance and Propulsion Characteristics of the VWS Hard Chine Catamaran Hull Series '89* (tech. rep.). https://www.researchgate.net/publication/269100646

Neary, V. S., Previsic, M., Jepsen, R. A., Lawson, M. J., Yu, Y.-H., Copping, A. E., Fontaine, A. A., Hallett, K. C., & Murray, D. K. (2014). *Methodology for Design and Economic Analysis of Marine Energy Conversion (MEC) Technologies* (tech. rep.). Sandia National Laboratories. Albuquerque. https://doi.org/10.13140/RG.2.2.10201.95846

Oosterveld, M. (1970). *Wake Adapted Ducted Propellers* (tech. rep.).

Papanikolaou, A., Xing-Kaeding, Y., Strobel, J., Kanellopoulou, A., Zaraphonitis, G., & Tolo, E. (2020). Numerical and experimental optimization study on a fast, zero emission catamaran. *Journal of Marine Science and Engineering*, *8*(9). https://doi.org/10.3390/JMSE8090657

Salvador, F., Forza, C., & Rungtusanatham, M. (2002). *Modularity, product variety, production volume, and component sourcing: theorizing beyond generic prescriptions* (tech. rep.).

Shadidi, B., Najafi, G., & Yusaf, T. (2021). A review of hydrogen as a fuel in internal combustion engines. https://doi.org/10.3390/en14196209

Stapersma, D., & Vos, P. (2015). *Dimension prediction models of ship system components based on first principles - final version* (tech. rep.).

Stapersma, D. (2010a). *Lecture Notes: Diesel Engines, Volume 1* (tech. rep.). Delft University of Technology. Delft.

Stapersma, D. (2010b). *Lecture Notes: Diesel Engines, Volume 3* (tech. rep.). Delft University of Technology. Delft.

Strobel, J., Xing-Kaeding, Y., & Papanikolaou, A. (2020). *Calm Water Model Tests for a 30 m Catamaran* (tech. rep.). Hamburgische Schiffbau-Versuchsanstalt. Hamburg. https://tramproject.eu/

Sun, Y. K. (2020). Promising All-Solid-State Batteries for Future Electric Vehicles. https://doi.org/10.1021/acsenergylett.0c01977

Taljegard, M., Brynolf, S., Grahn, M., Andersson, K., & Johnson, H. (2014). Cost-effective choices of marine fuels in a carbon-constrained world: Results from a global energy model. *Environmental Science and Technology*, *48*(21), 12986–12993. https://doi.org/10.1021/es5018575

Tarhan, C., & Çil, M. A. (2021). A study on hydrogen, the clean energy of the future: Hydrogen storage methods. https://doi.org/10.1016/j.est.2021.102676

Transparency Market Research. (2023). Passenger Ferries Market Outlook 2031. https://www.transparencymarketresearch.com/passenger-ferries-market.html

Tunér, M., Aakko-Saksa, P., & Molander, P. (2018). *SUMMETH-Sustainable Marine Methanol Deliverable D3.1 Engine Technology, Research, and Development for Methanol in Internal Combustion Engines* (tech. rep.).

Tupper, E. C. (2013). Propulsion. In *Introduction to naval architecture* (5th ed., pp. 161–203). Elsevier. https://doi.org/10.1016/B978-0-08-098237-3.00008-4

Ulreich, S. (2022). *Fuelling the Fourth Propulsion Revolution An Opportunity for All In collaboration with Professor Dr* (tech. rep.). www.ics-shipping.org

Van Lieshout, T. P. S., De Jonge, V., Verbeek, R., Vredeveldt, A. W., & Finner, S. (2020). *Green Maritime Methanol: WP3 factsheet and comparison with diesel and LNG* (tech. rep.). www.tno.nl

van Terwisga, T. (1997). A Parametric Propulsion Prediction Method for Waterjet Driven Craft.

VEM. (2023). Product Catalogue.

Verbeek, R. (1992). Application of waterjets in highspeed craft. *Hydrodynamics: Computations, Model Tests and Reality*, 133–138.

Wang, H., Zhou, P., & Wang, Z. (2017). Reviews on current carbon emission reduction technologies and projects and their feasibilities on ships. *Journal of Marine Science and Application*, *16*(2), 129–136. https://doi.org/10.1007/s11804-017-1413-y

Wang, X., Zhu, J., & Han, M. (2023). Industrial Development Status and Prospects of the Marine Fuel Cell: A Review. *Journal of Marine Science and Engineering*, *11*(2), 238. https://doi.org/10.3390/jmse11020238

Waterjets Product Guide. (2017). https://www.wartsila.com/docs/default-source/product-files/gears-propulsors/waterjets/product-guide-o-p-modular-waterjet.pdf?sfvrsn=4

Weir, R. J. (1987). *Ducted Propeller Design and Analysis* (tech. rep.). Sandia National Laboratories. Albuquerque, New Mexico.

Wu, S., Miao, B., & Chan, S. H. (2022). Feasibility assessment of a container ship applying ammonia cracker-integrated solid oxide fuel cell technology. *International Journal of Hydrogen Energy*, *47*(63), 27166–27176. https://doi.org/10.1016/j.ijhydene.2022.06.068

Xing, H., Stuart, C., Spence, S., & Chen, H. (2021a). Fuel cell power systems for maritime applications: Progress and perspectives. *Sustainability (Switzerland)*, *13*(3), 1–34. https://doi.org/10.3390/su13031213

Xing, H., Stuart, C., Spence, S., & Chen, H. (2021b). Alternative fuel options for low carbon maritime transportation: Pathways to 2050. *Journal of Cleaner Production*, *297*. https://doi.org/10.1016/j.jclepro.2021.126651

Zhao, D., Zhang, Y., He, Q., Sun, C., & Bi, M. (2022). Hydrodynamic and Flow Field Characteristics of Water Jet Propulsion under Mooring Conditions. *Journal of Marine Science and Engineering*, *10*(7). https://doi.org/10.3390/jmse10070953

Zhou, Y., Pavesi, G., Yuan, J., & Fu, Y. (2022). A Review on Hydrodynamic Performance and Design of Pump-Jet: Advances, Challenges and Prospects. https://doi.org/10.3390/jmse10101514

Zhou, Y., Wang, L., Yuan, J., Luo, W., Fu, Y., Chen, Y., Wang, Z., Xu, J., & Lu, R. (2021). Comparative Investigation on Hydrodynamic Performance of Pump-Jet Propulsion Designed by Direct and Inverse Design Methods. *Mathematics*, *9*(4), 343. https://doi.org/10.3390/math9040343

A

Reference vessel

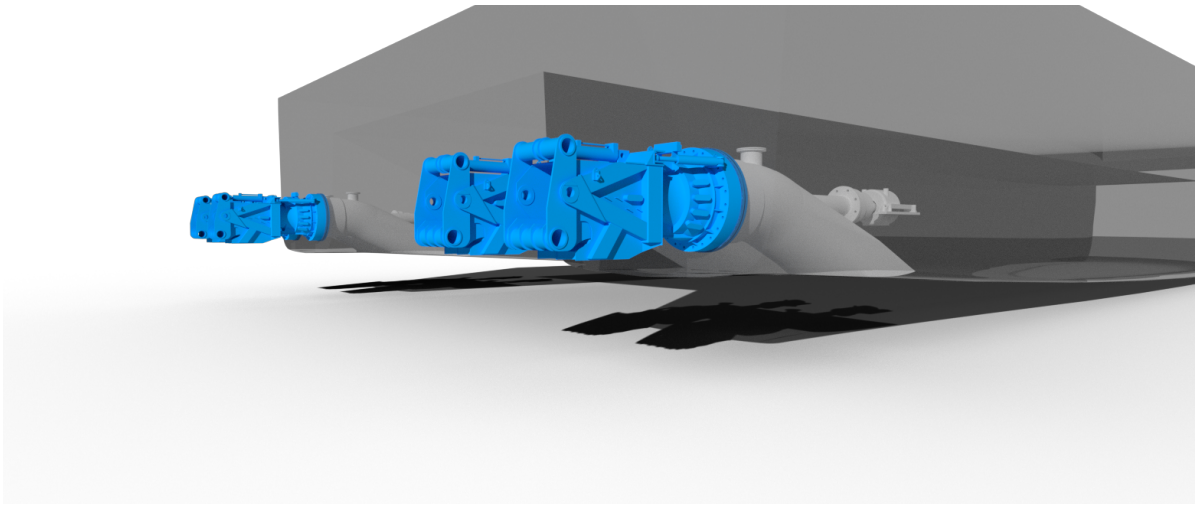

Figure A.1: Base hull with four waterjets representation

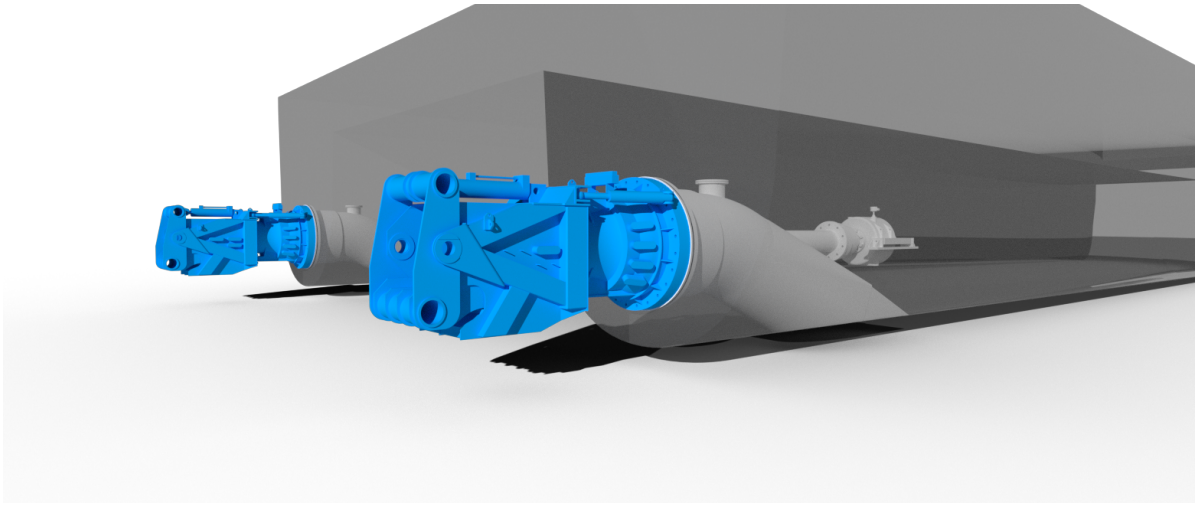

Figure A.2: Extended hull with two larger waterjets

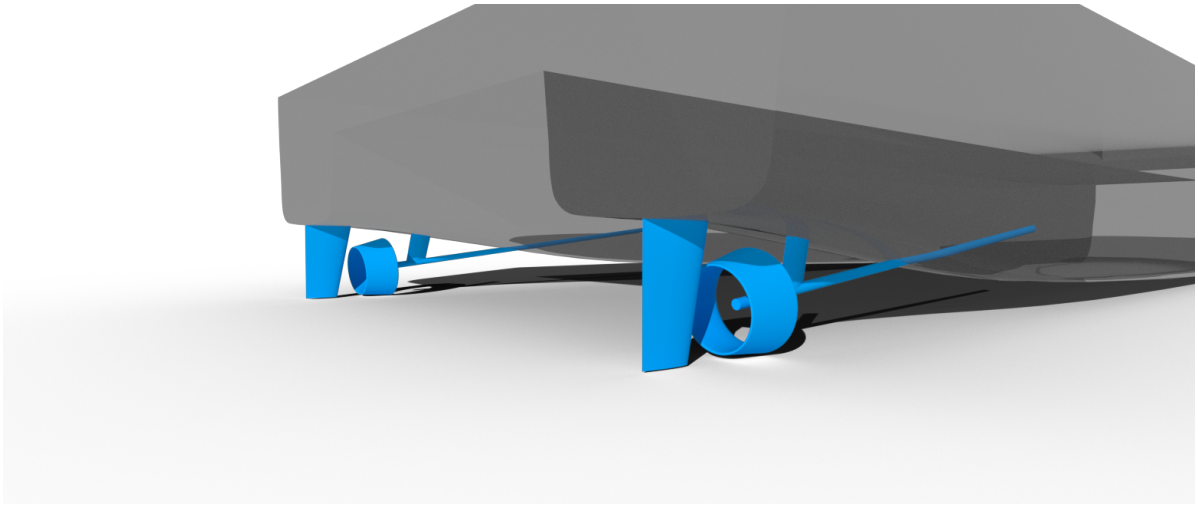

Figure A.3: Ducted Propeller hull

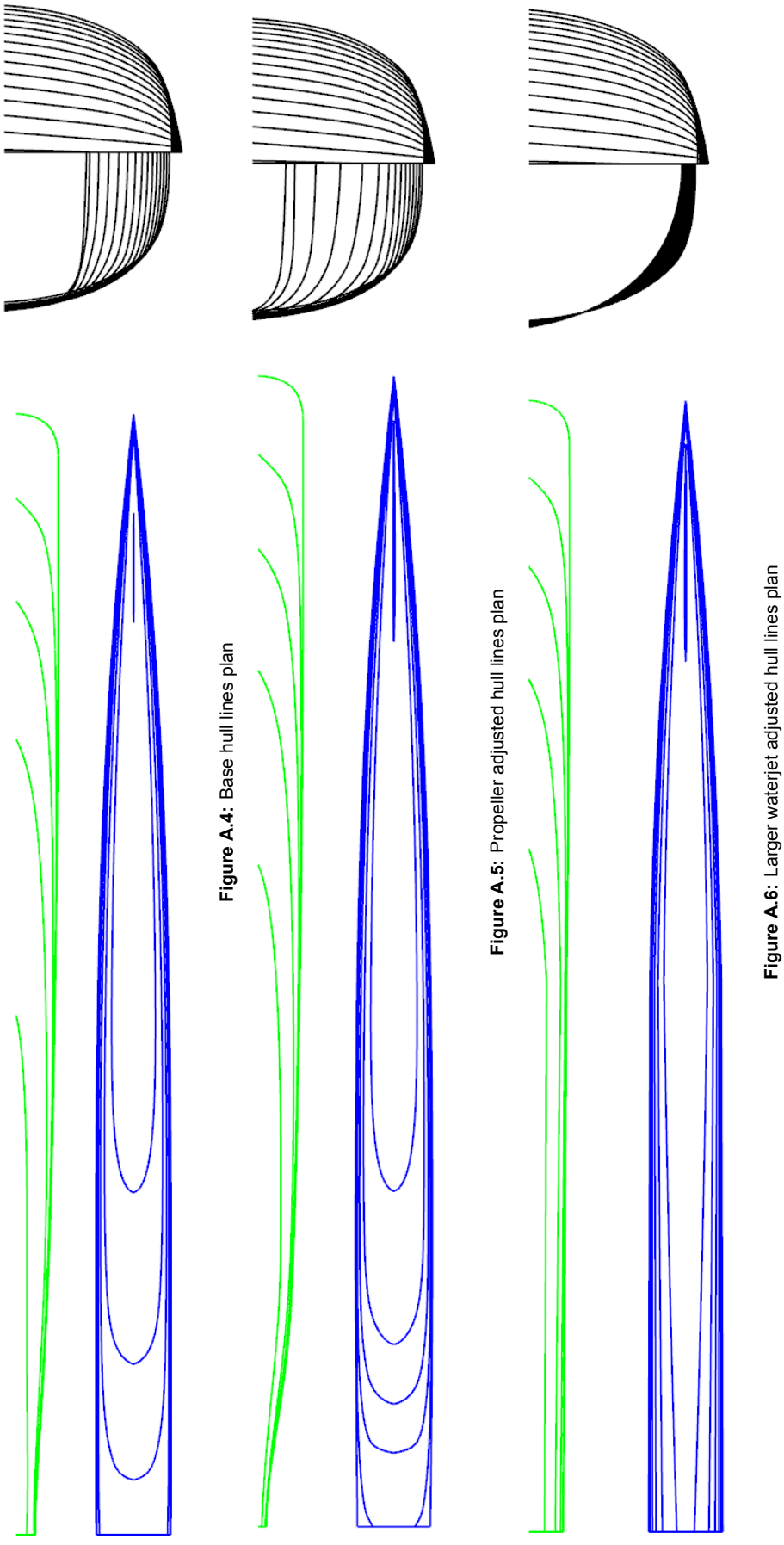

Figure A.4: Base hull lines plan

Figure A.5: Propeller adjusted hull lines plan

Figure A.6: Larger waterjet adjusted hull lines plan

B

Regression coefficients

Fn	a_1	a_2	a_3	a_4	a_5
0.20	0.02364	0.00208	-0.09802	0.00367	-0.00074
0.25	0.08105	-0.11406	-0.08112	0.00249	-0.00399
0.30	0.09203	-0.12002	-0.04730	-0.00032	-0.00962
0.35	0.09872	-0.14088	0.05087	-0.00119	-0.01753
0.40	0.11462	-0.18198	0.15454	-0.00345	-0.00860
0.45	0.19912	-0.36887	0.47748	-0.01172	-0.03507
0.50	0.25341	-0.51243	0.66013	-0.01491	-0.04746
0.55	0.23065	-0.47458	0.63852	-0.01406	-0.04424
0.60	0.18009	-0.37030	0.52675	-0.01145	-0.03065
0.65	0.15325	-0.31598	0.35717	-0.00734	-0.01231
0.70	0.14200	-0.29540	0.28432	-0.00570	-0.00455
0.75	0.11903	-0.24491	0.22942	-0.00432	-0.00114
0.80	0.11354	-0.23332	0.18725	-0.00331	0.00104
0.85	0.10354	-0.21127	0.15102	-0.00225	0.00249
0.90	0.08330	-0.16378	0.11757	-0.00129	0.00248
0.95	0.09060	-0.17985	0.09039	-0.00053	0.00308

Table B.1: NPL-Molland regression coefficients for residual resistance coefficient

Fn	a_1	a_2	a_3	a_4	a_5
0.20	8.60810	-18.62000	10.41700	-0.50534	-0.20518
0.25	13.17900	-27.89500	9.44030	-0.50136	-0.63251
0.30	11.16400	-23.23600	12.85600	-0.48311	-0.84645
0.35	7.93080	-18.55300	18.14000	-0.54882	2.79610
0.40	19.81400	-42.50100	79.98600	-2.17310	1.18870
0.45	41.68500	-78.47700	161.20000	-4.38950	-10.79700
0.50	57.81900	-109.75000	230.93000	-5.74290	-20.47400
0.55	77.38700	-158.09000	266.16000	-5.94060	-21.89300
0.60	74.97100	-156.37000	269.82000	-5.93160	-18.73700
0.65	60.44000	-128.09000	245.49000	-5.29750	-11.22100
0.70	54.96500	-118.19000	233.46000	-5.22510	-6.22420
0.75	61.06800	-134.51000	221.79000	-4.97590	-2.09950
0.80	72.46800	-161.88000	211.21000	-4.67040	0.64284
0.85	53.37200	-118.14000	198.67000	-4.26940	2.27600
0.90	52.17200	-113.93000	179.75000	-3.79840	3.71750
0.95	53.17100	-114.06000	164.69000	-3.59100	4.60620

Table B.2: NPL-Molland regression coefficients for the trim angle

Type of Analysis	Number of Coefficients	Regression Coefficients			
	N_{fit}	C_1	C_2	C_3	C_4
Moving Probe	2	0.157	1.835		
	3	0.1559	1.83	0.0158	
	4	0.002472	1.862	0.2859	0.3588
Transom Probe	2	0.08057	2.831		
	3	0.0734	2.835	0.1247	
	4	0.06296	2.834	0.1352	0.01338

Table B.3: Doctors et al. (2007) regression coefficients for transom ventilation

Appendages	$(1 + k_2)$
rudder behind skeg	1.5-2.0
rudder behind stern	1.3-1.5
twin-screw balance rudders	2.8
shaft brackets	3.0
skeg	1.5-2.0
strut bossings	3.0
hull bossings	2.0
shafts	2.0-4.0
stabilizer fins	2.8
dome	2.7
bilge keels	1.4

Table B.4: Appendages resistant coefficients

C

Single line diagrams

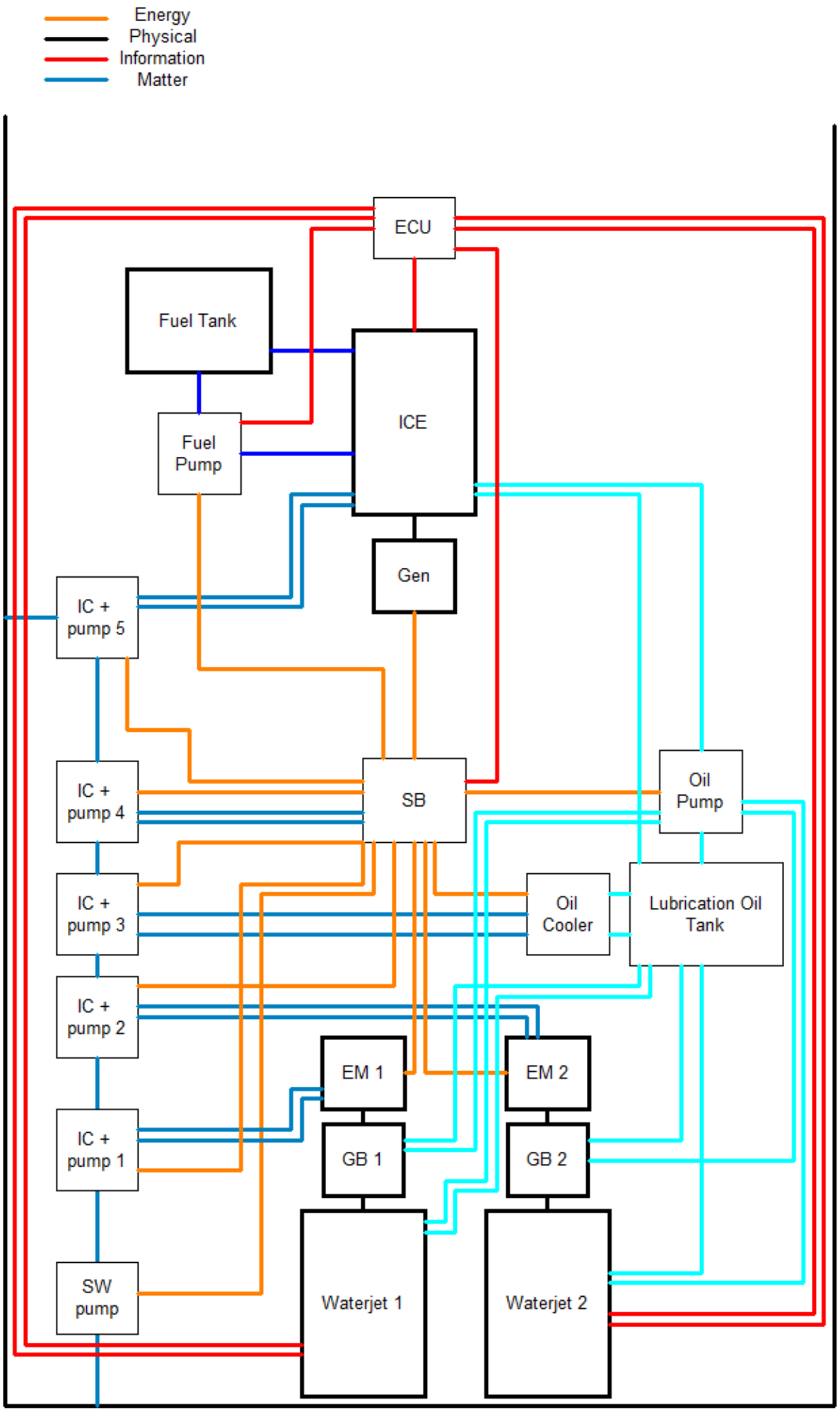

Figure C.1: Electrical architecture with two propulsors

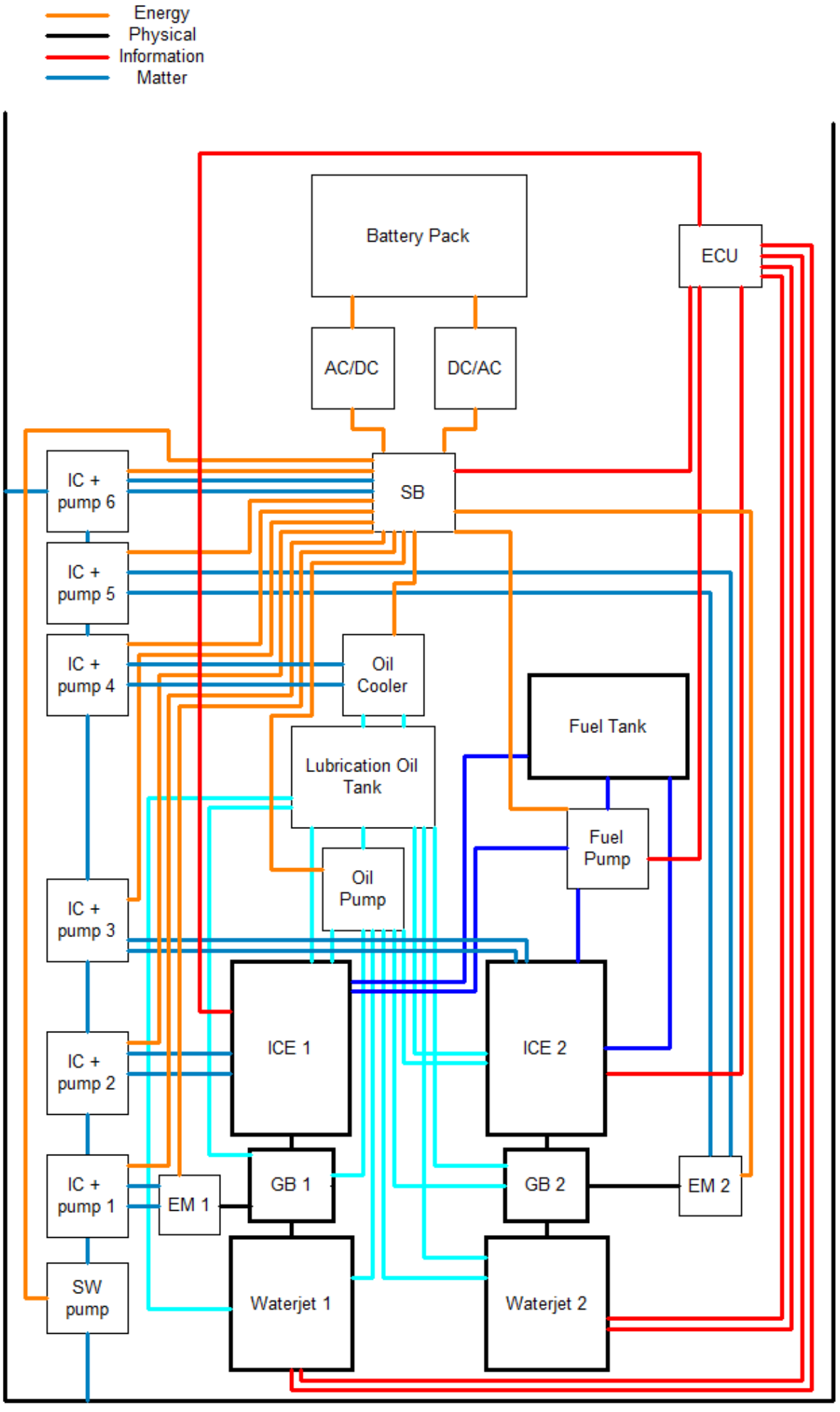

Figure C.2: Hybrid architecture with two propulsors

D

Data fit

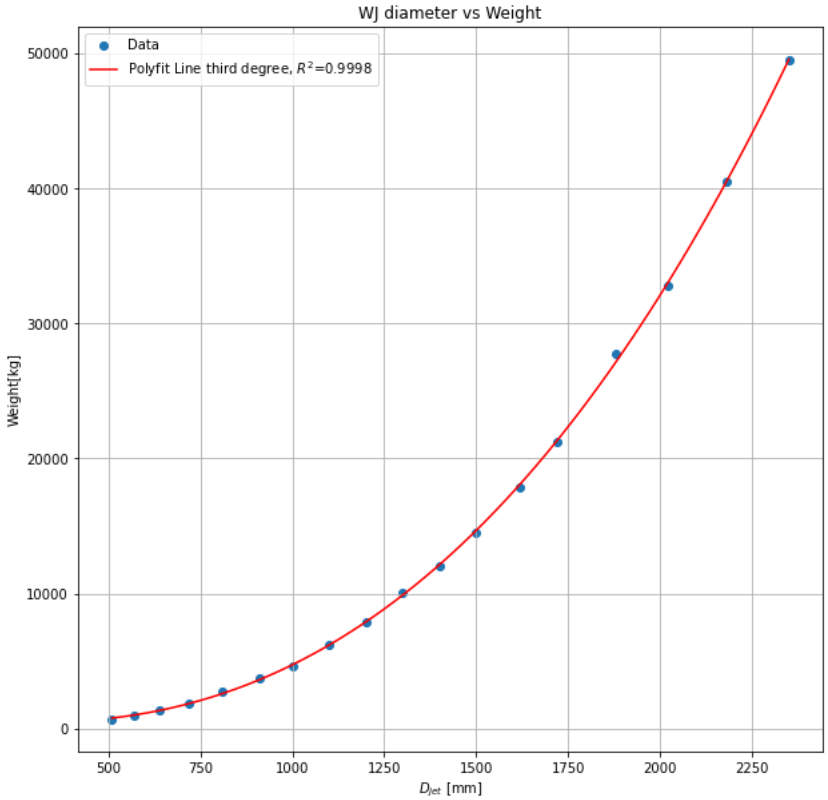

Figure D.1: Waterjet weight vs diameter

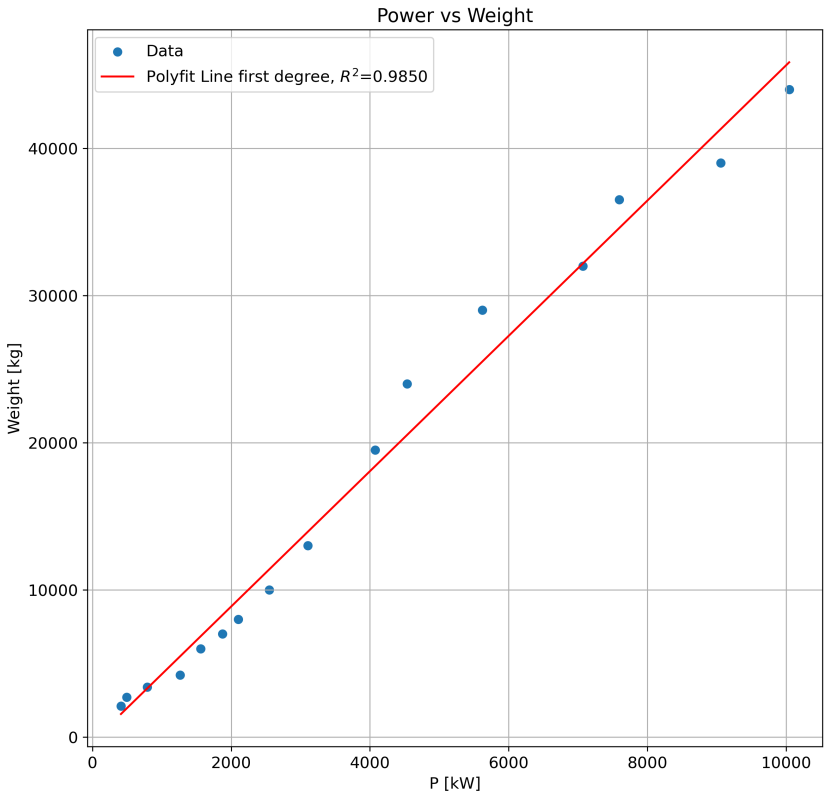

Figure D.2: Gearbox weight vs power

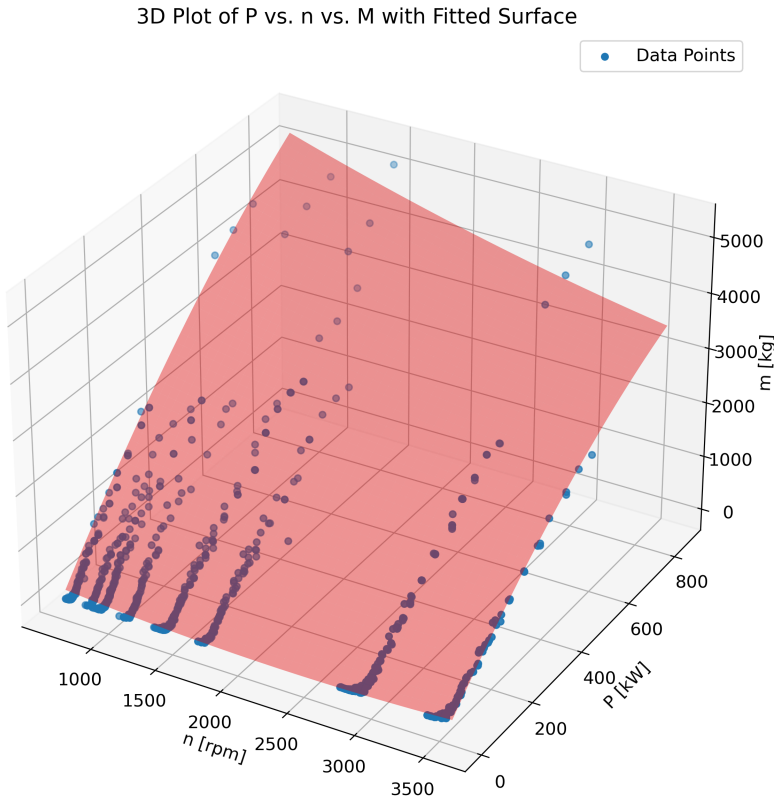

Figure D.3: Electric motor weight

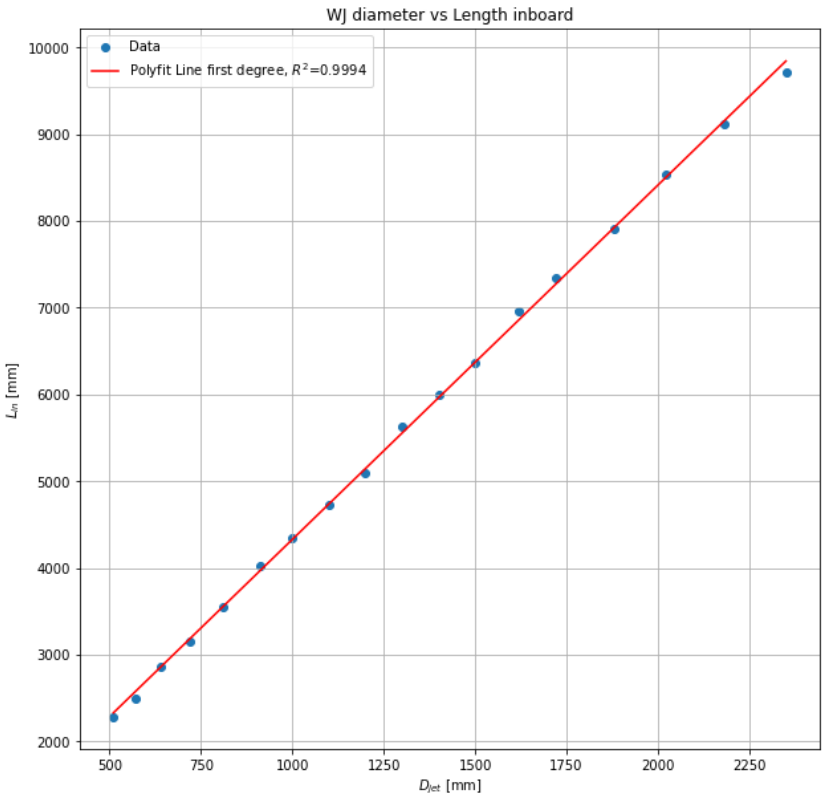

Figure D.4: Waterjet inboard length vs diameter

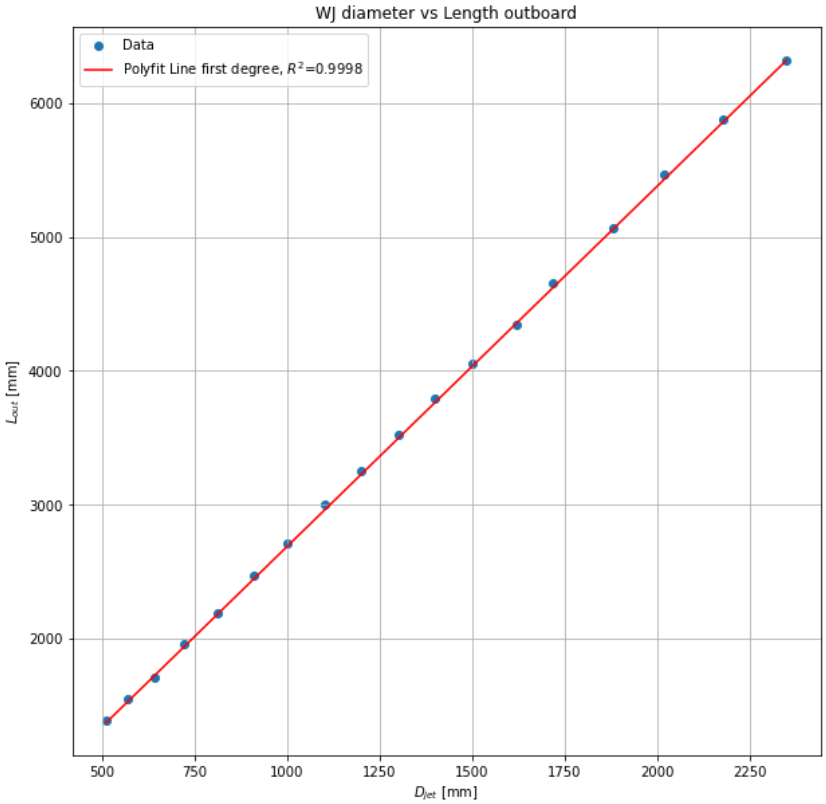

Figure D.5: Waterjet outboard length vs diameter

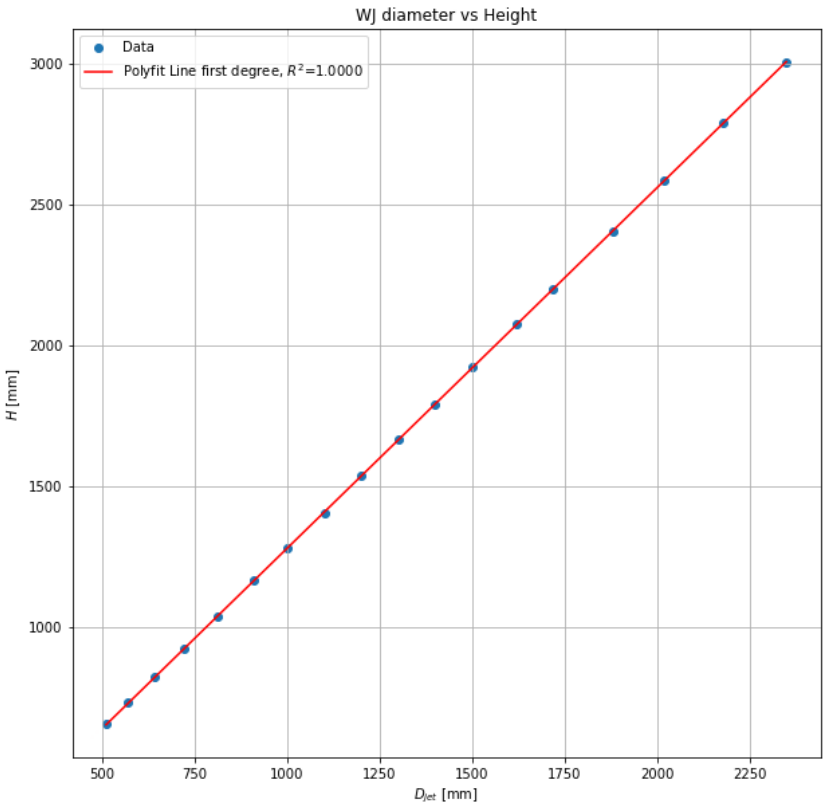

Figure D.6: Waterjet outboard height vs diameter (also represents the width)

D.1. Electro motor price

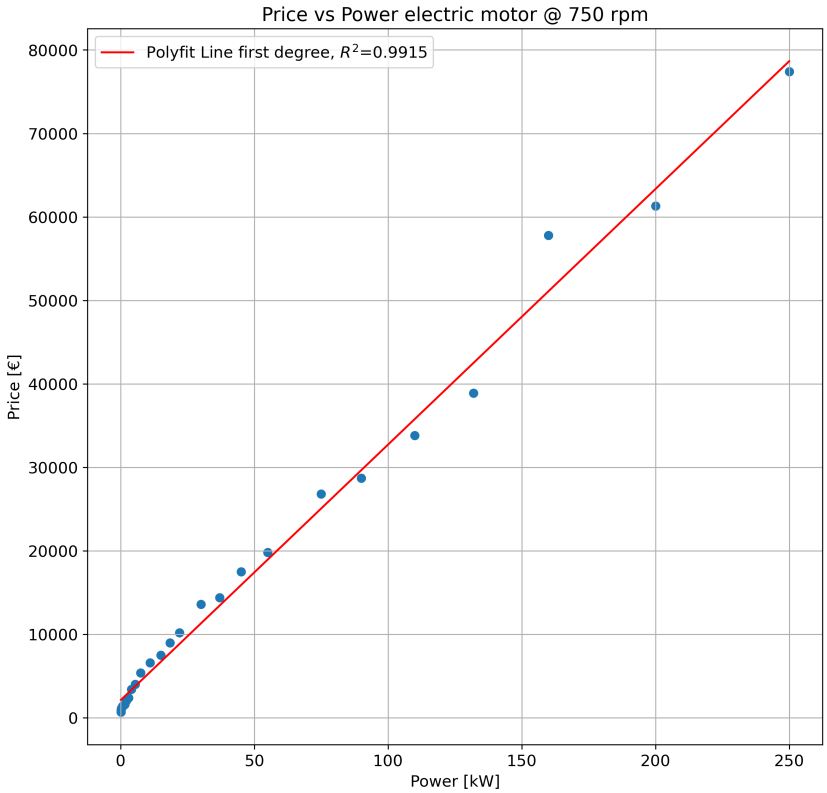

Figure D.7: Price vs weight electric motor ($CAPEX = 306.15 \cdot P + 2109.25$)

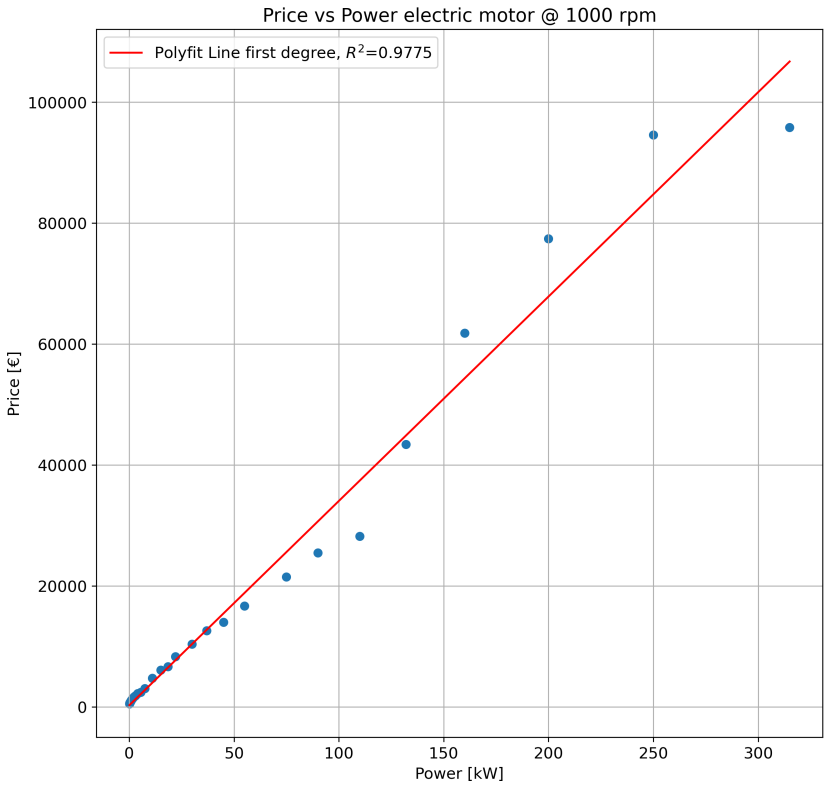

Figure D.8: Price vs weight electric motor ($CAPEX = 337.99 \cdot P + 255.33$)

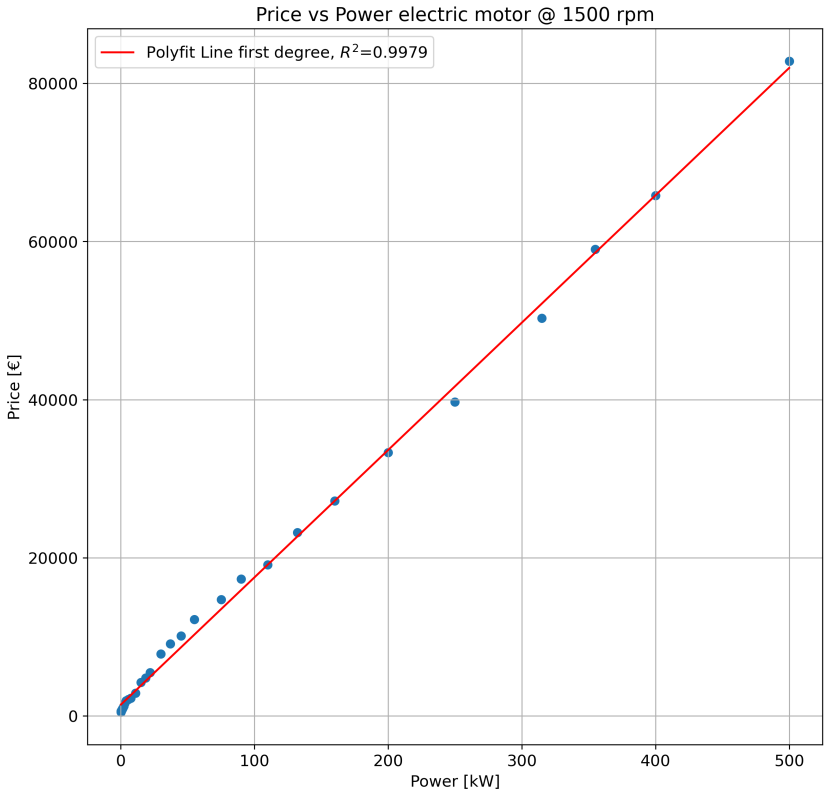

Figure D.9: Price vs weight electric motor ($CAPEX = 161.08 \cdot P + 1404.32$)

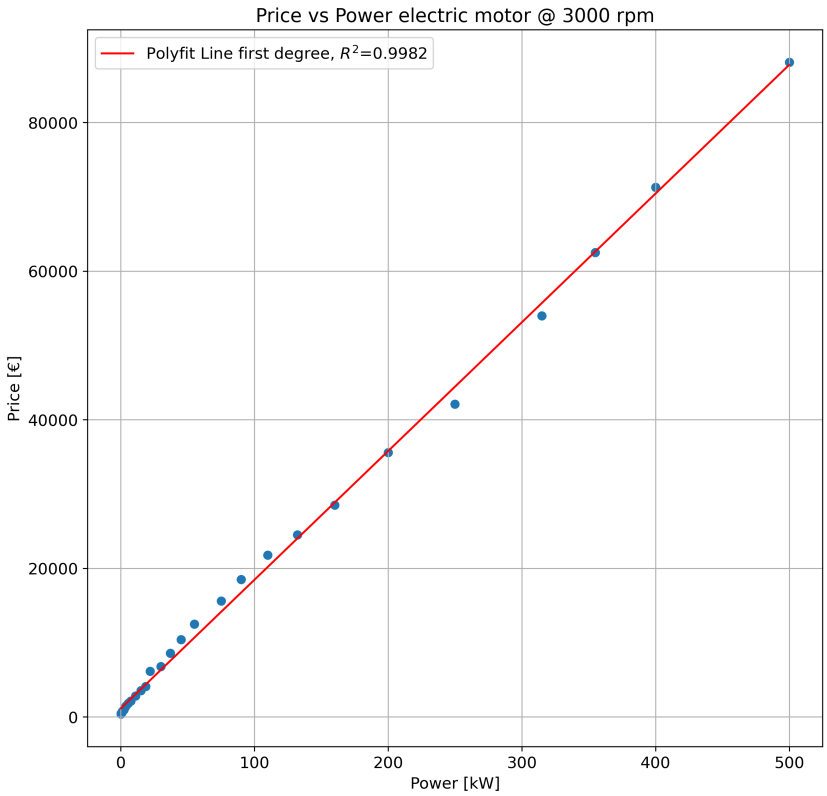

Figure D.10: Price vs weight electric motor ($CAPEX = 173.23 \cdot P + 1137.18$)

E

Fuel price forecasts

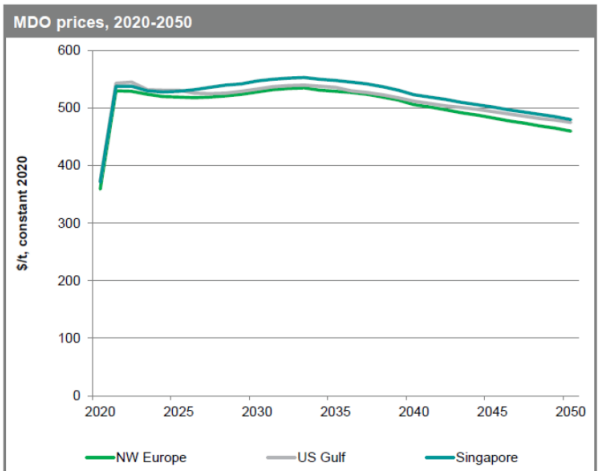

Figure E.1: MDO price forecast (Horton et al., 2022)

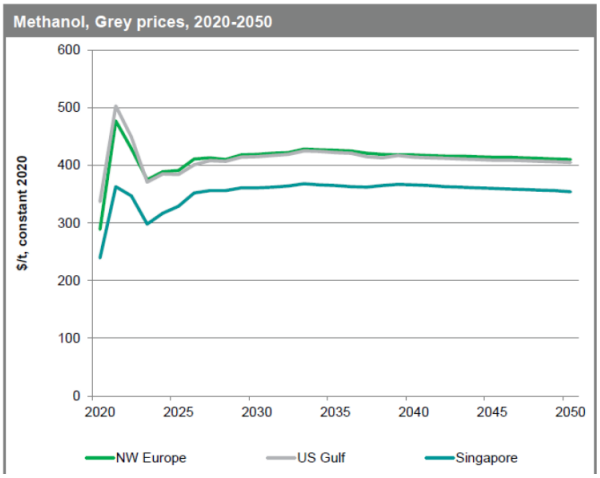

Figure E.2: Methanol price forecast (Horton et al., 2022)

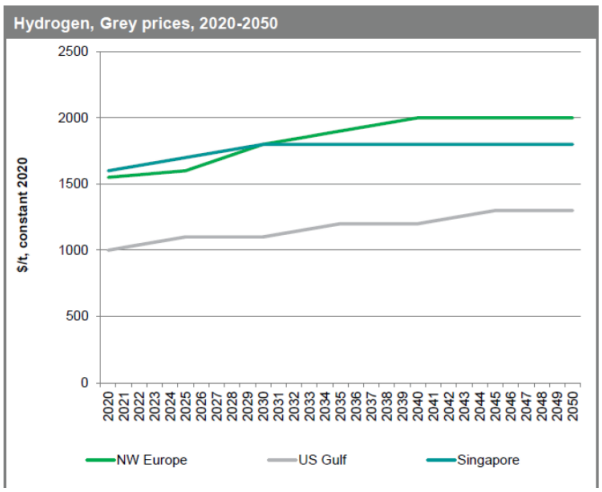

Figure E.3: H2 (grey) price forecast (Horton et al., 2022)

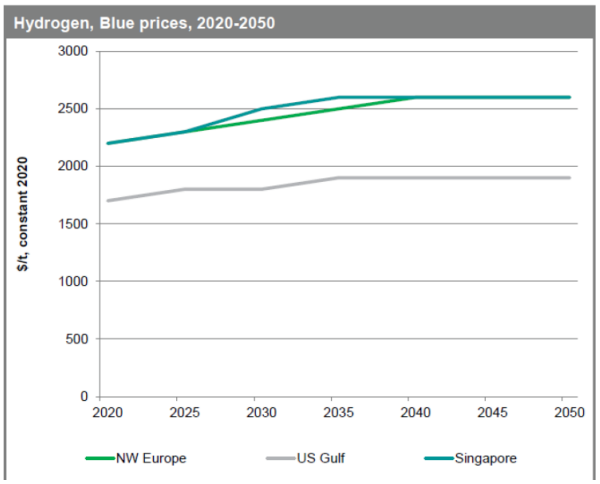

Figure E.4: H2 (blue) price forecast (Horton et al., 2022)

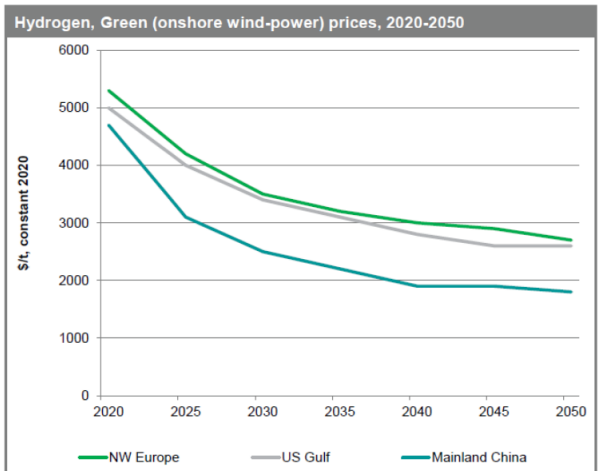

Figure E.5: H2 (green) price forecast (Horton et al., 2022)